# Identification and characterization of interactions between bacterial WxxxE-virulence proteins and host cell proteins

Von der Fakultät für Lebenswissenschaften

der Technischen Universität Carolo-Wilhelmina zu Braunschweig

zur Erlangung des Grades einer

Doktorin der Naturwissenschaften

(Dr. rer. nat.)

genehmigte

D i s s e r t a t i o n

von Nadiia Igorivna Sokolova
aus Slowjansk / Ukraine

1. Referentin: Professorin Dr. Theresia Stradal

2. Referent: Professor Dr. Martin Korte

eingereicht am: 26.09.2016

mündliche Prüfung (Disputation) am: 09.12.2016

Druckjahr 2016

## Vorveröffentlichungen der Dissertation

Teilergebnisse aus dieser Arbeit wurden mit Genehmigung der Fakultät für Lebenswissenschaften, vertreten durch die Mentorin der Arbeit, in folgenden Beiträgen vorab veröffentlicht:

### Tagungsbeiträge

Stefan Arens, Eric Meinhardt, Sonia Blasche, **Nadiia Soklakova**, Dominik von Tils, M. Alexander Schmidt, Manfred Kögl, Frank Schwarz, Theresia E. B. Stradal. Characterization of type-III secreted bacterial virulence factors that interfere with Rho-GTPase signalling. (Poster) International Joint Meeting of the German Society for Cell Biology (DGZ) and the German Society for Developmental Biology (GfE), Heidelberg (2013).

**Nadiia Soklakova**, Stefan Arens, Eric Meinhardt, Sonia Blasche, Dominik von Tils, M. Alexander Schmidt, Manfred Kögl, Frank Schwarz, Theresia E. B. Stradal. Identification and characterization of interactions between *Salmonella* bacterial virulence proteins SifA and SifB and EPEC EspT and host cell proteins. (Poster) 5$^{th}$ Summer School on Infection Research, Dresden (2014).

**Nadiia Soklakova**, Stefan Arens, Eric Meinhardt, Sonia Blasche, Manfred Kögl, Frank Schwarz, Theresia E. B. Stradal. Identification and characterization of interactions between *Salmonella* bacterial virulence proteins SifA and SifB and host cell proteins. (Poster) 7$^{th}$ International PhD Symposium, HZI, Braunschweig (2014).

**Nadiia Soklakova**, Stefan Arens, Eric Meinhardt, Sonia Blasche, Manfred Kögl, Frank Schwarz, Theresia E. B. Stradal. Novel interactions of *Salmonella* bacterial virulence proteins SifA and SifB and host cell proteins. (Poster) 8$^{th}$ International PhD and ESR Symposium, HZI, Braunschweig (2015).

**Nadiia Soklakova**, Stefan Arens, Eric Meinhardt, Sonja Blasche, Manfred Kögl, Frank Schwarz and Theresia E.B.Stradal.Identification and characterization of interactions between *Salmonella* bacterial virulence proteins SifA and SifB and host cell proteins.(Poster) Actin Dynamics Meeting, Regensburg (2015).

**Nadiia Soklakova**, Stefan Arens, Eric Meinhardt, Sonja Blasche, Manfred Kögl, Frank Schwarz and Theresia E.B.Stradal. Novel interactions of *Salmonella* bacterial virulence proteins SifA and SifB and host cell proteins. (Poster) International Meeting of the German Society for Cell Biology, Munich (2016).

# To my Family

# Table of contents

# 1. INTRODUCTION

Actin dynamics is essential for a variety of cellular processes, namely in supporting shape, division and motility of the cell, intracellular transport and cell signaling. The actin cytoskeleton shows a remarkable evolutionary conservation, from single cell organisms to highly complex mammals. Moreover, actin dynamics is a tightly regulated process, wherein the proteins of the family of Rho GTPases are the main players in controlling actin turnover. Considering its essential role in a variety of cellular activities, it is not surprising that the actin cytoskeleton is a prime target of an array of pathogens. Pathogenic bacteria have evolved to usurp actin either to pursue an intracellular lifestyle or to remain unperceived by the immune system of the host. In the present work, I address modulation of actin regulators by enteric pathogens during the course of infection.

Infectious diseases remain the major problem in developed and developing countries. Remarkably, although enteric bacteria target the same host, their disease causing mechanisms are distinct. For example, enteropathogenic and enterohemorrhagic *Escherichia coli* (EPEC and EHEC) adhere closely to the host cell plasma membrane, eliminate the enterocyte microvilli and induce cytoskeletal rearrangement resulting in the formation of pedestals beneath adherent bacteria (Lommel et al., 2004). Both EPEC and EHEC largely remain extracellular in the lumen of the gut (Wong et al., 2011). For intracellular bacteria, the main point is to get access to the intracellular space of the host cells. In particular, *Salmonella spp*. and *Shigella spp.* invade eukaryotic target cells by activating Rho GTPase signaling pathways, and internalize in beneficial replicative niches within the host. In this study, I focus mainly on *Salmonella* pathogenesis.

## 1.1 Rho GTPases

Rho GTPases are main actin regulators. Together with Ras, Rab, Arf and Ran they belong to the Ras- superfamily that comprises approximately of 150 members in humans (Vigil et al., 2010).Remarkably, all Rho proteins share a common G-domain (GDP/GTP-binding domain) and an isoprenylated moiety on the C-terminal region, which is essential for their membrane localization and for their association with guanine nucleotide dissociation inhibitor (GDI). Like other small GTPases, Rho proteins act as molecular switches that cycle between active GTP and inactive GDP forms. The activity of Rho GTPases is tightly coordinated by more than 85 guanine nucleotide exchange factors (GEFs), 60 GTPase-activating proteins (GAPs) and at least 3 GDIs (Jaffe & Hall., 2005;Cherfils & Zeghouf 2013). Indeed, GEFs promote the exchange of GDP to GTP, whereas GAPs catalyze the hydrolysis reaction of GTP to GDP+Pi, and GDIs prevent activation and degradation of Rho proteins in the cytosol (Figure 1) (Cherfils & Zeghouf 2013; Jaffe & Hall., 2005).

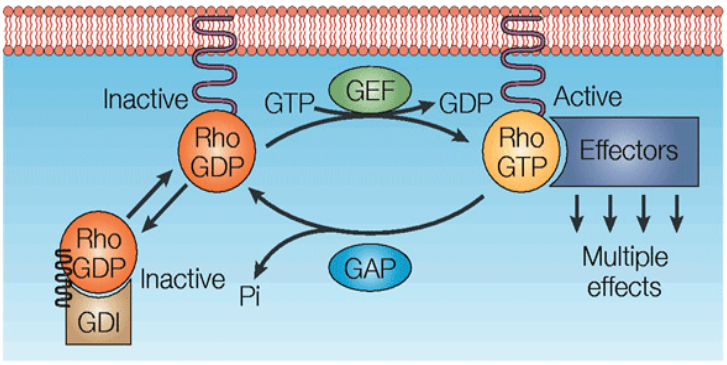


**Figure 1: Regulation of the Rho GTPases cycle by GEFs, GAPs, and GDIs.**The active conformation of Rho-family GTPases is characterized by hydrolysis of GDP to GTP, a process induced by GEFs. At the same time, Rho proteins are inactivated by certain GAPs. GDIs bind the Rho-GDP form and keep the protein in its inactive conformation in the cytosol (Aktories & Barbieri., 2005).

Members of the Rho GEF family, also known as Dbl family, commonly contain a Dbl-homology (DH) domain, encoding the catalytic activity, and a pleckstrin homology (PH) domain, which mediates membrane localization of these regulators (Bishop & Hall., 2000). Activation of Rho GTPases is mediated by binding of the DH domain of GEFs, resulting in the release of GDP and spontaneous binding of GTP (van Buul et al., 2014).

The most studied GTP-binding proteins of the Rho family are RhoA, Rac1 and Cdc42, which are all involved in regulation of the actin cytoskeleton. RhoA is a 22 kDa-protein which is involved in organizing contractile actin/myosin stress fibers and focal adhesions (Ridley & Hall., 1992). Rac1 is a 21 kDa-protein essential for the formation of focal complexes and

sheet-like leading edge protrusions, referred to as lamellipodia (Ridley et al., 1992). Cdc42 is known to induce the formation of filopodia or microspikes and to be important for cell polarity.

Rho GTPases are involved in many cellular functions such as cell polarity, cell cycle progression, apoptosis, transformation, microtubule dynamics, vesicular transport pathways and gene transcription, as well as a variety of enzymatic activities, to name only some. Regulation of the actin cytoskeleton during infection is another important function, which is not a surprise (Aktories & Barbiere., 2005; Heasman & Ridley, 2008; Etienne-Manneville & Hall, 2002; Lemichez & Aktories, 2013).

Due to these diverse cellular functions, host GTPases are preferred molecular targets for bacterial effector proteins that mimic eukaryotic regulators of the GTPases cycle (Boquet, 2000). Thereby, intracellular bacterial pathogens induce extensive changes in host signaling pathways allowing them, for instance to invade epithelial cells and establish the intracellular niche for further replication. *Salmonella* effectors proteins, including SopE, SopE2, SptP, SopB, SipC and SipA, are involved in the entrance of this pathogen into non-phagocytic cells. Functions of these virulence factors in the pathogenesis of *Salmonella* are described in more detail below.

### 1.2 Microtubule assembly, organization and dynamics

Together with actin (microfilaments), septins and intermediate filaments, microtubules participate in the maintenance of the cellular architecture. Microtubules are built as cylindrical filaments assembled as head-to-tail polymerized α- and ß- tubulin heterodimer subunits. The γ-tubulin acts as a basis for microtubule nucleation. A microtubule is a hollow tube with a diameter of 24 nm and consists of 13 protofilaments that are built from dimers of α- and ß-tubulin (Figure 2 A). Microtubules originate from γ-tubulin in the microtubule organizing center (MTOC) which forms around the centrosome (Fig. 2 C). Dynamic instability of these cytoskeleton polymers is characterized by a continuous process of polymerizing (growth) and depolymeriziting (shrinkage) of the microtubules on the faster-growing ends (plus end). Transition from growth to shrinkage is known as ‘catastrophe’ and the reverse process is termed ‘rescue’ (Figure 2 B) (Horio & Hotani, 1986; Walker et al., 1988). Polymerization of microtubules is a GTP-dependent process, in which both α- tubulin and ß- tubulin must be bound to GTP (Akhanova & Steinmetz, 2015; Wade, 2009). New αß-dimers are added to a

microtubule followed by hydrolysis of the GDP to GTP. The depolymerization phase is characterized by a rapid loss of GDP-tubulins from the protofilaments leading to rapid disassembly (Figure 2 B) (Desai & Mitchison, 1997; Conde & Caceres, 2009).

Motorproteins of the kinesin family transport various cargoes from the minus to plus end (i.e. from cell center to the periphery). At the same time, dyneins move cargo to the minus end towards the cell center. Thereby, these molecular motors facilitate intracellular transport along microtubules.

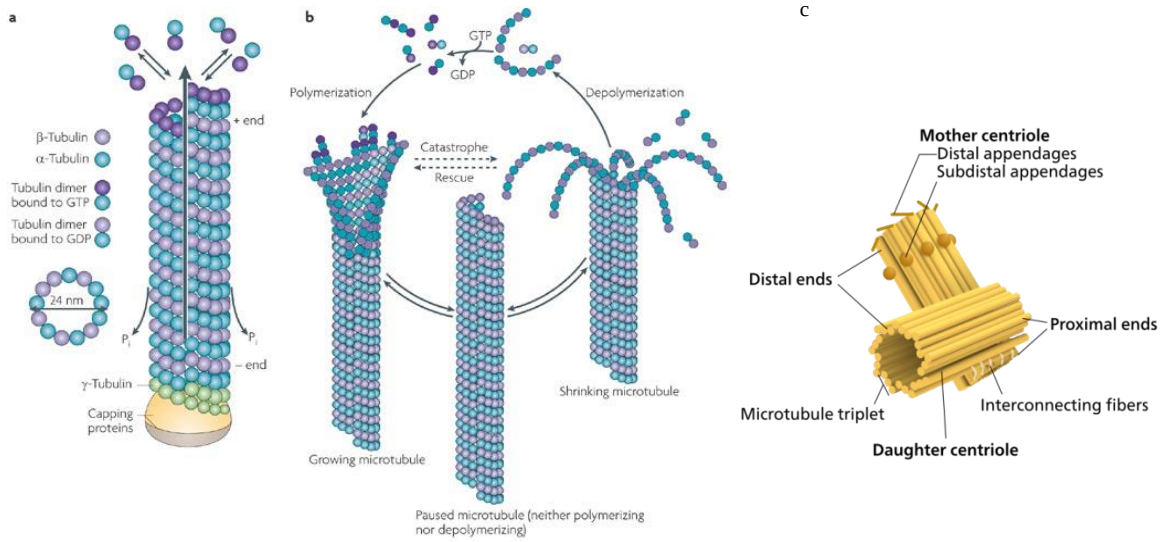


**Figure 2: Microtubules and centrosome.**

(A) Assembly of polar microtubules. (B) Microtubule dynamic instability (Conde & Caceres, 2009). (C) The structure of the centrosome that serves as the main MTOC (Wikimedia, https://commons.wikimedia.org).

Intracellular pathogens exploit the microtubule network and molecular motors, associated with it, in order to acquire nutrients coming from different host compartments. Indeed, *Salmonella* manipulates this molecular assembly for the establishment and the stability of the bacterial replicative niche (also compare below Figure 7).

## 1.3 *Salmonella*

*Salmonella* is a rod-shaped Gram-negative facultative intracellular pathogen, whose cells range from 0.7 to 1.5 µm in diameter and from 2 to 5 µm in length (Figure 3). The genus *Salmonella* is comprised of two species, *Salmonella bongori* and *Salmonella enterica*, which are in turn classified into six subspecies: enterica, salamae, arizonae, diarizonae, houtenae, and indica (de Jong et al., 2012). To date, more than 2500 serovars of *Salmonellaenterica* are known; however, I will be focussing on *Salmonella enterica* serovar Typhimurium in this thesis. Infection with non-typhoidal *Salmonella* (NTS), in particular *Salmonella enterica* serovar Typhimurium, is usually characterized by self-limiting diarrhea, with symptoms disappearing within 2-5 days. Infection with *Salmonella* Typhi results in the development of systemic infection, which manifests itself as typhoid fever and often leads to death of the patient.

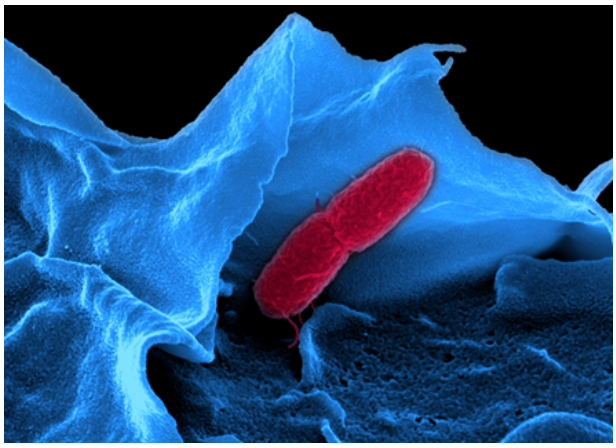

**Figure 3: *Salmonella* (red) invades a host cell (blue) by induction of membrane ruffling.** Image courtesy of Manfred Rohde (HZI).

Pathogenic *Salmonella* spreads through fecal contamination of food and water. Poultry, meat, dairy products, eggs are common sources of *Salmonella* infection. It is well known that the stomach has an acidic milieu (pH 2), and most of intracellular pathogens are unable to survive in such hostile environment; however, *Salmonella* is an exception. Due its adaptive acid tolerance, salmonellae are capable to survive in such harsh acidic condition within a host (Garcia-del-Portillo et al., 1993; Reisenberg-Wilmes et al., 1996). *Salmonella* overcomes multiple defense mechanisms of the small intestine in order to reach and attach to the intestinal epithelium, thus initiating infection.

## 1.4 Epidemiological situation of non-typhoidal Salmonellosis in EU/EEA countries

The European Centre for Disease Prevention and Control (ECDC) surveillance of food and waterborne diseases and zoonosis has rated *Salmonella* as the most frequently reported pathogen in foodborne outbreaks (for example 1 533 *Salmonella* outbreaks have been estimated in 2012) and the second most commonly reported enteric infection in the European Union/ European Economic Area (EU/EEA). The surveillance report indicates a 10% reduction in the number of cases of non-typhoidal salmonellosis from 2010 to 2012 (102 456 reported cases in 2010 to 92 443 cases in 2012). Total numbers of disease are quite different among EU/EEA countries: the highest notification rates have been documented in the Czech Republic and Slovakia (>70 cases per 100 000), followed by Hungary and Lithuania (>55 cases per 100 000), while the lowest rates have been reported in Portugal (<2 cases per 100 000) (Niskanen et al., 2015).

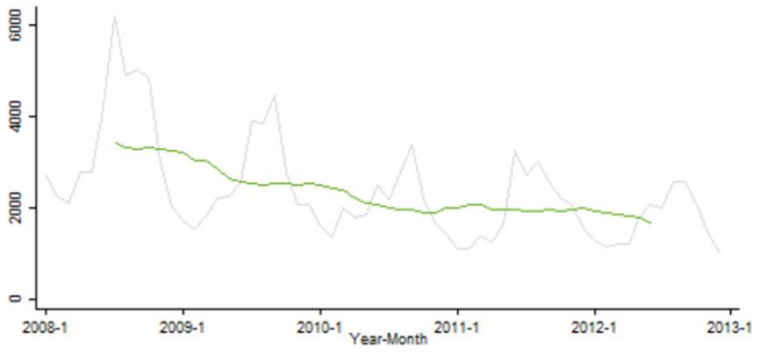


**Figure 4: Trend in the number of confirmed non-typhoidal salmonellosis cases in Germany.** Data were obtained from ECDCs surveillance, 2008-2012 (Niskanen et al., 2015).

The highest prevalence of salmonellosis has been reported in children between 1 and 4 years of age (>90 cases per 100 000), and the lowest in the age group 25-44 years (<12 cases per 100 000), for both males and females. Disease caused by *Salmonella typhimurium* has a strong seasonal pattern with the highest peak in the summertime and a second smaller peak in January (Niskanen et al., 2015).

## 1.5 Assembly of the bacterialT3SS

Like many other Gram-negative bacterial pathogens, *Salmonella*, as well as EPEC and EHEC,utilizes a needle-like type three secretion system (T3SS), also known as injectisome, to secret an arsenal of virulence factors into the host cytoplasm. The injectisome is built of approximately 25 proteins embodying a fascinating molecular machine composed of a basal body, and an extracellular needle that emerges from the outer membrane. Despite the fact that there are seven different families of injectisomes, the structure of the needle complex is universal among species (Cornelis, 2006). The basal body of T3SS comprises of two rings embedded into the inner and the outer bacterial membrane. The inner membrane (IM) ring contains 24 subunits of SctJ and SctD (united secretion and cellular translocation (Sct) names) (Prgk and PrgH in *Salmonella*) (Moest & Meresse, 2013). The outer membrane (OM) ring is composed of 12-15 copies of secretin protein SctC (*Salmonella's* InvG) (Schraidt & Marlovits, 2011). The extracellular hollow needle of approximately 60-80 nm in length functions as a sensory probe to detect a host cell and to secrete virulence effector proteins that promote bacterial infection. The needle is associated with the basal body of T3SS via the inner rod protein SctI (*Salmonella's* PrgJ) (Marlovits et al., 2004). An ATPase plays a key role in the release of bacterial effectors from chaperones and their secretion (SctN) (*Salmonella's* InvC) (Akeda & Galan, 2005). Finally, translocation of bacterial virulence effectors is facilitated by the translocon, a protein complex that forms a pore in the host cell membrane (Cornelis, 2006; Burkinshaw & Strynadka, 2014) (Figure 5).

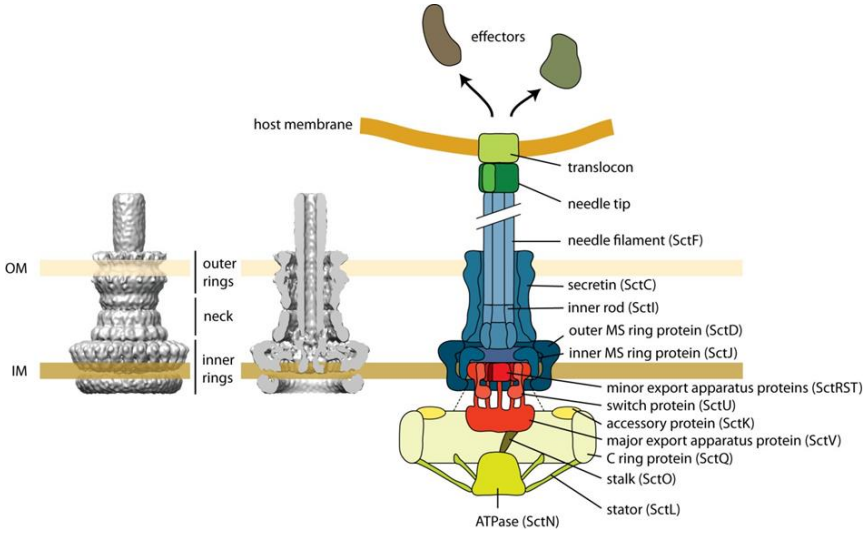


**Figure 5: Organization of the injectisome and its components.** Cryo-electromicroscopic data of a 3D surface representation of the needle complexes (left panel side view, middle panel cut view). The T3SS and its elements are schematically depicted (right panel). Cytoplasmic components are colored in yellow, export apparatus components in red, base and needle components in blue, and needle tip and translocator proteins in green (Diepold & Wagner, 2014).

Abbreviations: IM, inner membrane; OM, outer membrane; MS, membrane and supramembrane; Sct, secretion and cellular translocation (united Sct names).

It should also be pointed out that the fully assembled T3SS is activated only upon host cell contact. Using time-lapse microscopy, Hardt and colleagues demonstrated that *Salmonella* secretes the effector protein SipA into an eukaryotic cell within 10-90 seconds following direct contact with the host, and that the entire injection process proceeds for 100-600 seconds (Schlumberger *et al.* 2005).

There is no doubt that the utilization of a complex molecular machinery such as T3SS and secretion of bacterial virulence effectors plays a pivotal role in the pathogenicity of Gram-negative bacteria.

### 1.6 *Salmonella* invasion

For the successful infection, *Salmonella* utilizes two type 3 secretion systems (T3SSs) encoded within *Salmonella* pathogenicity islands-1 and -2 (SPI-1 and SPI-2) during pathogenesis. Through the action of SPI-1 T3SS effectors are translocated across the plasma membrane of host cell, enabling *Salmonella* to invade non-phagocytic cells, through re-arrangement and polymerization of actin and resulting in membrane ruffling. Manipulation of the host's actin cytoskeleton is achieved by activation of several T3SS-1 translocated effectors such as *Salmonella* invasion proteins (Sips) and Salmonella outer proteins (Sops) (Donnenberg, 2000; Schlumberger & Hardt, 2006). While SipA and SipC directly bind to actin and are involved in actin polymerization and bundling, SopE, SopE2 and SopB indirectly activate host actin remodeling by triggering Rho-GTPases. SopE functions as GEF for Cdc42 and Rac1, SopE2 targets Cdc42, and SopB activates host GTPases indirectly by manipulating the host phosphatidyl-inositol-phosphate metabolism (Hänisch et al., 2011; MgGhie et al., 2009; Friebel et al., 2001; Hardt et al., 1998; Agbor & McCormick, 2011). Later, upon completion of invasion, these small GTPases are downregulated by the GAP activity of T3SS effector SptP (Figure 6 A) (Rottner et al., 2005; Orchard & Alto, 2012; Fu & Galan, 1999; Hardt et al., 1998). Additionally an important feature of SptP is the ability to function as tyrosine phosphatase (Humphreys et al., 2009).

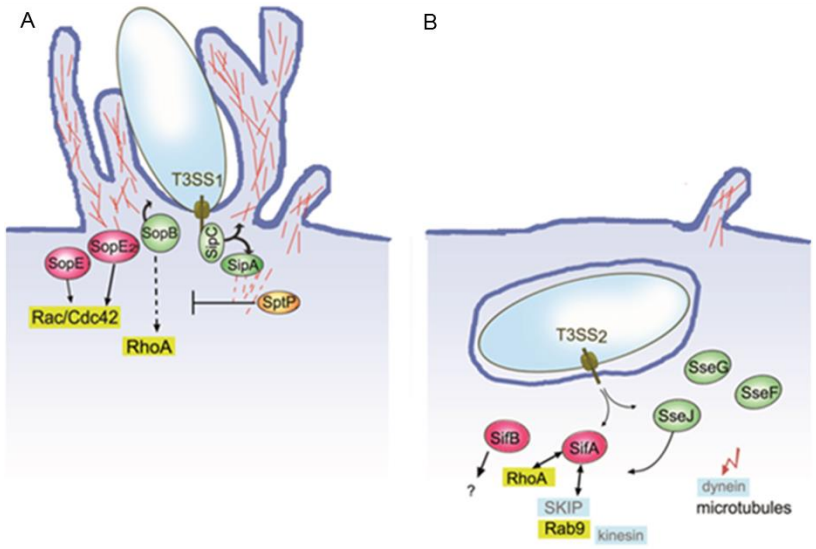


**Figure 6: *Salmonella* manipulates host cell behavior to its benefit.** A. *Salmonella* induces host cell invasion by delivering T3SS-1 bacterial virulence effectors into eukaryotic cells. While T3SS-1 effectors, SopE and SopE2, mimic eukaryotic GEF by triggering Rac1 and Cdc42, another effector, SptP, functions as GAP and downregulates the activity of these Rho GTPase. SipA and SipC directly interact with actin and stabilize F-actin. B. *Salmonella* resides in the intracellular niche, the so-called SCV, and translocates T3SS-2 effectors. SifA interacts with host protein SKIP and RhoA GTPase. SseF and SseG associate with microtubules. The function of SifB is not well defined (Rottner et al., 2005).

## 1.7 The *Salmonella*-Containing Vacuole

The host environment is rich in organic nutrients and serves a habitat for intracellular bacteria. Upon cell invasion, *Salmonella* resides in the so called *Salmonella*-containing vacuole (SCV). This unique compartment matures from the initial phagosome and contains early endosomal markers, such as early endosomal antigen 1 (EEA1), Rab5 and transferrin receptors. The latter is substituted within 20–40 min by late endosome/lysosome markers (LE/Lys), such as vacuolar ATPase (vATPase), lysosome-associated membrane proteins (LAMPs) and the lysosomal hydrolases such as cathepsins (Steele-Mortimer, 2008). Movement of SCVs from the site of bacterial internalization to the perinuclear region within 5 µm of the microtubule-organizing centre (MTOC) is controlled by the late endosomal GTPase Rab7 and its effector, Rab-interacting lysosomal protein (RILP) (Ramsden et al., 2007; Harrison et al., 2004).

After 2-4 hours post invasion, pathogenic bacteria employ SPI-2 T3SS effectors to mature the SCV and establish a niche for survival and replication within host cells (Hensel et al., 1995; Ruiz-Albert et al., 2002). A subset of T3SS-2 effectors, including SifA, PipB2, SopD2, SseG and SseF, is required for the formation of *Salmonella*-induced filaments (SIFs) (also see below section 1.8). At the same time, SseJ and SpvB down-regulate the appearance of highly

dynamic tubules from SCV (Ruiz-Albert et al., 2002; Figueira &Holden, 2012). Furthermore, SifA binds to the host protein SKIP (SifA and kinesin-interacting protein), an interactor of the endosomal GTPase Rab9 (Figure 6 B) (Diacovich et al., 2009; Jackson et al., 2008; Ohlson et al., 2008; Zhao et al., 2015). While SifA preferentially interacts with GDP-bound RhoA, SseJ binds to GTP-bound RhoA. Recent evidence suggests that the synergistic action of two T3SS-2 effectors, SifA and SseJ, along with host SKIP and RhoA to promote endosomal tubulation (Ohlson et al., 2008). Other virulence factors, namely SseF and SseG, that are also translocated by the SPI2-encoded T3SS, associate with microtubules and are engaged in alterations of the architecture of the microtubule network, including forcing of massive bundles close to SCV and tubular endosomal aggregates (Figure 6 B) (Kuhle et al., 2004; Abrahams et al., 2006). Much less is known about the biological function of the T3SS-2 effector protein SifB in *Salmonella* pathogenesis. BLAST database analyses of SifA and SifB bacterial effectors recognized 30% sequence similarity over the length of these proteins, thus SifB was named after its analog to SifA (Miao & Miller, 2000). However, infection experiments with bacteria lacking SifB demonstrate a phenotype similar to that of *Salmonella*-WT, at least *in vitro* (Rajashekar et al., 2014; Ruiz-Albert et. al., 2002). Detailed analysis of the role of SPI2 *in vivo* demonstrate that *Salmonella* strains harboring mutations in SPI-2 virulence genes are able to invade cells and reach host organs, but are attenuated in intracellular replication (Shea et al., 1999; Cirillo et al., 1998; Hensel, 2000).

### 1.8 SIFs, a dynamic tubular network induced by *Salmonella*

Pathogenic *Salmonella* induces a tubular network formation of the so called *Salmonella*-induced filaments (SIFs). These are characterized by the presence of a defined set of proteins, namely sorting nexins (SNX), *Salmonella*-induced secretory carrier membrane protein 3 (SCAMP3), and lysosome-associated membrane protein 1 (LAMP1). At different time points of infection some of these markers may be absent, defining specific subsets and stages of SIF formation (Figure 7) (Malik-Kale et al., 2011; Schroeder at al., 2011). Furthermore, *Salmonella*-induced tubules are formed along microtubules that serve as cytoskeletal scaffold for them. Previous publications report that (Brumell et al., 2002), inhibition of microtubules with nocadozole results in disruption of these tubulated membranes. Characteristic features and the mechanism of formation of early and late tubules are described in more detail below.

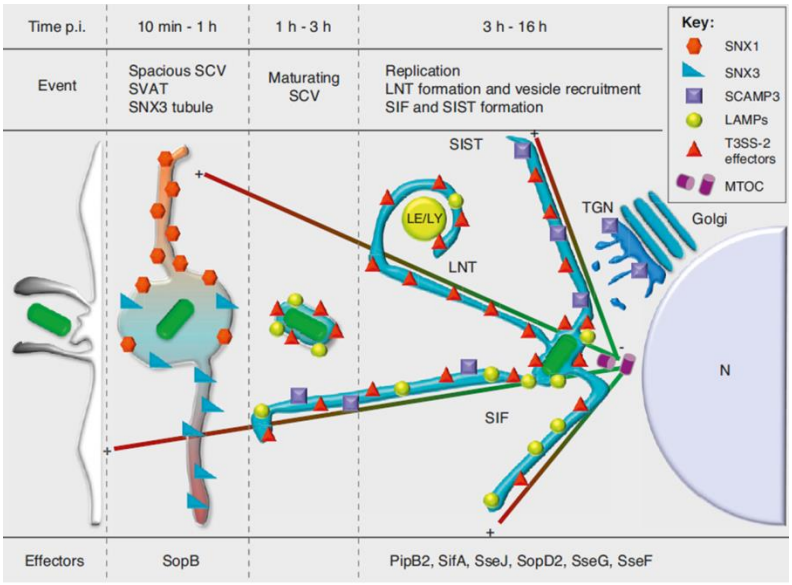


**Figure 7: *Salmonella*-induced tubular networks.** After its internalization, Salmonella (green rod) resides in SCV that is enriched in SNX1 and SNX3. At 10 min post invasion (p.i.) SVATs are formed by SNX1, at 30 min p.i. SNX3 tubules appear. The T3SS-1 effector SopB mediates the accumulation of the phosphoinositide [PI (3) P], followed by the recruitment of SNX1 and SNX3 on the vacuolar membrane. After 2 hours p.i. mature SCV moves to its replication niche, close to the MTOC. Then late T3SS-2 dependent tubular networks (SIFs, SISTs, and LNTs) are assembled (Schroeder at al., 2011). Abbreviations: MTOC, microtubule-organizing center; LAMPs, lysosome-associated membrane proteins; LNTs , LAMP1-negative tubules; SCV, Salmonella –containing vacuole; SNX, sorting nexin tubules; SIF, Salmonella-induced filaments; SISTs, Salmonella-induced secretory carrier membrane protein 3 (SCAMP3) tubules; SVATs, spacious vacuole-associated tubules; TGN, trans-Golgi network.

### 1.8.1 The early T3SS-1 dependent SNX tubules

Within the first hour post invasion, *Salmonella* develops sorting nexin (SNX) tubules, depending on the T3SS-1 bacterial effector SopB (Figure 1.7) (Bujny et al., 2008; Braun et al., 2010). Among the 30 proteins of the SNX family, SNX1 and SNX3 localize to the early SCV already after 10 min p.i., before they reach the cell center at 30-60 min p. i. SNX1 forms extensive highly dynamic spacious vacuole-associated tubules (SVATs) with peaks at 10-15 min post invasion, with a subsequent decrease in vacuole size (Bujny et al., 2008). SNX3 tubules appear at 30 min and disappear 2 hours after the invasion (Braun et al., 2010). The Bin-amphiphysin-Rvs (BAR) domain of SNX1 facilitates sensing of membrane curvature and induces tubulation (Van Weering et al., 2010; Cullen, 2008).

### 1.8.2 The late T3SS-2 dependent tubular networks: SIFs, SISTs and LNTs

#### 1.8.2.1 SIFs

In 1993 Garcia-del Portillo and colleagues were the first to identify the appearance of extensive highly dynamic filaments, with collapse velocities of 0.4-0.5 µm x $sec^{-1}$ during *Salmonella* infection. These compartments have been termed *Salmonella*-induced filaments (SIF) (Garcia-del Portillo et al., 1993; Krieger et al., 2014; Liss & Hensel, 2015). Activation of SPI-2 T3SS-translocated effectors is required for the induction of SIF which harbors late endosomal markers including lysosome-associated membrane protein 1(LAMP1), vacuolar vATPase (vATPase), endosome-associated GTPase Rab7 (Steele-Mortimer, 2008; Drecktrah et al., 2008; Garcia-del Portillo et al., 1993; Rajashekar & Hensel, 2011). Numerous studies have documented that after 3-4 h p.i. the formation of tubular endosomal aggregations occurs from the special vacuolar compartment, known as the *Salmonella*-containing vacuole. The late phase of *Salmonella* infection (8 h p.i.) is characterized by stabilization of an extensive tubular endosomal network (Drecktrah et al., 2008; Rajashekar et al., 2008). Dynamic behavior and morphologic variation of SIFs were extensively studied in the last years. Recent work by the group of Michael Hensel reported that infection with various mutant *Salmonella* strains defective in one of the effector proteins of the SPI2-T3SS leads to intracellular phenotypic differences. In contrast to wild-type *Salmonella* which induces the highly dynamic SIF of 160-200 nm in diameter, a pathogen defective in PipB2 effector induces bulky (with diameters of more than 500nm) non-dynamic SIFs, whereas the SseF- or SseG- mutant strains induce thin (with diameters of less than 100 nm) dynamic SIFs. The most dramatic phenotype, which is characterized by the entire absence of tubular membrane compartments, was observed in cells infected with a mutant strain deficient in SifA (Rajashekar et al., 2014; Brumell et al., 2001).

#### 1.8.2.2 SISTs

The members of the secretory carrier-associated membrane protein (SCAMP) family associate with the trans-Golgi network (TGN) and participate in protein trafficking along endosomal pathways. *Salmonella*-induced SCAMP3 positive tubules (SISTs) are not only characterized by the presence of SCAMP3 but also by the absence of late endosomal proteins, including LAMP1. Similar to SIF formation, SCAMP3 tubulation depends on the T3SS-2 effectors PipB2, SifA, SopD2, SseF and SseG (Haraga et al., 2008; Mota et al., 2009). The

molecular mechanism of SISTs forming likely involves formation of a PipB2-kinesin-1 complex, followed by a centrifugal extension of SCAMP3 tubules (Mota et al., 2009).

#### 1.8.2.3 LNTs

Finally, LAMP1 negative tubules (LNTs) act as precursors of SIFs and SISTs, thereby contributing to the recruitment of endocytic vesicles and to the membrane stability of SCVs. While the T3SS-2 effector SifA activates the formation of LNTs, the bacterial virulence protein SopD2 inhibits this process. Similar to SIFs, LNTs contain vATPase and cholestrerol, but they lack LAMP1 and Rab7 (Schroeder et al., 2010).

Remarkably, the T3SS-1 effector PipB2 interacts with kinesin light chain and regulates centrifugal extensions of SIFs, SISTs, and LNTs (Henry et al., 2006; Knodler & Steele-Mortimer, 2005; Mota et al., 2009; Schroeder et al., 2010). It has been suggested that the formation of early SNX tubules is essential for SCV maturation and its movement towards the MTOC (Bujny et al., 2008; Braun et al., 2010). SIFs, SISTs, and LNTs are important during the late stages of the intracellular lifestyle of *Salmonella*. The molecular mechanism of the formation of tubular networks as induced by *Salmonella*, and exact physiological functions of these tubules remain unclear.

## 1.9 Elimination and survival of *Salmonella* as a result of autophagy

Autophagy is derived from the Greek words "auto" ("self") and "phagein" ("to eat"). Autophagy is involved in the delivery of cytoplasmic material that is destined for degradation into lysosomes. This intracellular process is characterized by the formation of a double-membrane vesicle called autophagosome and the involvement of 36 autophagy-related (ATG) proteins. Beside its primary function, autophagy is tightly associated with the host immune defense mechanism against intracellular pathogens.

### 1.9.1 Autophagy of cytosolic bacteria

Recent studies highlight that *Salmonellaenterica* serovar Typhimurium can also survive in the cytosol of epithelial cells (Knodler et al., 2014; Malik-Kale et al., 2012). Interestingly, these cytosolic bacteria become ubiquitinated and can simply be recognized by autophagic adaptors, such as p62, nuclear dot protein (NDP52) and optineurin (OPTN) which belong to sequestosome 1/p62-like receptors (SLRs) family. These SLRs modify membranes for autophagosome formation through their interaction with an autophagosomal membrane-anchored member of the ATG8 family (LC3), resulting in degradation of intracellular bacteria (Figure 8, pathway 1) (Deretic, 2012).

### 1.9.2 Autophagy of bacteria in SCV

As mentioned earlier, *Salmonella* uses T3SS-1 to invade host cell by forming pores of ~3.5 nm in diameter in the host cell membrane (Knodler, 2015). Meanwhile, cytosolic galectins, particularly galectin 8, serve as danger receptors and accumulate on the damaged vacuole in order to protect host cells against penetration of pathogens. Galectin 8 triggers NDP-52 and LC3 accumulation to the defective SCV, thereby inducing antibacterial autophagy and elimination of cytoplasmic pathogens (Figure 8, pathway 2) (Thurston et al., 2012; Birmingham et al., 2006).

The work by the group of Prof. Dr. Wolf-Dietrich Hardt demonstrate that non-canonical autophagy is involved in repairing SCV membrane damaged by T3SS-1. Authors have identified that the sealing of endosomal membranes damaged by T3SS-1 effectors unexpectedly requires autophagy regulators (mTOR), recruitment factors (galectins, OPTN), initiation factors (ULK1, PI-3 kinase C3, Beclin1, ATG2A, and ATG9), ATG12- (ATG5,

ATG7, ATG12, and ATG16L1) and ATG8- conjugated systems, as well as regulators of SCV maturation (GTPases Rab5 and Rab7). Subsequently, it promotes bacterial maturation and replication by induction of T3SS-2 effectors. (Figure 8, pathway 3) (Kreibich et al., 2015). Nevertheless, the exact molecular mechanism of repairing the ruptured SCV remains poorly understood.

Recent findings shed light on different roles of the autophagy machinery during infection. Many questions remain open, for instance, it is unclear how the decision is made whether the autophagy machinery of the host that recognizes the damaged SCV membrane would either lead to degradation or to recovery.

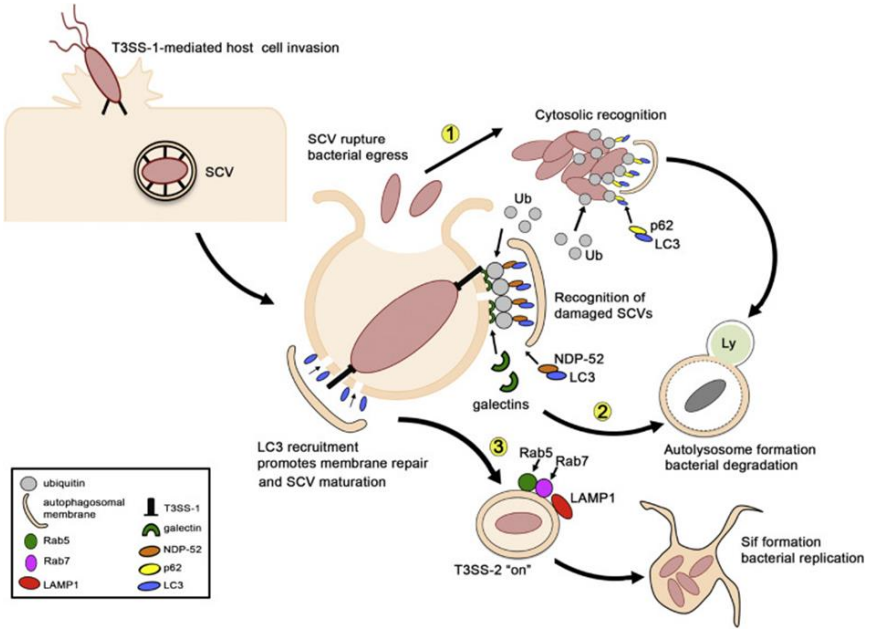


**Figure 8: Autophagy targets *Salmonella*.** After bacterial entry, *Salmonella* resides in a membrane bound compartment called the *Salmonella*-containing vacuole (SCV), docking early (Rab5, EEA1) and late (Rab7, Rab9, vATPase and LAMP1) endosomal markers. To invade a host cell, *Salmonella* secretes T3SS-1 effectors that form a pore in the host cell membrane which allow some bacteria to escape from the vacuole and enter the cytosol. (1) Antibacterial autophagy. Cytosolic salmonellae are ubiquitinated and became recognized by autophagy adapters including p62, nuclear dot protein (NDP52), and optineurin (OPTN). These adapters interact with LC3 to promote lysosomal killing of cytosolic bacteria. (2) Autophagy recognizes intracellular *Salmonella* in damaged vacuoles. In this case, carbohydrate modifications within the ruptured SCV are sensed by galectins, NDP-52, and recruit ubiquitin to the membrane, which subsequently activates the autophagy pathway leading to bacterial degradation. (3) Autophagic machinery repairs the damage of SCV mediated by T3SS-1 effectors. In contrast to antibacterial autophagy, *Salmonella* can manipulate the host autophagic system for its own benefit and to cause disease. SCV is saturated with autophagosome marker LC3 leading to the activation of the phagosomal repair pathway, followed by translocation of T3SS-2 effectors for SCV maturation process and SIF formation (Owen & Casanova, 2015).

### 1.10 WxxxE family

Work by the Alto group classify the WxxxE protein family composing of 24 bacterial effector proteins, including Map, EspM and EspT of EHEC/EPEC and the related *Citrobacter rodentium*, IpgB1 and IpgB2 of *Shigella* spp., and SifA and SifB of *Salmonella* spp. These distinct effectors harbor a common Trp-xxx-Glu (WxxxE) motif, comprising two invariant amino acids, tryptophan (W) and glutamic acid (E) (Alto et al., 2006). The best characterized member of this family is the T3SS effector protein Map that functions similar to a eukaryotic GEF for Cdc42, inducing the formation of filopodia during early stages of infection (Huang et al., 2009). Another WxxxE effector of the attaching and effacing (A/E) pathogen group, EspT, triggers cellular GTPases Rac and Cdc42, thereby inducing actin cytoskeleton rearrangements followed by the formation of membrane ruffles and lamellipodia (Raymond et al., 2011; Bulgin et al., 2009). The *Shigella* WxxxE effector IpgB1 induces the formation of membrane ruffles via activation of the Rho GTPase Rac1 and Cdc42, thereby facilitating *Shigella* invasion (Ohya et al., 2005). Furthermore, IpgB1 was reported to function as a bacterial GEF for Rac1 and Cdc42 (Huang et al., 2009). At the same time, IpgB2 stimulates formation of stress fibers by mimicking eukaryotic GEF-activity for RhoA (Klink et al., 2010).

The *Salmonella* WxxxE effector SifA comprises two domains. Via the N-terminal region, it binds to the C-terminal pleckstrin homology (PH) domain of a host protein SKIP (SifA and kinesin-interacting protein), whereas the C-terminal region of SifA consists of a canonical WxxxE-domain (Figure 9) (Diacovich et al., 2009; Jackson et al., 2008; Ohlson et al., 2008). This fold is highly similar to that of the *Salmonella* TTSS-1 effector SopE (Figure 9) (Buchwald et al., 2002).

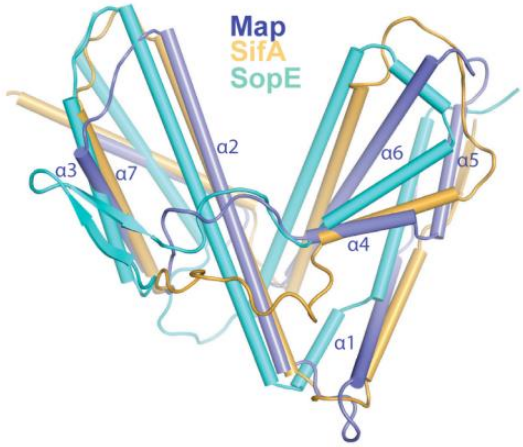


**Figure 9: Structural comparison of MAP, SifA, and SopE.** Superimposition of MAP (violet), SifA (gold) and SopE (turquoise). MAP, canonical bacterial GEF of the WxxxW family, targets Cdc42. The C-terminal region of SifA harbors a canonical WxxxE-domain. Salmonella SopE effector mimics eukaryotic GEFs by stimulation of Rho GTPases Cdc42 (Huang et al., 2009).

*Salmonella* proteins SopE and SopE2, which share 69% amino acid sequence identity, represent the second family of bacterial GEFs for Rho GTPases. SopE and SopE2 are shown to directly activate Rac1 and Cdc42 in a Dbl-like fashion, resulting in the formation of membrane ruffles (Friebel et al., 2001). Although SopE and SopE2 do not share sequence similarity with this Rho GEF family, these *Salmonella* effectors are able to mimic eukaryotic GEFs (Buchwald et al., 2002).

Strikingly, despite the lack of sequence homology between the two families of bacterial GEF-mimics, structure analysis of the WxxxE-family GEFs and of the *Salmonella* effectors SopE/E2 reveal that these effectors indeed share a common fold (Buchwald et al., 2002; Ohlson et al., 2008; Huang et al., 2009; Bulgin et al., 2010). This highlights the importance of efficient manipulation of Rho GTPases, because these bacteria independently invent such enzymes twice during co-evolution with their hosts. Noteworthy, *Salmonella* comprises bacterial GEFs of both families, namely SopE and -E2 as well as SifA and -B.

In this study, I focus on several members of the WxxxE group such as *Salmonella* SifA and SifB as well as EspT from EPEC and *Citrobacter rodentium*.

## 1.11 Aim of the study

Enteric Gram-negative pathogens utilize T3SS in order to export bacterial virulence proteins into host cells. These bacterial effector proteins modulate the host's actin cytoskeleton for the establishment of infection within or beyond the epithelial lining. The role of the secreted effectors during infection has been extensively studied in recent years. However, hitherto only a few host proteins have been discovered to directly interact with translocated virulence factors, most of them remaining unknown.

This study aims at defining host molecular targets of bacterial virulence factors, including SifA, SifB and EspT, and to understand how these bacterial virulence factors manipulate host cell signaling pathways.

In order to achieve this aim we have established the following tasks:

- validation of the Y2H hits using biochemical methods;

- mapping of interaction surfaces between a pair of proteins using deletion mutants and individual domain-based constructs in pull-down assays;

- investigation of subcellular localization and studies of co-localization of host and bacterial proteins;

- generation of somatic knockout cells using CRISPR-Cas approach;

- production of monoclonal antibodies against SifA and SifB;

- investigation of the role of potential interactions during long-term infection with a wild type and a mutant *Salmonella enterica* serovar Typhimurium using time-lapse microscopy.

# 2. MATERIAL

## 2.1 Chemicals

All used chemicals, reagents and solvents have been purchased from AppliChem GmbH (Darmstadt, Germany), Bio-Rad Laboratories GmbH (Munich, Germany), Fluka Chemie AG (Buchs, Switzerland), Macherey Nagel (Düren, Germany), Roche Diagnostics GmbH (Mannheim, Germany), Sigma-Aldrich Chemie GmbH (Munich, Germany), Thermo Fisher Scientific (Schwerte, Germany), Gibco by Life Technologies (Darmstadt, Germany), Polyplus transfection (New York, USA), Merck KGaA (Darmstadt, Germany), New England Biolabs (Ipswich, MA, USA) and Promega Corporation (Madison, WI, USA).

## 2.2 Plastic

Plastic ware has been purchased from Sarstedt (Nümbrecht, Germany).

## 2.3 Reagents

**Table 1: Commercial kits**

| Kit | Manufacturer |
|---|---|
| GeneJET Plasmid Miniprep Kit | Thermo Fisher Scientific, Schwerte, Germany |
| GeneJET Gel Extraction and DNA Cleanup | Thermo Fisher Scientific, Schwerte, Germany |
| Mix2Seq Kit | Eurofins Genomics GmbH (Ebersberg, Germany). |
| Pierce™ BCA Protein Assay Kit | Thermo Fisher Scientific, Schwerte, Germany |

**Table 2: DNA size markers**

| Marker | Fragment size, bp | Reference |
|---|---|---|
| Quick-Load 100 bp DNA Ladder | 1.517; 1.200; 1.000; 900; 800; 700; 600; 500; 400; 300; 200; 100 | New England Biolabs,Ipswich, MA, USA |
| Quick-Load 1 kb DNA Ladder | 10.000; 8.000; 6.000; 5.000; 4.000; 3.000; 2.000; 1.500; 1.000; 500 | New England Biolabs,Ipswich, MA, USA |

**Table 3: Protein size markers**

| Marker | Fragment size, kDa | Reference |
|---|---|---|
| Color Prestained Protein Standard, Broad Range | 245; 190; 135; 100; 80; 58; 46; 32; 25; 22; 17; 11 | New England Biolabs,Ipswich, MA, USA |
| PageRuler™ Prestained Protein Ladder | 180; 130; 100; 70; 55; 40; 35; 25; 15; 10 | Thermo Fisher Scientific, Schwerte, Germany |

**Table 4: Media and supplements for eukaryotic cell culture**

| Reagent | Description | Reference |
|---|---|---|
| DMEM (1X) | Dulbecco´s Modified Eagle Medium<br>[+] 4.5 g/L D-Glucose<br>[+] L-Glutamine<br>[-] Pyruvate | Gibco, Life Technologies, Darmstadt, Germany |
| Opti-MEM® (1X) | Opti-MEM® I Reduced-Serum Medium | Gibco,Life Technologies, Darmstadt, Germany |
| Trypsin-EDTA (1X) | Trypsin-EDTA (0.05%), phenol red | Gibco, Life Technologies, Darmstadt, Germany |
| L-Glutamine (100X) | 200mM L-Glutamine | Gibco,Life Technologies, Darmstadt, Germany |
| Pen Strep | Penicillin-Streptomycin (5,000 U/ml) | Gibco,Life Technologies, Darmstadt, Germany |
| FBS | Fetal bovine serum, sterile filtered | Sigma-Aldrich Chemie GmbH, Munich, Germany |
| Gentamicin solution | 10 mg/ml in deionized water, liquid, sterile filtered | Sigma-Aldrich Chemie GmbH, Munich, Germany |
| PBS | PBS tablets, Phosphate-Buffered Saline | Gibco, Life Technologies, Darmstadt, Germany |
| jetPRIME® | Transfection reagent | Polyplus transfection, New York, US |
| X-tremeGENE™ 9 | Transfection reagent | Roche, Mannheim, Germany |
| Fibronectin | Human plasma fibronectin | Roche, Mannheim, Germany |

## 2.4 Enzymes

**Table 5: Enzymes**

| Enzyme | Specific activity | Reference |
|---|---|---|
| Go Taq DNA polymerase | 5’ → 3’ DNA polymerase | Promega Corporation, Madison, WI, USA |
| Phusion DNA polymerase | 5’ → 3’ DNA polymerase Generates blunt-ended products | New England Biolabs,Ipswich, MA, USA |
| T4 DNA ligase | Formation of a phosphor-diester bond between 3’ and 5’-termini | New England Biolabs,Ipswich, MA, USA |
| **Restriction enzymes:** | | |
| *BamH1* | 5’-G^GATCC-3’ | Thermo Fisher Scientific, Schwerte, Germany |
| *BglII* | 5’-A^GATCT-3’ | Thermo Fisher Scientific, Schwerte, Germany |
| *SalI* | 5’-G^TCGAC-3’ | Thermo Fisher Scientific, Schwerte, Germany |
| *Eco47 III* | 5’-AGC^GCT-3’ | Thermo Fisher Scientific, Schwerte, Germany |
| *EcoRV* | 5’-GAT^ATC-3’ | Thermo Fisher Scientific, Schwerte, Germany |
| Bsp1407I | 5’-T^GTA CA-3' | Thermo Fisher Scientific, Schwerte, Germany |
| *BbsI* | 5’-GAAGACN2↓-3' | Thermo Fisher Scientific, Schwerte, Germany |
| Lysozyme from chicken egg white | Glycoside hydrolase | Sigma-Aldrich Chemie GmbH,Munich, Germany |
| Benzonase | Endonuclease | Merck KGaA, Darmstadt, Germany. |

## 2.5 Antibodies

**Table 6: Primary antibodies**

| Name | Target | mc/pc | Species | Reference | Application |
|---|---|---|---|---|---|
| 101G4B2 | GFP | mc | ms | Barbara Behrendt, HZI | WB |
| Ab290 | GFP | pc | rb | Abcam | WB |
| 9E10 | Myc | mc | ms | Commercial hybridoma, HZI | WB, IF |
| 9B11 | Myc | mc | ms | Cell Signaling | WB |
| | RFP | pc | rb | Jan Faix, MHH | WB |
| 5F8 | RFP | mc | rat | Chromotek | IF |
| HA | HA | mc | ms | Covance | WB |
| Y 1/2 | Tubulin | mc | rat | Jürgen Wehland, HZI | IF |
| 20C6 | Tubulin | pc | rb | | IF |
| ab24586 | Golgi | pc | rb | Abcam | IF |
| ab136044 | CLIP4 | pc | rb | Abcam | WB |
| HPA043366 | CLIP4 | pc | rb | Atlas | WB |
| 7H8/A10, 7H8/24 | SifA | mc | ms | TU Braunschweig,Sabine Buchmeier | WB |
| 7B10, 1G12 | SifB | mc | ms | TU Braunschweig,Sabine Buchmeier | WB |

Abbreviations: mc=monoclonal, pc=polyclonal, rb = rabbit, ms = mouse.

Antibodies were diluted according to manufacturer's instructions.

**Table 7: Secondary antibodies**

| Name | Description | Coupled to | Reference | Application |
|---|---|---|---|---|
| A4a | goat anti-mouse IgG & IgM (H+L) | HRPO | Dianova | WB 1:2000 |
| B4c | goat anti-rabbit IgG (H+L) | HRPO | Dianova | WB 1:2000 |
| A12c | goat anti mouse IgG (H+L) | Alexa Fluor™ 488 | Invitrogen | IF 1:100 |
| A13c | goat anti-mouse IgG (H+L) | Alexa Fluor™ 594 | Invitrogen | IF 1:100 |
| A16c | goat anti-mouse IgG (H+L) | Alexa Fuor™ 350 | Invitrogen | IF 1:100 |
| B12c | goat anti-rabbit IgG (H+L) | Alexa Fluor™ 488 | Invitrogen | IF 1:100 |
| B13c | goat anti-rabbit IgG (H+L) | Alexa Fuor™ 594 | Invitrogen | IF 1:100 |
| C13c | goat anti-rat IgG (H+L) | Alexa Fuor™ 594 | Invitrogen | IF 1:100 |

## 2.6 Fluorescent dyes

**Table 8: Fluorescent dyes**

| Name | Description | Reference | Application |
|---|---|---|---|
| DAPI | 4',6-diamidino-2-phenylindole | Invitrogen | IF 1:500 |
| PH12 | Phalloidin-Alexa 350 | Invitrogen | IF 1:100 |
| PH13 | Phalloidin-Alexa 594 | Invitrogen | IF 1:100 |

## 2.7 Oligonucleotide Primers

Designed oligonucleotide primers were synthesized by Eurofins Genomics GmbH (Ebersberg, Germany).All primers used in this study are listed in Table 9.

**Table 9: List of oligonucleotides**

| Oligonucleotide | Purpose | Sequence 5’ to 3’ |
|---|---|---|
| CLIP4Xba1fwdBamH1 | cloning | GGATCCATGCTTCTAGATGCGGTGCCTC |
| CLIP4M1252fwdBgl2 | cloning | AGATCTATGGATGTTGCCCTGCTTGGA |
| CLIP41228revSal1 | cloning | GTCGACTTTCTCTGTCACAGTTTTAAG |
| CLIP41849revSal1 | cloning | GTCGACCTTCACGCTCCCTTCAATG |
| pJET1.2 for | sequencing | CGACTCACTATAGGGAGAGCGGC |
| pJET1.2 rev | sequencing | AAGAACATCGATTTTCCATGGCAG |
| pEGFPC1for | sequencing | GATCACTCTCGGCATGGAC |
| pEGFPC1rev | sequencing | CATTTTATGTTTCAGGTTCAGGG |
| pGex for | sequencing | ATAGCATGGCCTTTGCAGG |
| pGex rev | sequencing | GAGCTGCATGTGTCAGAGG |

## 2.8 Plasmids

**Table 10: Plasmids**

| Plasmid | AR | Function | Source |
|---|---|---|---|
| pEGFP-C1 | kana | GFP-tagged expression vector | Clontech |
| pEGFP C1–APPL1 | kana | Transfection, IF, Pull down assay | this group |
| pEGFP C1-DYNLRB1 | kana | Transfection, IF, Pull down assay | this group |
| pEGFP C1-Cep70 | kana | Transfection, IF, Pull down assay | this group |
| pEGFP C1-CLIP4 | kana | Transfection, IF, Pull down assay | this group |
| pEGFP C1-CLIP4 ΔANK | kana | Transfection, IF, Pull down assay | this group |
| pEGFP C1-CLIP4 ΔCAP-Gly | kana | Transfection, IF, Pull down assay | this group |
| pEGFP C1 CLIP4 (1CAP-Gly) | kana | Transfection, IF, Pull down assay | this dissertation |
| pEGFP-CLIP4 (1+2 CAP-Gly) | kana | Transfection, IF, Pull down assay | this dissertation |
| pEGFP-CLIP4 (2 CAP-Gly) | kana | Transfection, IF, Pull down assay | this dissertation |
| pEGFP-CLIP4 (2+3 CAP-Gly) | kana | Transfection, IF, Pull down assay | this dissertation |
| pCB6-GFP-CLIPR5926R | amp | Transfection, IF, Pull down assay | Franck Perez, Severine Divoux |
| pCB6-GFP-CLIPR59AA | amp | Transfection, IF, Pull down assay | Institut Curie, Paris |
| pEGFP C2-CLIP115 CAP-Gly | kana | Transfection, Pull down assay | Marco Van Ham, HZI |
| pEGFP C2-CLIP170 CAP-Gly | kana | Transfection, Pull down assay | Marco Van Ham, HZI |
| pmCherry C1 | kana | RFP-tagged expression vector | Clontech |
| pmCherry C1-CLIP4 | kana | Transfection, IF | this dissertation |
| pETM-41 | kana | Protein expression vector | EMBL |
| pETM-41-SifA Δext | kana | Protein expression | this group |
| pETM-41-SifB Δext | kana | Protein expression | this group |
| pEGFP-C1-SifA Δext | kana | Transfection, IF | this group |
| pEGFP-C1-SifB Δ ext | kana | Transfection, IF | this group |
| pRK5-myc-SifB | amp | Transfection, IF | this dissertation |
| pSpCas9(BB)-2A-GFP | amp | cloning | Addgene |

Abbreviations: AR = encoded antibiotic resistance for selection in bacteria;

amp = ampicillin; kana = kanamycin; IF=immunofluorescence.

## 2.9 Cell lines and cell culture media

**Table 11: List of cell lines**

| Cell line | Description |
|---|---|
| B16-F1 | Mouse melanoma fibroblasts |
| NIH/3T3 | Mouse embryonic fibroblasts |
| Hek 293T | Human epithelial embryonic kidney cells |
| HeLa | Human epithelial carcinoma cells |
| A431 | Human epithelial carcinoma cells |
| Cos-7 | African green monkey kidney fibroblasts |
| HeLa-LAMP1-GFP | Epithelial carcinoma |

**Table 12: Cell culture media for B16-F1, NIH/3T3, Cos-7, HeLa and A431 cell lines**

| Components | |
|---|---|
| DMEM | |
| [+] 4.5 g/L D-Glucose | |
| [+] L-Glutamine | |
| [-] Pyruvate | |
| FBS | 10% (v/v) |
| Pen Strep | 1% (v/v) |
| L-Glutamine | 2mM Glutamine |

## 2.10 Microorganisms and bacterial growth media

**Table 13: List of microorganisms**

| Microorganism | Characteristics |
|---|---|
| *E.coli* DH5α | fhuA2 Δ(argF-lacZ)U169 phoA glnV44 Φ80 Δ(lacZ)M15 gyrA96 recA1 relA1 endA1 thi-1 hsdR17 (Invitrogen) |
| *E.coli* BL21 (DE3) | fhuA2 [lon] ompT gal (λ DE3) [dcm] ΔhsdS λ DE3 = λ sBamHIo ΔEcoRI-B int::(lacI::PlacUV5::T7 gene1) i21 Δnin5 (Invitrogen) |
| *Salmonella enterica* serovar Typhimurium SL1344 | |
| *Salmonella enterica* serovar TyphimuriumMvP389 | ΔsifB::FRT (Prof.Dr. Michael Hensel) |
| *Salmonella enterica* serovar Typhimurium MvP503 | ΔsifA::FRT (Prof.Dr. Michael Hensel) |

**Tabel 14: Bacterial growth media**

| LB medium ("Luria Bertani broth") | |
|---|---|
| Trypton | 10 g/l |
| Yeast extract | 5 g/l |
| NaCl | 7.5 g/l |

**Table 15: Supplements for bacterial growth media**

| Supplement | Stock solution | Working concentration |
|---|---|---|
| Ampicillin | 100 mg/ml, sterile filtered | 100 µg/ml |
| Kanamycin | 30 mg/ml, sterile filtered | 30 µg/ml |
| Gentamicin | 10 mg/ml | 100 µg/ml |
| Glucose | 1 M, sterile filtered | 2 g/l |
| Isopropyl-ß-D-thiogalactopyranoside (IPTG) | 1 M, sterile filtered | 0.5 mM |

# 3. METHODS

## 3.1. Molecular biological methods

### 3.1.1. LB agar plates

LB agar plates were poured under sterile conditions from an autoclaved LB agar stock (0.4% (w/v) agar in LB medium). Appropriate antibiotics were added to the solution once it cooled down to about 55°C. Approximately 20 ml of LB agar solution were required per Ø100 mm polystyrene Petri dish.

### 3.1.2. Storage of bacterial strains

For daily use, bacterial working stocks were streaked onto agar plates, incubated up-side-down overnight at 37ºC and stored at 4°C for several weeks. For long-term storage, glycerol stocks were prepared. To do so, bacterial cultures were supplemented with an appropriate volume of glycerol 10% (v/v) during exponential growth phase and then snap-frozen and stored at -80°C.

### 3.1.3. Polymerase chain reaction (PCR)

In order to successfully amplify the region of interest in a DNA sequence, specific PCR primers were designed (Mullis et al., 1986). All reaction components were mixed on ice and then quickly transferred to a thermocycler preheated to the denaturation temperature (95°C). Basic reaction components are listed in Table 16.

**Table 16: Basic reaction mixture for PCR**

| Component | Final Volume | Final Concentration |
|---|---|---|
| Nuclease-Free $H_2O$ | 33 µl | |
| 5xPhusion HF or GC Buffer | 10 µl | 1X |
| 10 mM dNTPs | 1 µl | 200 µM |
| 10 µM Forward Primer | 2.5 µl | 0.5 µM |
| 10 µM Reverse Primer | 2.5 µl | 0.5 µM |
| Template DNA | 0.5 µl | 0.5µg |
| Phusion DNA Polymerase | 0.5 µl | 1.0 units/ 50µl PCR |

The standard program used for PCRs is described in Table 17.

**Table 17: Thermocycling conditions for a routine PCR**

| Step | Temperature | Time | Number of Cycles |
|---|---|---|---|
| Initial Denaturation | 95°C | 2 min | 1X |
| Denaturation | 95°C | 20 sec | 20 X |
| Annealing | 55°C | 1 min | |
| Extension | 72°C | 1 min | |
| Final Extension | 72°C | 10 min | 1 X |

Desired PCR products were detected via agarose gel electrophoresis and purified with GeneJET Gel Extraction and DNA Cleanup kit (Thermo Fisher Scientific, Schwerte, Germany).

### 3.1.4. Agarose gel electrophoresis

Agarose gel electrophoresis was applied for effective separation of DNA fragments according to their size. The gel was prepared by dissolving agarose powder in heated 1xTAE buffer. The solution was then poured into a gel chamber. For detection of DNA fragments in the gel, 5 µl of Midori Green (Biozym, # 617004) were added to 100 ml of agarose gel after the solution cooled to ~60°C. The appropriate DNA ladder and DNA samples were mixed with Fast digest loading buffer (Thermo Fisher Scientific, Schwerte, Germany) before they were loaded onto the gel. The electrophoresis was executed at 80-150 V. DNA fragments were detected by using a strong UV light source and documented using Gel Image (Intas). Desired DNA fragments were excised from the gel for further purification using GeneJET Gel Extraction and DNA Cleanup Kits (Thermo Fisher Scientific, Schwerte, Germany). TAE buffer was prepared as described in Table 18.

**Tabel 18: TAE buffer**

| Stock solution | |
|---|---|
| 2 M | Tris base |
| 1 M | Acetic acid |
| 50 mM | EDTA |

### 3.1.5. Plasmid DNA extraction and purification

Isolation and purification of high quality plasmid DNA from recombinant *E.coli* cultures was carried out by using the GeneJET Plasmid Midiprep Kit (Thermo Fisher Scientific, Schwerte, Germany) according to the manufacturer's instructions.

### 3.1.6. DNA gel extraction and purification

DNA was fragmented in an agarose gel and the desired band was excised from the gel with a scalpel. Excised DNA was purified by removing the agarose with the GeneJET Gel Extraction and DNA Cleanup Kit (Thermo Fisher Scientific, Schwerte, Germany) according to the manufacturer's instructions.

### 3.1.7. DNA digestion with restriction enzyme

Plasmid vector and insert were cleaved with suitable restriction enzymes to create blunt-ended DNA fragments. Digestion reactions were performed according to the setup listed in Table 19.

**Table 19: Digestion reaction**

| Stock solution | Amount |
|---|---|
| DNA | 5 µl |
| H2O | 3 µl |
| 10X Fast Digest Buffer | 1 µl |
| Fast Digest Enzyme | 1 µl |

The reaction mixture was incubated at 37°C in a heat block for at least 20 min. Afterwards, the digestion products were separated using agarose gel electrophoresis and subsequently purified.

### 3.1.8. Dephosphorylation of linearized vectors

To avoid self-ligation of a vector and therefore reduce the amount of false-positive clones, the plasmid was dephosphorylated. Dephosphorylation of the cleaved vector was accomplished using Antarctic phosphatase (New England Biolabs, Ipswich, MA, USA) in 1x Antarctic phosphatase reaction buffer. The reaction mixture was incubated at 37°C for 15 min and

inactivated by heating at 70°C for 5 min. The dephosphorylated vector and the insert were separated in an agarose gel, purified and subjected to ligation.

### 3.1.9. Ligation of DNA fragment and vector

Ligation was the final step in the construction of a recombinant plasmid. This approach allowed the integration of an insert DNA into a compatibly cleaved vector backbone. Ligation was performed according to the setup listed in Table 20.

**Tabel 20: Ligation reaction**

| Stock solution | Amount |
|---|---|
| Vector | 1 µl |
| Insert | 7 µl |
| 10X T4 DNA Ligase Buffer | 1 µl |
| T4 DNA Ligase | 1 µl |

Ligation reactions were performed overnight at 16°C in a sterile PCR tube. Upon completion of the reaction, 5 µl of the ligated DNA were used to transform electro-competent *E. coli* DH5α. Transformed bacteria were then plated on LB agar containing the appropriate antibiotic. Positive clones were selected by means of digestion analysis of plasmid DNA and finally verified by sequencing.

### 3.1.10. Generation of electrocompetent *E.coli*

*E.coli* DH5α were streaked on LB plates and grown overnight at 37°C. The next day a single colony was used to inoculate 3-5ml of LB medium. This culture was again incubated at 37°C overnight and subsequently diluted 1:100 - 1:500 in 0.5-1 L of LB medium. The resulting culture was grown for approximately 18 h at room temperature with agitation (1000 rpm) until the optical density (OD600nm) reached 0.6-1. Afterwards, the cell suspension was chilled on ice for at least 15 min and bacteria were harvested by centrifugation at 8000 rpm and 4°C for 10 min (JA-10 rotor, Beckman Avanti J-25 centrifuge). The cell pellet was resuspended in 200 ml of cold sterile water. This washing procedure was repeated 3 times. Finally, the pelleted cells were resuspended by gentle pipetting in 3-6 ml ice-cold 15% (v/v)

glycerol and aliquoted into individual pre-chilled microfuge tubes. The aliquots were then snap-frozen in liquid nitrogen and stored at -80°C.

### 3.1.11. Transformation of electro-competent *E.coli*

A 50 µl aliquot of electro-competent bacterial cells was thawed on ice and mixed by pipetting with 1 µg of salt-free plasmid DNA. This mixture was then transferred to a pre-chilled electroporation cuvette, and the cells were subjected to electroporation (Gene Pulser® II Electroporation System, BIO-RAD) according to the manufacturer's instructions. Immediately after the pulse, 1 ml of room temperature LB medium was added, and the cells were allowed to recover at 37°C for 1 h in a shaker. Bacteria were then pelleted (12000 rpm, 1min, Centrifuge 5427R from Eppendorf) and resuspended in 50-100µl of LB medium. Finally, the cells were plated on a pre-warmed LB-agar plate containing the appropriate antibiotic incubated up-side-down overnight at 37ºC.

### 3.1.12. DNA Quantification

A DS-11 Spectrophotometer (DeNovix Inc., Wilmington, DE USA) was used to quantify nucleic acid samples based upon their absorbance value at 260 nm.

### 3.1.13. DNA sequencing

DNA sequencing was carried out by Eurofins Genomics GmbH (Ebersberg, Germany). The sequences were analyzed using the Basic Local Alignment Search Tool (BLAST, http://blast.ncbi.nlm.nih.gov/Blast.cgi) and the free software ApE, a plasmid editor (http://biologylabs.utah.edu/jorgensen/wayned/ape/).

## 3.2. Cell biological methods

### 3.2.1. Culture of eukaryotic cells

For sterile conditions, subculturing of eukaryotic cell lines took place under a laminar-flow hood (Maxisafe 2020, Thermo Scientific, Langenselbold, Germany). Cells were maintained in appropriate medium in a sterile Ø100 mm dish. Upon reaching confluency, the cell monolayer was washed twice with room temperature PBS, covered with pre-warmed Trypsin (0.05 %) and incubated at 37°C until cells detached. Next, the cells were resuspended in pre-warmed medium and centrifuged at room temperature (5 min, 1000 rpm, Centrifuge 5804 R from Eppendorf). Finally the cell pellet was resuspended in complete growth medium and cells were seeded at a dilution of 1/5 or/and 1/10. Cell lines were subcultured up to 3 months and then a new cryovial of cells was thawed.

### 3.2.2. Thawing of cryoconserved eukaryotic cells

A cryovial of frozen cells was thawed rapidly in a water bath at 37°C for max. 1 min. The freezing medium was diluted slowly by adding pre-warmed growth medium. Cells were pelleted (5 min, 1000 rpm, Centrifuge 5804 R from Eppendorf) and finally resuspended in a proper volume of growth medium. Thawed cells were seeded into sterile Ø100 mm dishes. The growth of eukaryotic cells was controlled under the light microscope.

### 3.2.3. Freezing and storage of eukaryotic cells

For long-term storage, eukaryotic cells were expanded and then cryopreserved as early as possible. Cells were frozen slowly by reducing the temperature by approximately 1°C per minute using a cryo-freezing container (CoolCell® Cryopreservation Alcohol-Free Cell Freezing Containers, BioCision®, USA). The freezing medium contained 10% DMSO as a cryoprotective agent. The next day, cryovials were transferred to liquid nitrogen and stored in the gas phase.

### 3.2.4. Transfection of Eukaryotic Cells

The transfer of nucleic acids (DNA or RNA) into living cells has been referred to as transfection. Cells that had been seeded the day before were transfected at a stage of 60-80% confluency. Transfections with the commercial lipid-based agents jetPRIME® (Polyplus-transfection, New York, US) or X-tremeGENE™ 9 (Roche, Mannheim, Germany) were carried out according to the manufacturer's recommendations.

Briefly, X amount of plasmid DNA were diluted in W volume of buffer, then Y volume of transfection reagent was added to the mixture (Table 21 and Table 22). This master mix was vortexed for 10 s and spun down, incubated for 10 min at room temperature and added to the cells. Rocking the plate back and forth allowed gentle mixing of the components.

**Table 21: DNA transfection using jetPRIME®**

| Culture vessel | **W** volume of jetPRIME® buffer | **X** amount of DNA added | **Y** volume of jetPRIME® reagent |
|---|---|---|---|
| 24-well | 50 µl | 0.5 µg | 1µl |
| 6-well/35mm | 200 µl | 2 µg | 4 µl |
| 100 mm | 500 µl | 10 µg | 20 µl |

**Table 22: DNA transfection using X-tremeGENE™ 9**

| Culture vessel | **W** volume of Opti-MEM® | **X** amount of DNA added | **Y** volume of X-tremeGENE™ 9 reagent |
|---|---|---|---|
| 24-well | 50 µl | 0.25 µg | 0.75 µl |
| 6-well/35mm | 200 µl | 1 µg | 3 µl |
| 100 mm | 500 µl | 5 µg | 15 µl |

## 3.3. Biochemical Methods

### 3.3.1. Bradford-Test

Protein concentration was determined via Bradford assay (Bradford, 1976). First, several dilutions of a protein standard (BSA) in a range of 2 to 10 µg protein were prepared as described in Table 23.

**Table 23: Bradford assay set up**

| | BSA concentration | | | | | |
|---|---|---|---|---|---|---|
| Stock solution | Blank | 2 µg/µl | 4 µg/µl | 6 µg/µl | 8 µg/µl | 10 µg/µl |
| H2O | 800 µl | 798 µl | 796 µl | 794 µl | 792 µl | 790 µl |
| BSA/Protein | 0 | 2 µl | 4 µl | 6 µl | 8 µl | 10 µl |
| Bradford | 200 µl | 200 µl | 200 µl | 200 µl | 200 µl | 200 µl |

Standard solution and samples were transferred into new test tubes and incubated with the Bradford solution, as shown in Table 23, for 15 min. Next, 200µl of each standard or sample were placed in a 96 well microplate in duplicates. The absorbance was measured at 595 nm on a plate reader (VICTOR™ X 5 Multilabel Plate Reader, Perkin Elmer™, USA). Microsoft Excel software was used to create a correlation curve and determine the protein concentration of the sample.

### 3.3.2. Sodium dodecyl sulfate polyacrylamide gel electrophoresis (SDS-PAGE)

For the best resolution of respective proteins, 7.5%-15% SDS- polyacrylamide gels were prepared by using the Mini PROTEAN® 3 System (BIO-RAD, Munich, Germany) (Laemmli, 1970). First, the resolving gel mixture was prepared as listed in Table 24, poured between two clean glass plates and left to polymerize. To avoid bubbles and for the even edge of the resolving gel, isopropanol was added. After 30 min, isopropanol was discarded and the stacking gel was poured as listed in Table 25. Gels were used directly or stored wrapped in wet tissue paper in a plastic bag at 4°C. Equal amounts of protein were loaded onto SDS-PAGE gels along with prestained protein ladder. Afterwards, the gel was subjected to an electric field of 100 V for 2 h or 200 V for 1 h.

**Table 24: SDS-PAGE mixture for two resolving mini-gels**

| Stock solution | 7.5% | 10% | 12% | 15% |
|---|---|---|---|---|
| 30% Acrylamide/ 0.8% Bisacrylamide (37.5:1) | 4.6 ml | 6.6 ml | 8 ml | 10 ml |
| 1.5M Tris pH 8.8 | 5 ml | 5 ml | 5 ml | 5 ml |
| $H_2O$ | 10.2 ml | 8.2 ml | 6.8 ml | 4.8 ml |
| 10%w/v SDS | 200 µl | 200 µl | 200 µl | 200 µl |
| 10% w/v APS | 100 µl | 100 µl | 100 µl | 100 µl |
| TEMED | 10 µl | 10 µl | 10 µl | 10 µl |

**Table 25: SDS-PAGE mixture for two stacking mini-gels**

| Stock solution | |
|---|---|
| 30% Acrylamide/ 0.8% Bisacrylamide (37.5:1) | 650 µl |
| 0.5M Tris pH 6.8 | 1.25 ml |
| H2O | 3.05 ml |
| 10% w/v SDS | 50 µl |
| 10% w/v APS | 25 µl |
| TEMED | 5 µl |

**Table 26: SDS running buffer**

| Stock solution | |
|---|---|
| 25 mM | Tris base |
| 192 mM | Glycine |
| 0.1 % (v/v) | SDS |

### 3.3.3. Protein staining with Coomassie

To visualize proteins separated by gel electrophoresis, SDS gels were stained by soaking in the Coomassie Brilliant Blue R-250 solution (Table 27). After one hour of incubation gels were incubated in destaining solution to reduce background (Table 28). Finally, the gel was washed in $H_2O_{dd}$ and documented using a scanner (HP Scanjet G2710).The Adobe® Photoshop CS6 Extended software was used to analyze the stained proteins.

**Table27: Coomassie Brilliant Blue solution**

| Stock solution | % |
|---|---|
| Coomassie R-250 | 0.1% (w/v) |
| Acetic Acid | 10% (v/v) |
| Methanol | 25% (v/v) |
| H2Odd | 65% (v/v) |

**Table28: Coomassie destaining solution**

| Stock solution | % |
|---|---|
| Acetic Acid | 10% (v/v) |
| Methanol | 40% (v/v) |
| H2Odd | 50% (v/v) |

### 3.3.4. Expression of recombinant proteins

For high-level protein production, the recombinant plasmid was introduced into electro-competent *E.coli* BL21 (DE3) and the transformants were selected on agar plates containing the respective antibiotic. To prepare a pre-culture, 50 ml of LB medium supplemented with the appropriate antibiotic were inoculated with a single colony and cultured overnight at 37°C. The next morning bacteria were diluted 1:10 in 500 ml LB medium supplemented with 2 g/l glucose and the antibiotic, and grown at 37°C to an OD600 of 0.5-0.8. Expression of the recombinant protein was induced with 0.5 mM isopropyl β-D-1-thiogalactopyranoside (IPTG) overnight at 20°C. Next, the bacterial culture was harvested by centrifugation at 6000 rpm for 20 min at 4°C (JA-10 rotor, Beckman Avanti J-25 centrifuge) and resuspended in 10 ml of ice cold lysis buffer supplemented with a spatula tip of lysozyme (Table 29). The suspension was incubated at 4°C with rotary agitation for 15 min. The cells were disrupted by ultrasonic treatment on ice (5 pulses, 30 sec each, with 1 min pause between each round of sonification, Branson Sonifer 250); cell debris was removed by centrifugation at 14000 rpm for 30 min at 4°C (JA-17 rotor, Beckman Avanti J-25 centrifuge). Meanwhile, 500 µl of Ni-NTA agarose beads (Qiagen, Hilden, Germany) were loaded onto a PD10 plastic column and equilibrated with two column volumes of wash buffer (Table 30). Afterwards, the bacterial supernatant was mixed with the beads and incubated overnight at 4°C on a rotary wheel. Next, beads were washed with 100 ml of washing buffer containing 20 mM Imidazole to remove unbound components and resuspended in 2 ml resuspension buffer. The aliquots of the immobilized protein were frozen in liquid nitrogen and stored at −80°C. To confirm the expression of the fusion protein, sodium dodecyl sulfate polyacrylamide gel electrophoresis (SDS-PAGE) was applied. After every purification step, samples were taken and prepared for SDS-PAGE. For that purpose, the samples were mixed with 4xSDS PAGE sample buffer, boiled for 5 min at 95°C and loaded on a gel. Using Coomassie staining, the size of the protein as well as the intensity of the bands and the purity of the samples could be checked.

**Table29: Lysis buffer (10 ml)**

| Stock solution | |
|---|---|
| 50 mM | $NaH_2PO_4$ |
| 300 mM | NaCl |
| 10 mM | Imidazol |
| set pH 8.0 using NaOH | |
| 10 mM | β-Mercaptoethanol |
| 1 µl | Benzonase |
| 1x Protease inhibitor cocktail EDTA free | |
| Spatula tip of lysozyme | |

**Table30: Washing buffer**

| Stock solution | |
|---|---|
| 50 mM | $NaH_2PO_4$ |
| 300 mM | NaCl |
| 20 mM | Imidazol |
| set pH 8.0 using NaOH | |
| 0.05% (v/v) | Triton X-100 |

### 3.3.5. Pull-down Assay

One method to determine the physical interaction between two or more proteins was the pull-down assay. The minimal requirements for this technique were purified recombinant fusion-tagged protein (the bait) and a protein-binding partner (the prey). One day prior to the experiment, HEK293T or B16-F1 cells were transfected with the plasmid of interest and incubated overnight under normal cell culture conditions. The next day, the cells were washed twice with PBS on ice, lysed in 500 µl of ice-cold IP buffer (Table 32) and removed from the plate using a cell scraper. The lysed cells were incubated on ice for 15 min and centrifuged at 4°C (15 min, 12000 rpm, Centrifuge 5427R from Eppendorf) to pellet the cellular debris. 50µl of the supernatant were taken as a loading control. Immobilized His-MBP-beads bound to prey protein were rotated on a rocking platform at 4°C for 2 h. Next, this complex was centrifuged at 4°C (500xg, 5 min, Centrifuge 5427R from Eppendorf) and the supernatant was discarded. Beads were collected by brief centrifugation and washed three times in ice cold IP-buffer containing 1 % Triton X-100 but no protease inhibitor. Washed beads were resuspended in 4x SDS PAGE sample buffer (Table 31), boiled for 5 min at 95°C and loaded on a gel. Results of Pull-down assays were verified by Western blotanalysis.

**Table 31: 4x SDS sample buffer**

| Stock solution | |
|---|---|
| 25 mM | Tris pH 6.8 (HCl) |
| 29 % (v/v) | Glycerin |
| 3.3 % (v/v) | SDS |
| 3.3 % (v/v) | 2-Mercaptoethanol |
| 0.17 % (w/v) | Bromphenolblue |

**Table 32: IP-Buffers**

| **IP buffer „A“ standard** | |
|---|---|
| Stock solution | |
| 15 mM | KCl |
| 50 mM | NaCl |
| 8 mM | Tris, free base |
| 12 mM | Hepes, free base |
| 5 mM | MgCl2 |
| Added freshly before use: | |
| 1x Protease inhibitor cocktail EDTA free | |
| 1% (v/v) | Triton X 100 |

| **IP-Buffer „B“ ‘lipid friendly’** | |
|---|---|
| Stock solution | |
| 15 mM | KCl |
| 50 mM | NaCl |
| 8 mM | Tris, free base |
| 12 mM | Hepes, free base |
| 5 mM | MgCl2 |
| Added freshly before use: | |
| 1x Protease inhibitor cocktail EDTA free | |
| ultrasonic treatment on ice (5 pulses, 30 sec each, Branson Sonifer 250 | |

| **IP-Buffer „C“** | |
|---|---|
| Stock solution | |
| 15 mM | KCl |
| 50 mM | NaCl |
| 8 mM | Tris, free base |
| 12 mM | Hepes, free base |
| 1mM | EDTA |
| Added freshly before use: | |
| 1x Protease inhibitor cocktail EDTA free | |
| 1% (v/v) | Triton X 100 |

| **IP-Buffer „D“** | |
|---|---|
| Stock solution | |
| 30 mM | KCl |
| 150 mM | NaCl |
| 8 mM | Tris, free base |
| 12 mM | Hepes, free base |
| 5 mM | MgCl2 |
| Added freshly before use: | |
| 1x Protease inhibitor cocktail EDTA free | |
| 1% (v/v) | Triton X 100 |

## 3.4. Immunological methods

### 3.4.1. Generation of monoclonal antibodies

For the generation of monoclonal anti-SifA and anti-SifB antibodies, HisMBP-SifA and SifB were expressed and purified by pull down assays as described in 3.3.5. To concentrate samples for immunization of mice, the ultrafiltration concentrators Vivaspin®6 PES membranes (Viva Products) with a cutoff of 10.000 Da were used. The subsequent immunization of a mouse with the protein of interest was done at the Antibody Facility of the TU Braunschweig by Sabine Buchmeier.

### 3.4.2. Immunofluorescence microscopy

#### 3.4.2.1. Preparation of coverslips

At first, coverslips (Ø12 mm or 15 mm) were soaked in a mixture of 60% ethanol (v/v) and 40% hydrochloric acid (v/v) for at least 30 min, repeatedly washed with $H_2O_{dd}$ at room temperature and then dried and autoclaved. Next, sterilized coverslips were carefully placed into the wells of a microplate. Afterward, the coverslips were coated with fibronectin (1 mg/ml in 2 M urea, Roche, Mannheim, Germany) to promote adhesion of cells to the glass surface, and incubated for 1 h at room temperature. After three washing steps with PBS, the cells were seeded in an appropriate growth medium onto the coated coverslips and incubated in normal cell culture conditions. Cells were fixed the next day.

#### 3.4.2.2. Fixation of samples

In order to detect intracellular antigens, cells were previously fixed with pre-warmed 4% (w/v) paraformaldehyde (PFA) in PBS at 37°C for 20 min. Afterwards, cells were permeabilized with 0.1% Triton X-100 in PBS at room temperature for up to 1 min. Finally, the permeabilized cells were washed several times with PBS.

### 3.4.2.3. Immunofluorescence staining

To avoid non-specific staining, coverslips were incubated for 1 h at room temperature in blocking solution (5% horse serum in PBS containing 1% BSA). After several washing steps with PBS, coverslips were placed upside down on a 15 µl drop of diluted primary antibody in PBS containing 1% BSA and incubated for 1 h. The washing procedure was repeated and samples were then incubated with the respective secondary antibody in PBS containing 1% BSA, supplemented with Phalloidin and/or Dapi (4',6-diamidino-2-phenylindole) if required. At this step, in order to protect the fluorescent dyes from light, coverslips were incubated for 1 h in the dark and then washed three times with PBS. One drop of Mowiol or ProLong®Gold antifade reagent (Thermo Scientific, Schwerte, Germany) was dispensed onto a glass slide and coverslips were carefully mounted upside-down with the cells facing the glass slide. Finally, the samples were dried at room temperature for 1 h and then stored in a slide box at 4°C.

### 3.4.2.4. Image acquisition

Imaging studies were done using an inverted microscope (Axiovert 135TV, Zeiss) equipped for epifluorescence and phase-contrast microscopy. Image acquisition was performed using a 63X objective Plan-Neofluar (Carl Zeiss) equipped with an HXP 120 lamp (Kubler) for epifluorescence illumination; the refraction index of the employed immersion oil (Carl Zeiss) was 1.518. Images were acquired with a back-illuminated, cooled charge-coupled-device (CCD) Coolsnap-K4 camera (Photometrics) driven by Metamorph software (Molecular Devices Corp.). Primary images were stored as a TIFF format and refined using ImageJ, Adobe® Photoshop CS6 Extended software, Metamorph.

### 3.4.2.5. Time-lapse microscopy

The time-lapse experiments were carried out at the Nikon BioStation IM which provides consistent environmental control of temperature, humidity and gas concentration in combination with phase and fluorescence imaging.

To study formation and dynamics of SIFs during infection with WT and mutant *Salmonella* strains, HeLa cells constitutively expressing LAMP1-GFP were used. These cells were plated on a µ-dish $^{35mm,\ high}$ glass bottom (Ibidi) 24 hours before the experiment to obtain 80%

confluency at the time of transfection. The next day, HeLa cells were transfected as described in chapter 3.2.4. To visualize CLIP4 for live cell imaging, transfection with the pmCherry-C1 plasmid was performed. The next morning, transfection efficiency was determined by using EVOS fluorescence microscopy with red and green channels. Hereafter, infection with various *Salmonell*a strains was performed as described in the chapter 'Bacterial infection'. The time-lapse microscopy was carried out 2 h post infection with *Salmonella* WT or mutant strains defective in single effector. The interval between recording images was 5-10 min for the duration of 8-12 h.Image data were analyzed by the following software: ImageJ, Adobe® Photoshop CS6 Extended software and Metamorph.

### 3.4.3. Western blotting

Western blotting allowed for identification of specific proteins from a complex protein mixture which have been separated by SDS-PAGE. The Thermo Scientific™ Pierce™ G2 Fast Blotter (Thermo Fisher Scientific, Schwerte, Germany) was employed to transfer proteins onto a membrane. First, sheets of Whatman paper and PVDF membrane were equilibrated in Pierce 1-Step Transfer Buffer for a minimum of 5 min. Prior to equilibration, the PVDF membrane was activated with methanol. Afterwards, the transfer stack was assembled as follows: one sheet of ~1.5 mm thick Whatman paper on the bottom (anode), followed by membrane, gel and one sheet of ~1.5 mm thick Whatman paper on top. The blot roller was used to remove any trapped air bubbles. Then an appropriate fast-blotting program was chosen for transfer. The successful transfer of proteins onto the membrane was confirmed by soaking in the Ponceau S solution before the blocking step. The membrane was blocked in 10% (w/v) milk powder in TBS-T for 30 min at room temperature and incubated with primary antibody at 4°C overnight on a shaker. On the following day, the blot was washed three times in TBS-T before it was incubated with a secondary antibody conjugated with horseradish peroxidase (PO) for 1 h at room temperature on a shaker. Afterwards, the blot was washed again three times in TBS-T and one time in $H_2O_{dd}$.Finally LumiLight Western Blotting Substrate (Roche, Mannheim, Germany) was added to the membrane. The exposure rate of the membrane in Intas ECL Chemocam Imager lasted from 5 seconds to 30 minutes. Finally, analysis of protein bands was carried out using the Adobe® Photoshop CS6.

**Table 33: TBS(-T)**

| Stock solution | |
|---|---|
| 0.2 M | Tris base |
| 1.37 M | NaCl |
| set pH 7.6 using HCl | |
| 0.1% (v/v) | Tween 20 |

**Table 34: Ponceau S solution**

| Stock solution | |
|---|---|
| 5 g | Ponceau-S |
| 0.4% (v/v) | Methanol |
| 15 % (v/v) | Acetic acid |

### 3.5. Bacterial infections

For infection assays, cells were maintained in antibiotic-free growth medium. Overnight bacterial cultures were diluted 1:100 in 5 ml LB medium and grown at 37°C to an OD600 of 0.5-0.8. Before infection, bacteria were harvested by centrifugation at 12000 rpm for 3 min (Heraeus™ Pico™ Micro centrifuge Thermo Fisher Scientific, Schwerte, Germany), washed once in the sterile PBS, and diluted 1:100 in antibiotic-free tissue culture medium.Cells were infected at a multiplicity of infection (MOI) of 50. After inoculation, the plates were centrifuged (5min at 2000 rpm in Centrifuge 5810 from Eppendorf) to initiate contact between bacteria and epithelial cells. 20 min after infection (37°C, 5 % $CO_2$ in Nuaire incubator NU-5800E,Tecnomara GmbH, Fernwald, Germany) cells were washed several times with antibiotic-free tissue culture medium and incubated for 1 h in medium containing 100 µg/ml gentamycin to kill any extracellular bacteria. The cells were washed again and growth medium containing 10 µg/ml gentamycin was used for further culturing during the infection assay

For live cell imaging, the cell culture dish was placed on the Nikon BioStation IM as described in part 3.4.2.5.

### 3.6. Generation of a knockout CLIP4 cell line using the CRISPR/Cas9 system

The Clustered Regularly Interspaced Short Palindromic Repeats (CRISPR) Type II system, a bacterial immune system, had been modified for genome editing (Ran et al., 2013).The CRISPR design web tool (http://crispr.mit.edu/) was employed to create the appropriate guide RNA (~20 nucleotides) which defines the location of the genomic target. To generate pSpCas9 (sgRNA), a pair of annealed oligonucleotides was ligated into the expression plasmid pSpCas9 (BB)-2A-green fluorescent protein (GFP).

**Table 35: Annealing buffer**

| Stock solution | |
|---|---|
| 100 mM | KAc ( Potassium acetate) |
| 2 mM | MgAc (Magnesium acetat) |
| 30 mM | HEPES |
| set pH 7.4 | |

**Table 36: Annealing of the oligonucleotides**

| Stock solution | |
|---|---|
| 1µl | Design forward primer |
| 1 µl | Design reverse primer |
| 48 µl | Annealing buffer |

The annealing reaction mixture was first incubated at 95°C for 4 min, then at 70°Cfor 10 min, then slowly cooled down and stored on ice.

The digestion reaction of the pSpCas9 (BB)-2A-GFP vector was performed according to the setup listed in Table 37.

**Table 37: Digestion reaction of the pSpCas9 (BB)-2A-GFP vector**

| Stock solution | Amount |
|---|---|
| DNA (pSpCas9(BB)-2A-GFP) | 3 µl |
| $H_2O$ | 22 µl |
| 10X Fast Digest Buffer | 3 µl |
| Fast Digest Enzyme (BbsI) | 1 µl |

The reaction mixture was incubated at 37°C in a heat block for at least 20 min. Afterwards, the digestion products were separated using agarose gel electrophoresis and then purified

using GeneJET Gel Extraction and DNA Cleanup kit (Thermo Fisher Scientific, Schwerte, Germany).Ligation reaction of DNA fragment and vector was performed as described in 3.1.9. Finally, the ligation product was transformed into electro-competent *E. coli* DH5α. Plasmid DNA was isolated using GeneJET Plasmid Miniprep Kit (Thermo Fisher Scientific, Schwerte, Germany) according to the manufacturer's instructions. The DNA concentration was quantified using a DS-11 Spectrophotometer (DeNovix Inc., Wilmington, DE USA). Samples were analyzed by double digestion using BbsI and EcoRV restriction enzymes. Afterwards a 1% (w/v) agarose gel containing the samples was subjected to an electric field of 100 V. Finally selected samples were sequenced by Eurofins Genomics GmbH (Ebersberg, Germany) to identify positive clones**.** The sequencing results were analyzed using the free software ApE a plasmid editor (http://biologylabs.utah.edu/jorgensen/wayned/ape/). To generate CLIP4 knockout cell lines, NIH/3T3 and A431 cells were transfected with appropriate plasmid DNA using X-tremeGENE™ 9 transfection reagent (Roche, Penzberg, Germany). Medium was changed after 48 h post transfection, cells were washed twice with PBS, trypsinized, centrifuged (5 min, 1000 rpm, Centrifuge 5804 R from Eppendorf) and resuspended in 1 ml growth medium supplemented with Penicillin-Streptomycin. Non-transfected WT A431 cells served as control samples for fluorescence activated cell sorting (FACS). FACS Sorting was carried out by Lothar Gröbe (HZI, Braunschweig). Cells were sorted and seeded as single cells into normal growth medium on 96-well plates. Single cell clones were expanded stepwise and cryopreserved as described in 3.2.3. Western Blot analysis was used to determine if the gene of interest was successfully knocked out by the CRISPR/Cas 9 system.

### 3.7 Isolation of primary mouse tissues

Preparation of murine tissues was performed by Stephanie Stahnke (HZI, Braunschweig). Briefly, an 8 weeks old mouse (strain C57BL/6, commonly referred to as "black 6" mice) was sacrificed via CO2 inhalation. To avoid protein destruction during enzymatic lysis of tissue, cryogenic grinding was performed. For that, a ceramic mortar and a pestle were pre-chilled with liquid nitrogen and the dissected tissues (skin, spleen, lung, kidney, liver, intestine (large and small), stomach and pancreas) were snap-frozen in liquid nitrogen. Finally, tissues were ground to fine powder, transferred to a pre-chilled cryo-tube, and the specimens were stored at - 80°C. The samples were mixed with 4xSDS-PAGE sample buffer, boiled and analyzed by Western blotting.

# 4. RESULTS

## 4.1 Identification of novel interactors by performing a Yeast-2-Hybrid screening

Project I focused on the identification of potential host binding partners of different bacterial virulence factors and the characterization of their function. In this perspective, the lab had initially performed Y2H screening in collaboration with the German Cancer Research Centre in Heidelberg in order to generate a list of potential effector binding partners. Using this approach, a human cDNA-based protein library served as prey and full-length or truncated versions of WxxxE bacterial effector proteins SifA and SifB of *Salmonella*, and EspT from enteropathogenic *E. coli* (EPEC) and *Citrobacter rodentium*, were used as baits. Remarkably, SifA and SifB shared an extension at the N-terminal region, which - in the case of SifA- required for the formation of highly dynamic tubules, so-called SIFs, which extended from the SCV, in addition to the WxxxE-GEF-like domain at the C-terminal region. The spectrum of host proteins that binded to the above bacterial virulence factors was explored using the Y2H screening approach, and the final list of putative interaction partners was about 30 hits per bait. Prior to any experimental validation, we carefully considered the biological function of these potential interaction partners. Involvement of these host proteins in such fundamental processes as migration, endocytosis, and cellular transport made them highly interesting candidates for our research.

As a result of the procedure described above, four host-pathogen pairs were pre-selected based on the known or anticipated biological relevance of these host proteins. These pre-selected Y2H hits are presented in Table 38.

**Table 38: List of most promising host-pathogen interactions**

| Bait | Prey | Prey function |
|---|---|---|
| EspT | APPL1 | Adaptor protein |
| SifA | Cep70 | Centrosomal protein |
| SifA | DYNLRB1 | Dynein Light Chain protein |
| SifB | CLIP4 | CAP-GLY domain containing linker protein 4 |

A combination of different methods, such as pull-down assay, co-immunoprecipitation assay and co-localization analysis by fluorescence microscopy, was used to validate the Y2H hits

and to gain more insight into biological activities of these virulence factors. Looking for the interaction partners of WxxxE effector proteins, in our experimental setup we used truncated versions of SifA and SifB (SifA Δext and SifB Δext) that harbored the WxxxE sequence motif.

Hence, the current project was aimed at defining the molecular targets of SifA, SifB and EspT and trying to understand how these bacterial virulence factors manipulate host cell signaling pathways.

## 4.2 Expression and purification of recombinant fusion proteins

In order to verify physical interaction between a presumable host target protein and its corresponding bacterial factor in pull-down assays, we expressed recombinantly the bacterial effector protein of interest. For this purpose, all recombinant proteins were overexpressed as His-MBP fusion proteins in *E. coli* BL21 (DE3) according to standard procedures (chapter 3.3.4). Purification of the proteins was carried out as described in chapter 3.3.4. Samples from every purification step were collected and then analyzed by SDS gel electrophoresis (chapter 3.3.2, 3.3.3). The results of the SDS-PAGE analyses of the purified recombinant proteins have been depicted in Figure 10.

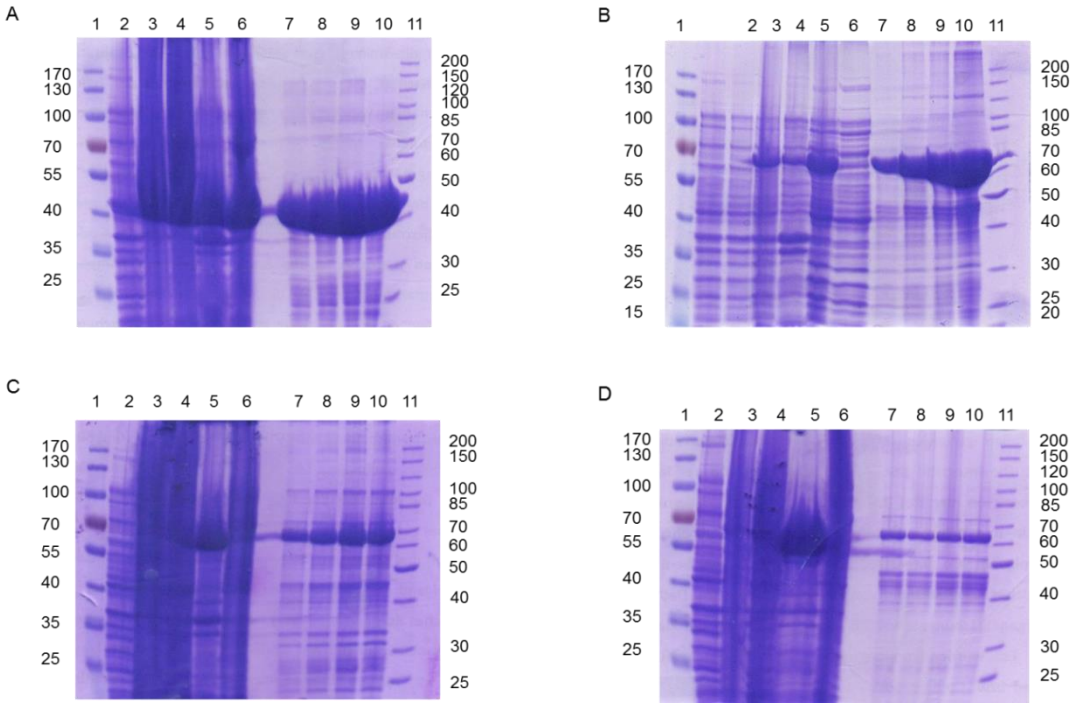


**Figure 10: SDS-PAGE analysis of expression and purification steps of recombinant SifA, SifB and EspT fusion proteins.**

Recombinant proteins were expressed in E. coli BL21 (DE3) as 6xHis-tagged fusion proteins using the pET-41-vector and purified. Gels were stained with Coomassie Brilliant Blue R-250. (A) Expression of a 45 kDa His-MBP. (B) Expression of a 72 kDa recombinant SifA Δext protein that contain WxxxE-GEF-like domain. (C) Expression of a 71 kDa recombinant SifB Δext protein that harbor WxxxE motif. (D) Expression of a 68 kDa recombinant EspT protein. Lanes are loaded as follows: 1. Prestained protein ladder; 2. Sample before induction; 3. Sample after induction; 4. Insoluble fraction after ultrasonication; 5. Soluble fraction after ultrasonication; 6. Supernatant after coupling to His-MBP beads; 7. His-MBP beads 5µl; 8. His-MBP beads 7µl; 9. His-MBP beads 10µl; 10. His-MBP beads 15µl; 11. Unstained protein ladder.

The His-tagged maltose-binding protein (MBP) encoded on the pET-41-vector, had a molecular weight of 45 kDa and could be immobilized either on amylose resin, or on Ni-NTA affinity resin. SDS-PAGE-analysis of the purification samples of His-MBP-SifA Δext confirmed the calculated molecular weight of the protein 72 kDa (Figure 10 B). Also His-MBP-SifB Δext (Figure 10 C) appeared as a band of the calculated molecular weight of 71 kDa. The recombinant EspT protein was detected as a band of approximately 68 kDa, which was in agreement with the calculated size of His-MBP-EspT (Figure 10 D). The purified recombinant proteins were then used for pull-down assays and antibody production.

### 4. 3 Bacterial virulence factor EspT and its predicted molecular target APPL1

An adaptor protein termed phosphotyrosine interacting with PH domain and leucine zipper 1 (APPL1) was identified as a possible interaction partner of EspT. APPL has been described to possess two isoforms, APPL1 and APPL2, both of which interact with Rab5, an important regulator of endocytosis, through the N-terminal BAR-PH domain (Miaczynska et al., 2004; Zhu et al., 2007; Li et al., 2007). APPL was originally identified as an interacting partner of the oncoprotein serine/threonine kinase AKT2 (Mitsuuchi et al., 1999). APPL interacts with the tumor suppressor protein DCC (deleted in colorectal cancer), and therefore it has been referred to as DCC-interacting protein (DIP)-13a (Liu et al., 2002; Li et al., 2007). In addition, APPL1 has been reported as a multifunctional endosomal adaptor protein (Nechamen et al., 2007). APPL1 composed a BAR domain (initially identified as the leucine zipper motif), a PH domain and a PTB domain (Figure 11).


**Figure 11: Schematic representation of human APPL1 domain structure.** APPL1 harbors unique BAR domain that contains two four-helical bundles (Li et al., 2007). The PTB domain of APPL1 interacts with both Akt2 (Mitsuuchi et al.,

1999) and the adiponectin receptors AdipoR1 and AdipoR2 (Mao et al., 2006). Interaction between APPL1 and Rab5 is mediated by the BAR-PH domain (Miaczynska et al., 2004).

To further investigate the ability of APPL1 to interact with EspT, pull-down assays were performed, in which purified recombinant His-MBP-EspT was used as bait and incubated with B16-F1 cell lysates of ectopically expressing GFP-APPL1 as prey. As a negative control for the experiment, His-MBP alone was used. Representative results of biochemical analyses have been illustrated in Figure 12.

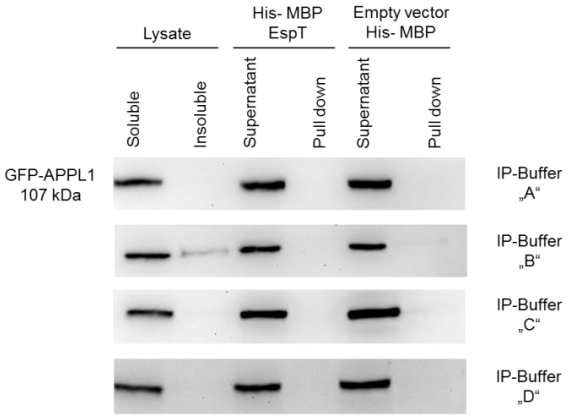


**Figure 12: Pull-down assays to probe binding of EspT to APPL1.**B16-F1 cells were transfected with GFP-APPL1 and lysed with ice-cold IP buffer. Lysates were incubated with recombinant proteins immobilized on Ni-NTA affinity resin. Samples were separated by SDS-PAGE and visualized by Western Blotting with anti-GFP antibody. Note that IP-Buffer „A“ is a standard IP buffer as described in chapter 3.3.5; IP-Buffer „B“ is a 'lipid friendly' buffer lacking Triton-X-100 (cells lysed by ultrasound); IP-Buffer „C“ contains 1mM EDTA instead of 5mM $MgCl_2$; IP-Buffer „D“ contains high concentration of salts (30 mM KCl and 150 mM NaCl) (chapter 3.3.5). Note that GFP-APPL1 was not bound by EspT in all four IP buffer conditions.

The Western blot result revealed that APPL1 was readily expressed and soluble, but does not bind to immobilized EspT under given conditions. GFP-APPL1 was detected by a monoclonal GFP antibody. Four different buffer conditions were tested, however no binding could be observed.

Taken together, the data presented in Figures 12 could not readily validate the putative interaction of EspT and APPL1 in the given experimental setup. This subproject was therefore not followed up in the framework of this thesis.

## 4.4 Bacterial virulence factor SifA and its predicted molecular target Cep70

### 4.4.1 Subcellular localization of GFP-tagged Cep70 and co-localization studies of GFP-Cep70 and Myc-SifA

Based on the results of the Y2H screen, Cep70 was identified as a potential molecular target of the *Salmonella* bacterial virulence factor SifA. Recently, it was published that Cep70 localizes to the centrosome throughout the cell cycle and interacts with γ-tubulin (Shi et al., 2011). Its centrosomal localization was mediated via the coiled-coil domains (Shi et al., 2011). Beside other functions, Cep70 has been reported to act as a regulator of microtubule assembly by promoting microtubule elongation rather than microtubule nucleation (Shi, 2012).

In order to learn more about the potential role of Cep70 in *Salmonella* infection, we first studied its subcellular localization in the presence and absence of SifA. Subcellular localization of GFP-tagged Cep70 was investigated by immunofluorescence microscopy in Cos-7 fibroblasts. In accordance with previously published data (Shi et al., 2011), analysis of immunofluorescence images in Cos-7 fibroblasts transiently transfected with GFP-Cep70 confirmed that in most cases Cep70 localizes exactly at two centrosomes (Figure 13, top panel). However, in some cases I had observed a higher number of differently sized spots (Figure 13, middle panel) which might well correspond to the structures that were described as centriolar satellites (Tollenaere et al., 2015).

Next, co-localization of GFP-Cep70 and Myc-SifA was further tested by immunofluorescence. Figure 13 shows corresponding images of fixed Cos-7 fibroblast cells overexpressing GFP-Cep70 with Myc-SifA. While SifA broadly distributed all over the cell, Cep70 signals were distinctly visible as discrete dots (Figure 13, bottom panel). Interestingly, at later stages of infection the *Salmonella*-containing vacuole (SCV) was positioned in close proximity to the microtubule-organizing center and, hence, centrosomes (Ramsden et al., 2007).

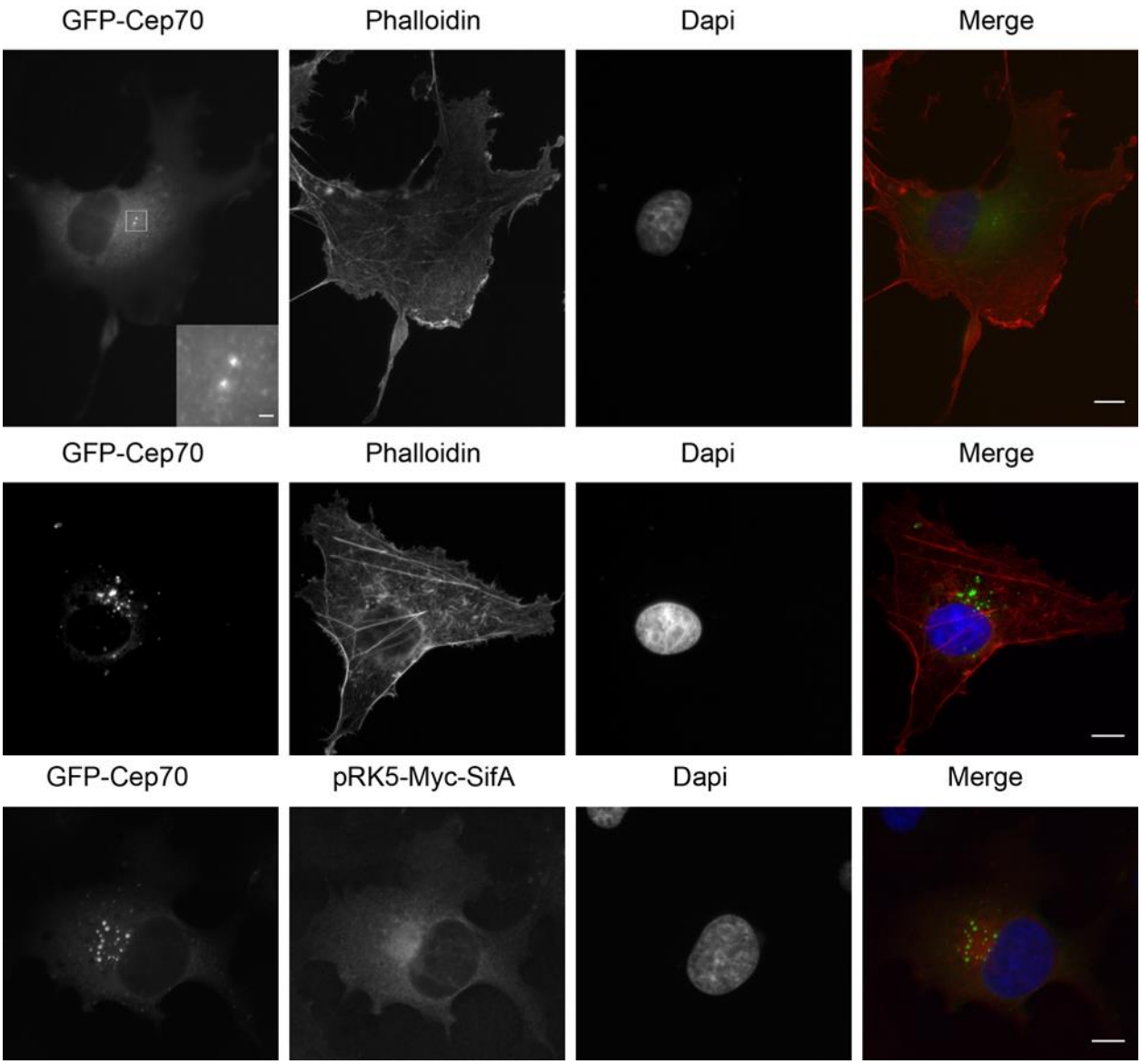


**Figure 13: Subcellular localization of GFP-tagged Cep70 and co-localization of Cep70 & SifA in Cos-7 fibroblasts.**

Cos-7 cells were transfected with the respective constructs, fixed 24 hours later with PFA and permeabilized. Nuclei were stained with DAPI. The actin cytoskeleton was stained with phalloidin as described in chapter 3.4.2. Merge shows an overlay of the green (GFP-Cep70), red (phalloidin and anti-Myc, respectively) and blue (Dapi) channel. Scale bars in full panels and the zoomed panel correspond to 10 µm and 1 µm, respectively. The insert of the marked region is enlarged 5 times.

### 4.4.2 Cep70 is largely Triton X-100 insoluble

Since I noticed a very poor expression of GFP-Cep70 in the Triton X-100 soluble fraction, I have analyzed the Triton X-100 solubility properties of this construct. For this, Hek293T cells were transiently transfected with GFP-Cep70 and subsequently analyzed by Western Blotting. I detected protein bands corresponding to the predicted molecular weight of 97 kDa. As shown in Figure 14, the Cep70 signal is mainly found in the Triton X-100 insoluble fraction of cell lysate.

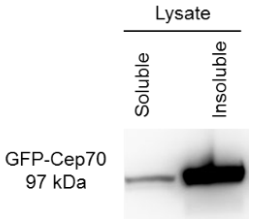


**Figure 14: Analysis of the Triton X-100 solubility of Cep70.** Hek293T cells were transfected with GFP-Cep70 and lysed with ice-cold IP buffer "A" (chapter 3.3.5). Samples were applied to SDS-PAGE and analyzed by Western Blotting with anti-GFP antibody.

Therefore, biochemical analysis of the interaction between Cep70 and SifA in standard assays was hampered, since this centrosomal protein resides in a triton-insoluble fraction. In order to find out whether Cep70 plays a role during *Salmonella* infection, further studies should be carried out. It would be interesting to look if Cep70 influences SCV positioning close to the centrosome, for instance by Cep70 RNA interference (RNAi) in cell infected with *Salmonella*.

## 4.5 Bacterial virulence factor SifA and its predicted molecular target DYNLRB1

### 4.5.1 Subcellular localization of DYNLRB1, SifA and Rab6a, and their co-localization studies

Dynein Light Chain Roadblock type-1 protein (DYNLRB1), an 11 kDa protein has been reported to belong to the LC7/roadblock protein family. Dynein comprised of two heavy chains, two intermediate chains, four light intermediate chains and light chains of the LC7/roadblock, LC8 and Tctex1/rp3 protein families (Wanschers et al., 2008). As a multifunctional protein, DYNLRB1 has been involved in many cellular processes, such as cargo transport along microtubules, regulation of cell migration, cell division, maintenance of Golgi apparatus integrity, and transport of intracellular vesicles (Ashokkumar et al., 2009).

It has recently been reported that DYNLRB1 specifically interacts and co-localizes with the small GTPase Rab6 in the Golgi (Wanschers et al., 2008).Furthermore, the cytoplasmic dynein interacted with N-acetylglucosamine kinase (GlcNAc kinase or NAGK), and this binding occurred on MT fibers at dendritic branch points (Islam et al., 2015). NAGK-DYNLRB1 interaction played an essential role in dendritogenesis. Finally, DYNLRB1 has been reported to interact with human reduced folate carrier (Ashokkumar et al., 2009) and the transforming growth factor-β receptor complex (Tang et al., 2002).

In order to probe the localization of GFP-DYNLRB1 subcellularly, Cos-7 cells were transfected with this construct. After fixation with PFA 24 hours post transfection, cells were permeabilized, treated with anti-Giantin antibody to visualize the Golgi, and stained with DAPI to visualize the cell nuclei. Immunofluorescence analyses in Cos-7 fibroblasts transiently transfected with GFP-DYNLRB1 revealed that this host proteinwas diffusely distributed throughout the cytoplasm. Represenative images have been depicted in Figure 15 (top panel).

Since *Salmonella* T3SS-2 effector SifA was identified as a potential interaction partner of the host protein DYNLRB1, I performed localization studies of the bacterial virulence protein SifA as well as co-localization studies of both proteins. Remarkably, the *Salmonella* virulence factor SifA was mostly distributed throughout the cytoplasm (Figure 15, bottom panel). When GFP-DYNLRB1 and Myc-SifA were co-expressed, I observed only a slight co-localization of both proteins in the area surrounding the Golgi (Figure 16, top panel).

Following the published findings from the group of Prof. Dr. Jack Fransen (Wanschers et al., 2008), we aimed to extend this observation and questioned whether DYNLRB1 is recruited to the Golgi upon expression of active Rab6. At first, we investigated the subcellular localization of Rab6a and subsequently performed co-localization studies of GFP-DYNLRB1 and mCherry-Rab6a. Indeed, Rab6 alone localized to the Golgi structure (Figure 15, middle panel) and was moreover able to recruit DYNLRB1 to this site. Consequently, DYNLRB1 had not distributed within the cytoplasm any longer but distinctly localized to the Golgi together with Rab6 (Figure 16, upper middle panel) (Wanschers et al., 2008).

Next, the interesting question arose whether the T3SS-2 effector SifA co-localizes with the GTPase Rab6 that is involved in microtubule-dependent transport pathways through the Golgi and from endosomes to the Golgi (Short et al., 2002). To answer this question, Cos-7 fibroblasts were co-transfected with GFP-SifA and mCherry-Rab6a. I found that the small GTPase Rab6a can also force SifA to localize to Golgi-like structures (Figure 16, lower middle panel).

Finally, I tested whether DYNLRB1 competes with Rab6 for SifA Golgi binding. For this purpose, Cos-7 fibroblasts were triple-transfected with GFP-DYNLRB1, mCherry-Rab6a and Myc-SifA. The results of this experiment clearly showed a compact co-localization of all three proteins in the Golgi region (Figure 16, bottom panel), suggesting that this triade does not show a competitive behavior.

Taken together, the data presented in Figures 15 and 16 suggest that DYNLRB1 and SifA were diffusely distributed throughout the cytoplasm when expressed alone, whereas mCherry-Rab6a was found exclusively in the Golgi (Figure 15). DYNLRB1 could be recruited to the Golgi by Rab6 (Figure 16, upper middle panel), which was in accordance with previously published data (Wanschers et al., 2008). Similarly, Rab6 could recruit SifA to Golgi-like structures (Figure 16, lower middle panel). Finally, co-expression of all three proteins resulted in significant co-localization in the Golgi region (Figure 16, bottom panel). As Rab6 was the master regulator of DYNLRB1 and SifA localization, we tested whether SifA might also interact with Rab6, assuming that the binding was mediated by its GEF-like domain (see below Figure 18).

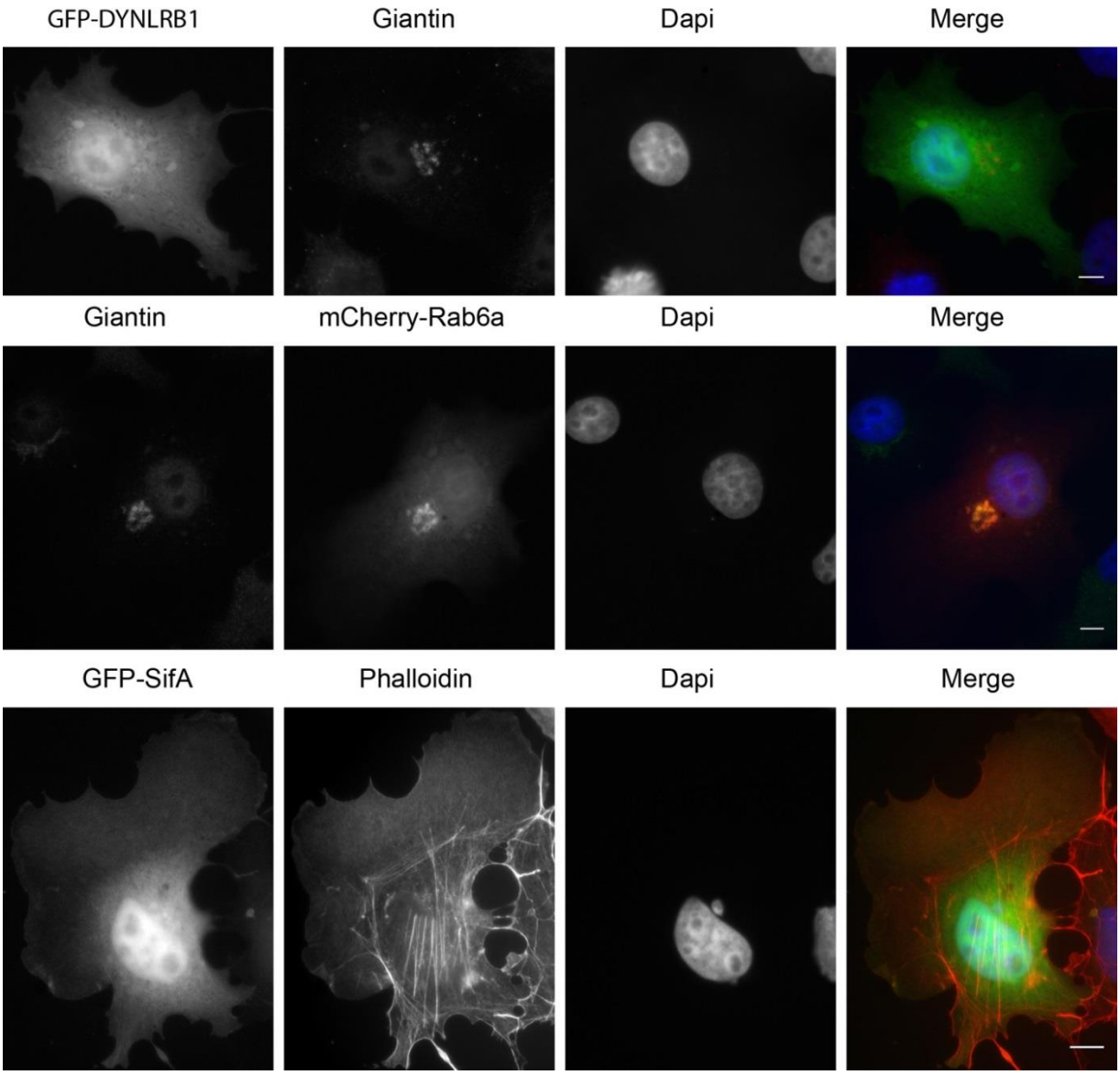


**Figure 15: Subcellular localization of GFP-DYNLRB1, GFP-SifA and mCherry-Rab6a.** Cos-7 cells were transfected with respective constructs, fixed 24 hours later with PFA and permeabilized. Nuclei were stained with DAPI. Golgi was stained with anti-Giantin rabbit polyclonal antibody as described in chapter 3.4.2. The scale bar indicates 10 µm.

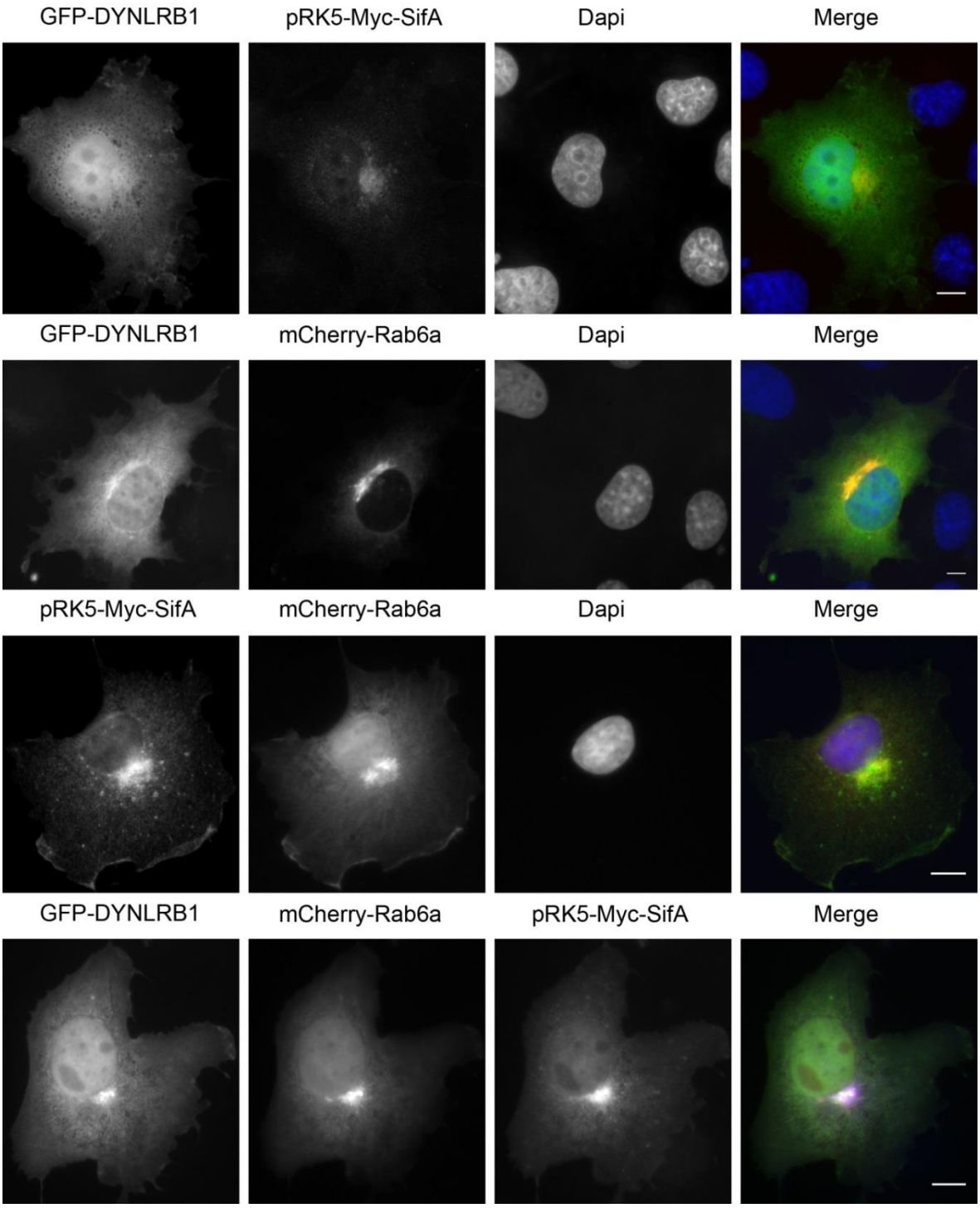


**Figure 16: Co-localization studies of DYNLRB1 & SifA (top panel); DYNLRB1 & Rab6a (upper middle panel); SifA & Rab6a (lower middle panel) and DYNLRB1 & SifA & Rab6a (bottom panel).** Cos-7 cells were transfected with respective constructs, fixed 24 hours later with PFA and permeabilized. Nuclei were stained with DAPI (blue in merge). Myc-tagged SifA protein was labeled with mouse anti-Myc antibody (red in merge). The scale bar is 10 µm.

### 4.5.2 Biochemical analysis of the interaction of DYNLRB1 with SifA

The potential interaction between the host protein DYNLRB1 and the bacterial virulence protein SifA was further scrutinized *in vitro*, as described in chapter 3.3.5. Purified recombinant His-MBP-SifA Δext and GFP-DYNLRB1 were used in a pull-down assay as bait, and prey, respectively. As a negative control I used His-MBP in the experiments. The results of these experiments have been shown in Figure 17.

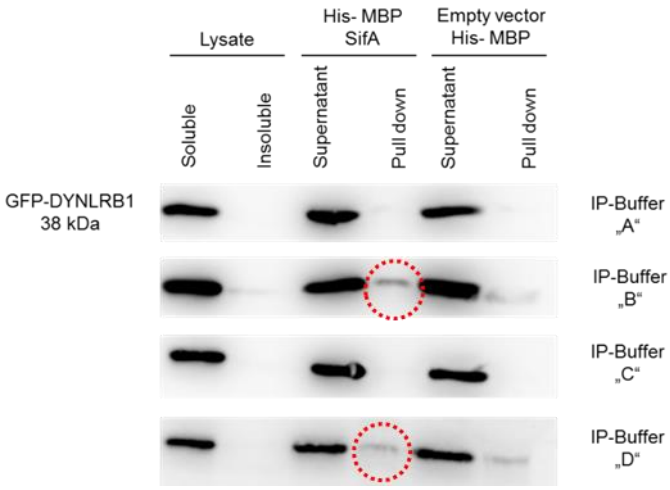


**Figure 17: Pull-down assays to probe binding of SifA to DYNLRB1.** B16-F1 cells were transfected with GFP-DYNLRB1, lysed with ice-cold IP buffer and the lysates were incubated with recombinant proteins immobilized on Ni-NTA beads. Samples were analyzed by SDS-PAGE and Western Blotting using anti-GFP antibody. Note that IP-Buffer „A“ is a standard IP buffer as described in chapter 3.3.5; IP-Buffer „B“ is a 'lipid friendly' buffer lacking Triton (cells lysed by ultrasound); IP-Buffer „C“ contains 1mM EDTA instead of 5mM MgCl2; IP-Buffer „D“ contains high concentration of salts (30 mM KCl and 150 mM NaCl) (chapter 3.3.5). DYNLRB1 only weakly bound to SifA in 2 of 4 different IP buffer conditions.

As expected, I detected a band of approximately 38 kDa, corresponding to the predicted molecular weight of GFP-DYNLRB1, when using a monoclonal antibody against GFP. There were strong signals in the load controls and supernatant after pull-down. In the pull-down lanes corresponding to His-MBP no bands could be observed. The same results were obtained when buffers with different salt concentrations were used. Only under conditions where membrane lipids were present (B) or when the water activity was reduced due to high salt (D), a weak interaction of His-MBP-SifA Δext and GFP-DYNLRB1 was detected.

Since immunofluorescence analysis clearly illustrated co-localization of all three proteins, DYNLRB1, SifA and Rab6a, in the Golgi region, we hypothesized that DYNLRB1 might interact with SifA more strongly or even only in the presence of small GTPase Rab6a. In order to explore the putative interaction of DYNLRB1 and SifA and its potential dependence

on Rab6a, we repeated our analysis using Hek293T cells co-transfected with the GFP-DYNLRB1 and the mCherry-Rab6a constructs. Using these lysates, we performed pull-down assays with recombinant His-MBP-SifA Δext as bait. His-MBP-SifB Δext and His-MBP-EspT were used as controls. Representative results of the biochemical analyses have been illustrated in Figure 18.

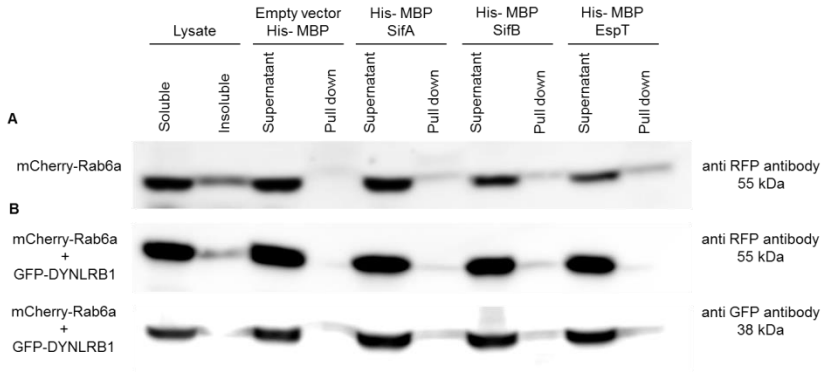


**Figure 18: Pull-down assays to probe binding of SifA to DYNLRB1 in the presence of Rab6a.** Hek293T cells were transfected with mCherry-Rab6a alone or co-transfected with GFP-DYNLRB1, lysed with ice-cold IP buffer and the lysates were incubated with immobilized recombinant proteins (chapter 3.3.5). Samples were analyzed by SDS-PAGE and visualized by Western Blotting with anti-RFP and anti-GFP antibodies. Note that Rab6a was not bound to SifA (A) and that in the presence of Rab6a, DYNLRB1 was not bound to SifA under these conditions (B).

These co-precipitation experiments revealed that small GTPase Rab6 does not directly interact with WxxxE family members such asSifA and SifB of *Salmonella,* and EspT from EPEC and *C. rodentium*. Moreover, the biochemical data suggested that Rab6a-DYNLRB1 complexes (Wanschers et al., 2008) do not bind SifA under these conditions.

In summary, I was not able to observe any notable differences in the pull-down assays (Figure 18, B) as compared to previous experiments (Figure 17). Unfortunately, these results could not confirm my hypothesis that Rab6a has an influence on the interaction between host DYNLRB1 and bacterial SifA proteins.

In conclusion, the data presented in Figures 17 and 18 indicated that interaction between DYNLRB1 and SifA couldnot unequivocally be demonstrated using this technique. However, the co-localization data and the results of Y2H screening strongly argued for this interaction. In addition, interaction studies have shown that SifA does not directly bind to Rab6. Nevertheless, co-expression of Rab6 and SifA led to a significant recruitment of SifA to the Golgi. A better understanding of this dynamic co-localization would require further experiments that were beyond the scope of this thesis.

## 4.6 Bacterial virulence factor SifA and Rab9

### 4.6.1 Biochemical analysis of the interaction of SifA with Rab9

During parallel studies in our lab it was discovered that among all members of Rab GTPases family, only Rab9 interacts with SifA (e.g. PhD Thesis of S. Arens). It has been found that up to 18 Rabs were present on the SCV during its maturation (Brumell & Scidmore, 2007). Recent evidence highlighted a new function of Rabs, namely that Rab9 and Rab7 regulate membrane trafficking processes at the late endosome-lysosome system. One of the most interesting features of both Rabs was that Rab7 and Rab9 were shown to be essential for SIFs formation (Smith et al., 2007; Brumell & Scidmore, 2007). This finding made Rab9 a highly interesting candidate for our research. Aiming to confirm interaction between SifA and Rab9, we transfected Hek293T cells with mCherry-Rab9 and performed pull-down assay. Purified recombinant His-MBP-SifA Δext and mCherry-Rab9 were used as bait and prey, respectively. His-MBP, His-MBP-SifB Δext and His-MBP-EspT were used as controls. The experimental results have been shown in Figure 19.

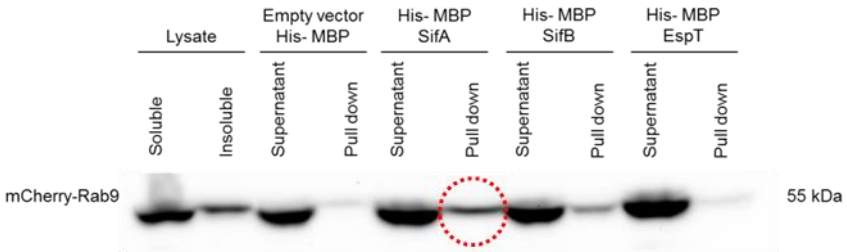


**Figure 19: Pull-down assays to probe binding of SifA toRab9.** Hek293T cells were transfected with mCherry-Rab9, lysed with ice-cold IP buffer and the lysates were incubated with immobilized recombinant proteins. Samples were analyzed by SDS-PAGE and visualized by Western Blotting with anti-RFP antibody as described in chapter 3.3.5. Note that Rab9 interacts with SifA.

As shown in Figure 19, I observed both Rab9 and SifA in the pull-down sample probed with an anti-RFP antibody, which confirmed a weak interaction between these proteins. However, additional studies would be required to explore the molecular mechanisms underlying this interaction. Nonetheless, these experiments further corroborated that the lack of SifA binding to Rab6 was specific.

### 4.6.2 Biochemical analysis of the potential interaction between DYNLRB1 and SifA in the presence of Rab9

Due to the fact that Rab9 interacted with SifA, as shown above by the pull-down assays, I raised the hypothesis that Rab9 may affect interaction between DYNLRB1 and SifA. For that, I co-transfected Hek293T cells with GFP-DYNLRB1 and mCherry-Rab9 and used recombinantly expressed His-MBP-SifA Δext as bait in pull down assays, His-MBP, His-MBP-SifB Δext and His-MBP-EspT were used as negative controls. Representative results of the biochemical analysis have been illustrated in Figure 20.

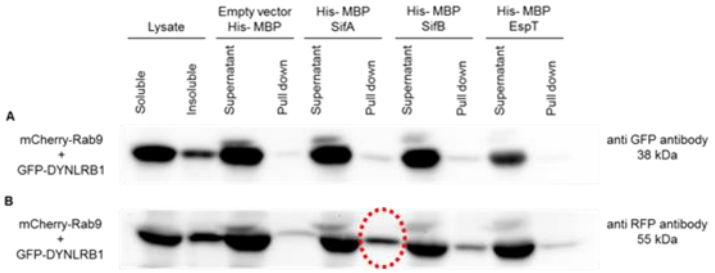


**Figure 20: Pull-down assays to probe binding of SifA to DYNLRB1 in the presence of Rab9.** Hek293T cells were co-transfected with GFP-DYNLRB1 and mCherry-Rab9 constructs; the cells were lysed with ice-cold IP buffer and the lysates were incubated with recombinant proteins as described in chapter 3.3.5. Samples were analyzed by SDS-PAGE and visualized by Western Blotting with anti-GFP (A) and anti-RFP antibodies (B). Note that Rab9 but not DYNLRB1 binds to SifA Δext.

Western blot analyses using an anti-GFP antibody showed that GFP-DYNLRB1 was not detected in the pellet after pulling down with recombinant SifA (Figure 20 A). I however detected a band of approximately 55 kDa, corresponding to mCherry-Rab9, in the pellet after incubation with SifA (Figure 20 B). I observed traces of the protein in the respective pull down samples of SifB and EspT, but still, the signal was much less than in pull down samples of SifA. These experiments suggested that the presence of Rab9 does not mediate an interaction between DYNLRB1 and SifA, but confirms the binding of SifA Δext to Rab9 (see Figure 19).

### 4.6.3 Subcellular localization of mCherry-tagged Rab9 and co-localization studies of this GTPase with DYNLRB1, SifA and these two proteins together.

In order to compare this influence of co-expression of Rab9 together with either DYNLRB1 or SifA alone of both proteins together, I initially performed localization analysis of mCherry-Rab9 in Cos-7 cells. This GTPase predominantly localized in the Golgi region (Figure 21, top panel), as visualized by a high degree of mCherry-Rab9 co-localizing with Giantin, a marker for the Golgi, reminiscent of Rab6 (Figure 15, middle panel).

To address whether the Rab9-like Rab6a recruited DYNLRB1 to the Golgi region, we performed co-localization studies in Cos-7 fibroblasts transiently transfected with GFP-DYNLRB1 and mCherry-Rab9 (Figure 21, upper middle panel). GFP-DYNLRB1 appeared to localize mainly in the cytoplasm, both in presence and in absence of ectopically expressed Rab9. Results of these experiments indicated that both proteins, although they partially overlap in the Golgi region, do not co-localize in a manner comparable to that of Rab6 and DYNLRB1 (Figure 21, upper middle panel).

Since I noticed the biochemical interaction of Rab9 with SifA, I was prompted to analyze whether Rab9 could affect the localization of SifA. While SifA overexpression alone in the Golgi, co-expression of Myc-SifA and mCherry-Rab9 led to the co-localization of both proteins at the Golgi (Figure 21, lower middle panel), indicating that Rab9 could effect SifA localization.

Finally, I investigated the effect of Rab9 on the co-localization of DYNLRB1 and SifA. For this purpose, Cos-7 fibroblasts were triple-transfected with GFP-DYNLRB1, mCherry-Rab9 and Myc-SifA (Figure 21, bottom panel). Noteworthy, DYNLRB1 was co-recruited together with SifA to the Golgi by Rab9, but not alone. This indicated that Rab9 couldnot recruit DYNRB1 directly, but rather via SifA. This was in contrast to Rab6, which recruits DYNLRB1 directly in the absence of SifA.

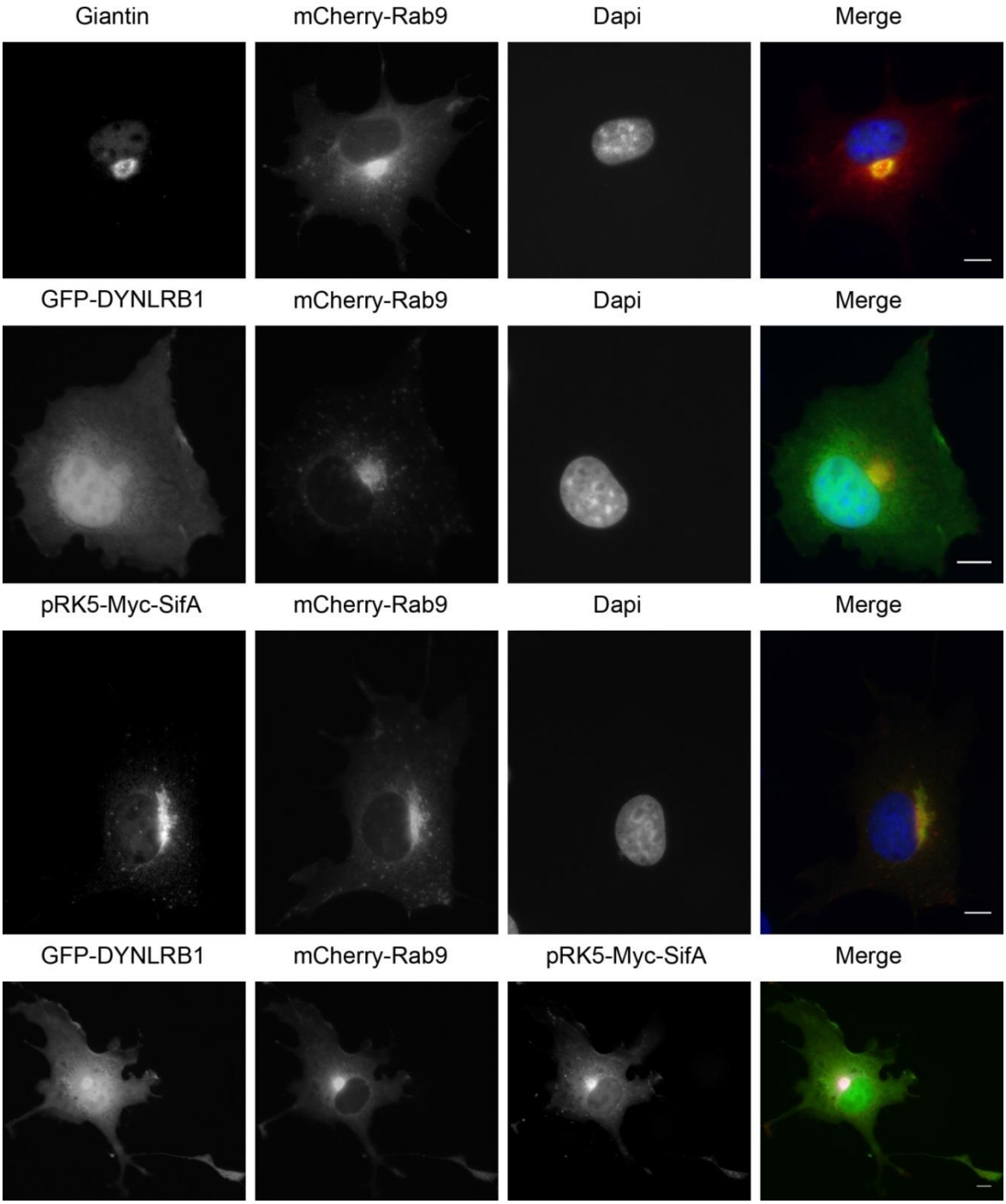


**Figure 21: Subcellular localization of mCherry-tagged Rab9 and co-localization studies of this GTPase with DYNLRB1, SifA and these two proteins together.** Cos-7 cells were transfected with respective constructs and fixed 24 hours later with PFA. Nuclei were stained with DAPI (blue). The Golgi was stained with anti-Giantin rabbit polyclonal antibody and is shown in green. The Myc tag was labeled with a mouse anti-Myc antibody. As secondary antibodies, anti-mouse Alexa Fluor® 350, Alexa Fluor® 488, were used, respectively (chapter 3.4.2). The scale bar indicates 10 µm. Note that SifA is recruited to the Golgi region by Rab9.

## 4.7 Bacterial virulence factor SifB and its predicted molecular target CLIP4

### 4.7.1 Subcellular localization of GFP-tagged CLIP4

CLIP4 was a not yet characterized protein of so far unknown function that harbors Ankyrin-repeats (ANK) and cytoskeleton-associated protein-glycine-rich (CAP-Gly)-domains. CLIP4 belonged to the CAP-GLY Domain Containing Linker Proteins (CLIP) family, which comprises four members (Figure 22 A). The first identified member of this family was CLIP 170 (cytoplasmic linker protein of 170 kDa), also termed CLIP1. CLIP1 and CLIP2, also referred to as CLIP115, have been the most investigated proteins of this family and have been also known as MT-tip binding proteins (Perez et al., 1999).

(A)

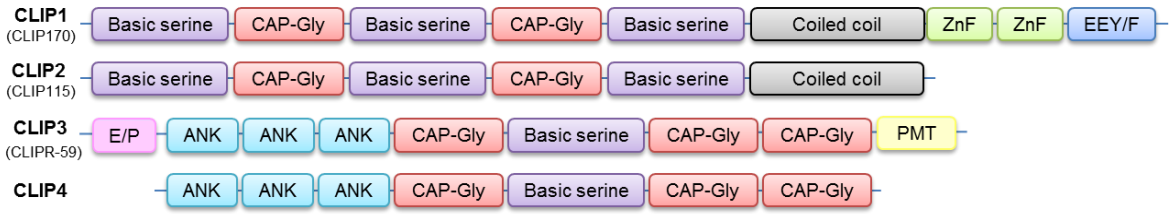


(B)

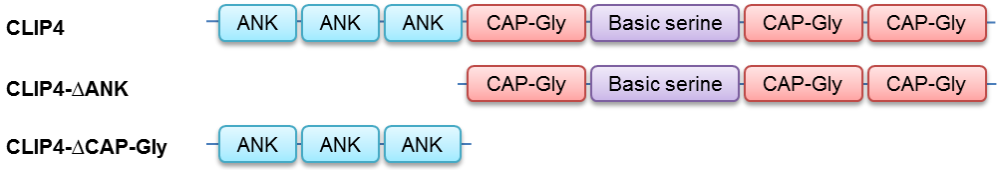


**Figure 22: Schematic domain overview of CAP-Gly proteins and CLIP4-constructs.** (A) Schematic representation of the CAP-Gly family of proteins with the conserved domains. These proteins share CAP-Gly domains, which in the case of CLIP1 and CLIP2 localize to microtubule plus ends. In addition, CLIP1 contains EEY/F motif, which binds to the end-binding proteins (EB) (Gupta et al., 2010). In contrast to CLIP1, CLIP2 lacks the zinc finger domain (ZnF) and thus does not bind to the dynein-dynactin complex (Steinmetz et al., 2008). Beside CAP-Gly domains, CLIP3 and CLIP4 harbor Ankyrin repeat (ANK) domain consisting of two α-helices separated by loops. Whereas most CAP-Gly proteins bind to MTs, CLIP3 localizes to the trans-Golgi by a palmitoylation membrane-targeting motif enclosed within the last 30 amino acids (PMT) (Lallemand-Breitenbach et al., 2004; Perez et al., 2002). (B) Schematic representation of full-length and truncated versions of CLIP4 protein used for immunofluorescence and pull down assays. CLIP4-ΔANK is a construct lacking ANK-repeats domain on the N-terminal region of the full-length CLIP4. CLIP4-ΔCAP-Gly is a construct lacking CAP-Gly and basic serine domains on the C-terminal region of the full-length CLIP4. Abbreviations: ANK, ankyrin repeats; E/P, glutamate-proline rich; PMT, palmitoylation membrane-targeting motif; ZnF, zinc finger domain.

Since CLIP4 was likely associated with the cellular microtubule system and since SIFs spread through the cell by using MTs, we decided to put effort into analyzing this hit from our Y2H screen.

To investigate the cellular function of CLIP4, I studied its subcellular localization. For that, Cos-7 fibroblasts were fixed 24 hours post transfection with GFP-CLIP4 and labeled with antibodies against tubulin (Figure 23, top panel). The subcellular distribution of CLIP4 strongly overlapped with MTs in transiently transfected Cos-7 fibroblasts. These results suggested that CLIP4 was a microtubule-binding protein (Figure 23, top panel) rather than a MT-Tip protein. In order to identify the domains needed for microtubule localization, we generated various truncated forms of CLIP4 protein tagged with GFP (Figure 22 B).

Hence, I tested individually the localization of the N-terminal Ankyrin-repeats and the C-terminal CAP-Gly-domains of CLIP4 protein. The construct lacking the ANK-repeats but harboring the CAP-Gly domains displayed characteristic microtubule localization (Figure 23, middle panel). In contrast, a construct lacking the CAP-Gly domains could not decorate microtubules and appeared cytoplasmic (Figure 23, low panel). This led us to the conclusion that localization of CLIP4 to MTs was mediated by the CAP-Gly domains and not the Ankyrin repeats (Figure 23).

Taken together, the data presented in Figures 23 indicate that the microtubule localization of CLIP4 depended on its CAP-Gly domains (C-terminal region), which are similar to those of CLIP 170 and CLIP 115.

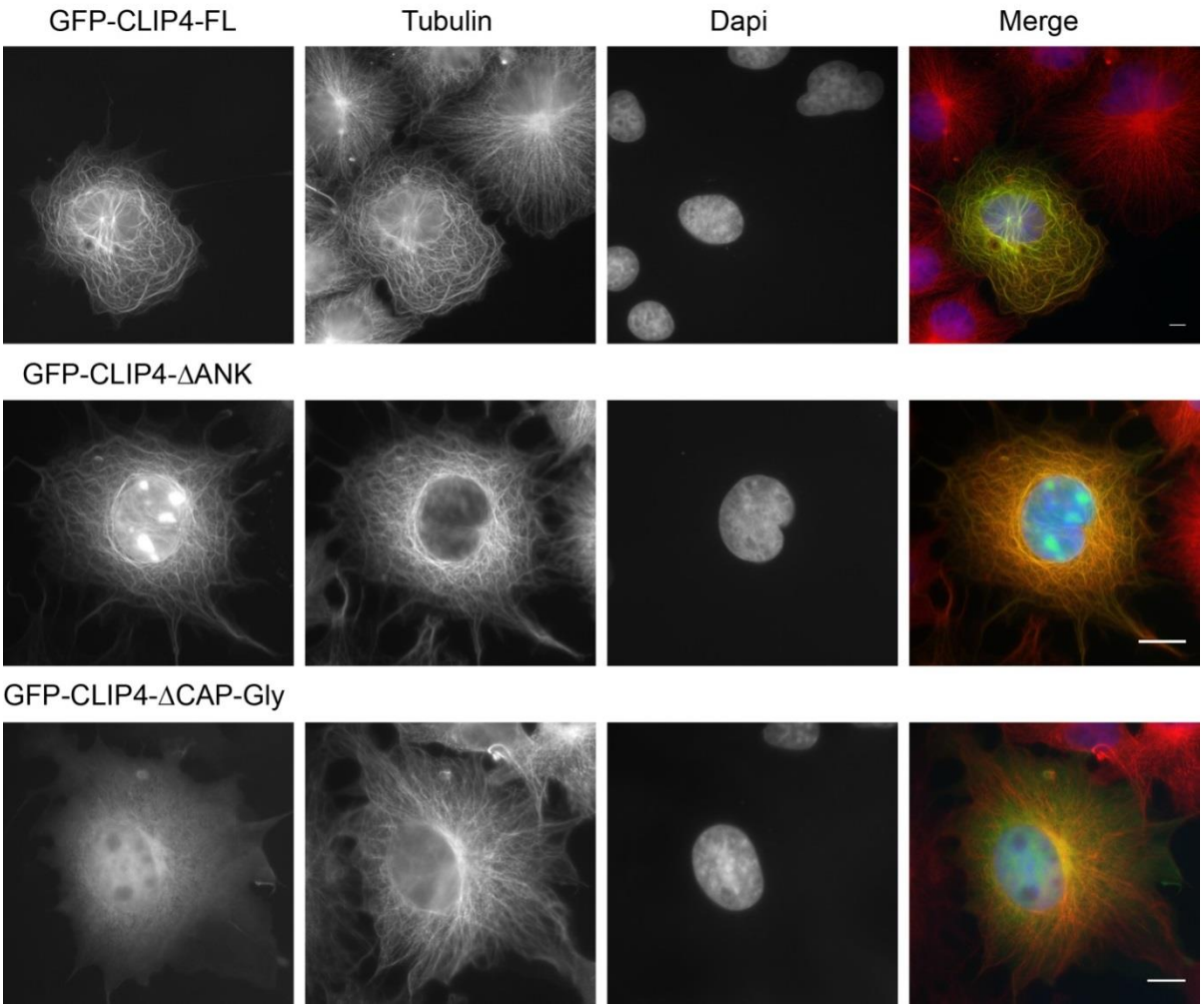


**Figure 23: Subcellular localization of GFP-tagged CLIP4 and localization of truncated constructs lacking the N-terminal ANK-repeats and the C-terminal CAP-Gly-domains, respectively in Cos-7 fibroblasts.** Cos-7 cells were transfected with respective GFP-tagged constructs of CLIP4, fixed 24 hours later with PFA and permeabilized. Nuclei were stained with DAPI. Staining of the transfected cells with anti-tubulin (YL ½) antibody revealed that CLIP4 is a microtubule-binding protein. The overlay shows the respective GFP-construct in green, Tubulin in red and Dapi in blue. The scale bar indicates 10 μm.

### 4.7.2 Time-lapse imaging of GFP-labelled CLIP4

In addition to immunostaining experiments of fixed cells, I studied the behavior of transfected GFP-CLIP4 cells using time-lapse fluorescence microscopy. This approach allowed visualization of the dynamic localization of CLIP4 on MTs. For this purpose, Cos-7 fibroblasts were transfected with GFP-tagged CLIP4 and fluorescent signals were recorded over time as described in chapter 3.4.2.5. During time-lapse acquisition, I monitored movement patterns within individual GFP-CLIP4 transfected cells. I made the observation that many cells died during the first hours. Nevertheless, I succeeded to record the dynamics of CLIP4, the fourth member of the CAP-Gly family. Representative images have been shown in Figure 24. Live cell imaging confirmed our previous assumption that CLIP4 is a microtubule-binding protein.

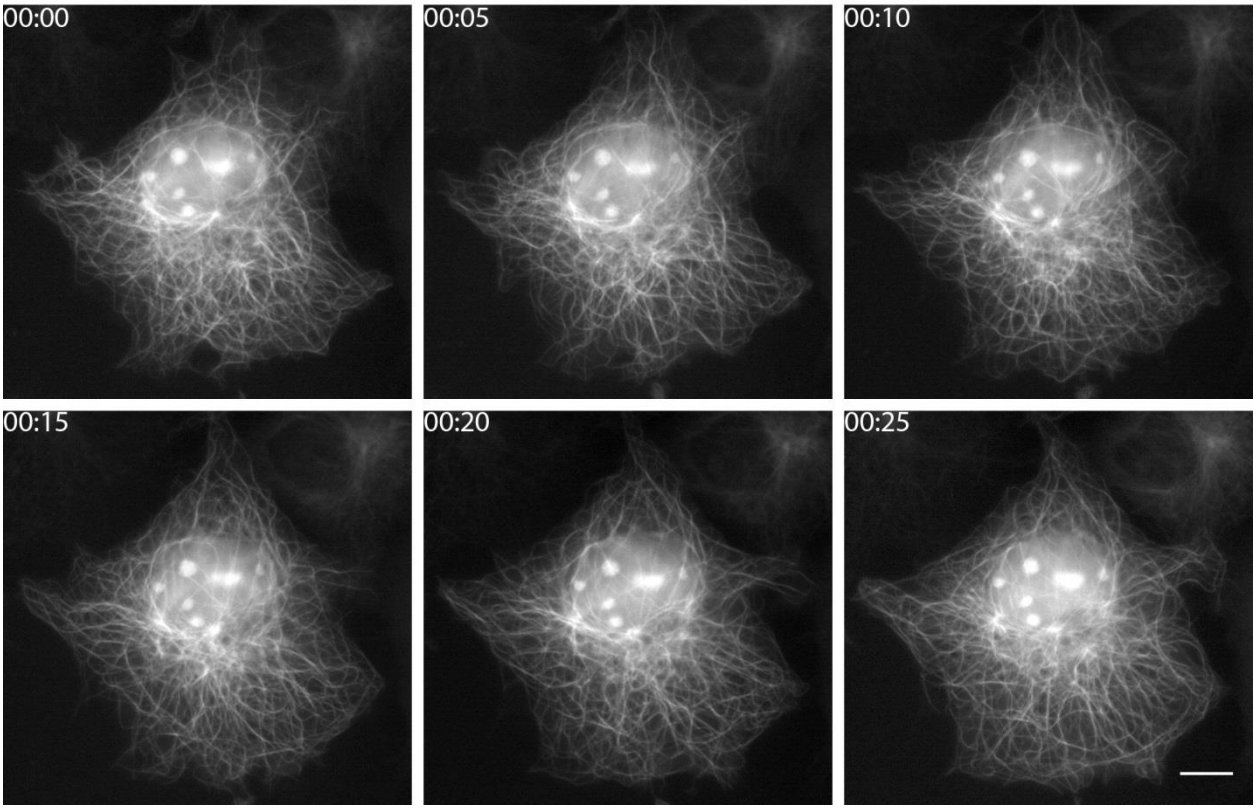


**Figure 24: Time-lapse imaging of dynamic of microtubule protein CLIP4.** Cos-7 cells were transfected with GFP-tagged CLIP4 construct and seeded onto Ø35 mm glass bottom µ-dishes (Ibidi) covered with fibronectin. Dynamics of CLIP 4 protein was visualized at Nikon BioStation IM (40X magnification) over 8 hours in 5 min intervals. The scale bar indicates 10 µm. The images were extracted from the supplementary movie 1. Time (h:min) is indicated in the upper left corner of each image.

### 4.7.3 Biochemical analysis of the potential interaction between CLIP4 and SifB

Based on Y2H screening results, I commenced to investigate the potential interaction between the host protein CLIP4 and the bacterial virulence protein SifB. For this, I performed pull-down assays, as described above, with Hek293T cells transiently transfected with GFP-tagged CLIP4. Purified recombinant His-MBP-SifA Δext and His-MBP-SifBΔext were used as baits, and expressed GFP-CLIP4 protein served as prey. As a negative control for our experiment, we used His-MBP and His-MBP-EspT. Representative results of biochemical analysis have been given in Figure 25.

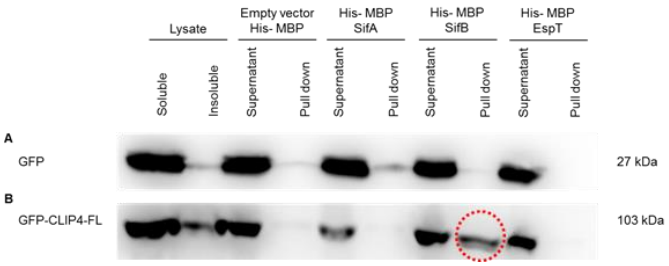


**Figure 25: Pull-down assays to probe binding of SifB to CLIP4.** Hek293T cells were transfected with GFP or GFP-CLIP4 constructs, lysed with ice-cold IP buffer and the lysates were incubated with recombinant proteins as described in chapter 3.3.5. Samples were analyzed by SDS-PAGE and visualized by Western Blotting with anti-GFP antibody. (A) Note that GFP alone was not bound by either SifA or SifB. (B) Note that GFP-CLIP4 readily bound to SifB, but not to SifA.

GFP alone, which served as a negative control, did not bind either SifA or SifB in all experiments performed (Figure 25 A). In contrast, I detected GFP-CLIP4 of the expected molecular weight (103 kDa) in the pellet where SifB Δ ext was used as bait. Therefore, this assay confirmed a positive interaction between CLIP4 and SifB, but not SifA (Figure 25 B), which has been in line with our Y2H result.

### 4.7.4 Mapping the interaction surface of SifB and CLIP4

In order to gain detailed knowledge about the interaction surfaces of the two proteins, I generated various truncated forms of human CLIP4 tagged with GFP, and performed pull-down assays as described above. As previously mentioned, the purified recombinant His-MBP-SifA Δext and His-MBP-SifB Δext were used as baits while the ectopically expressed GFP-CLIP4 protein was used as prey. As negative controls, I used His-MBP and His-MBP-EspT.

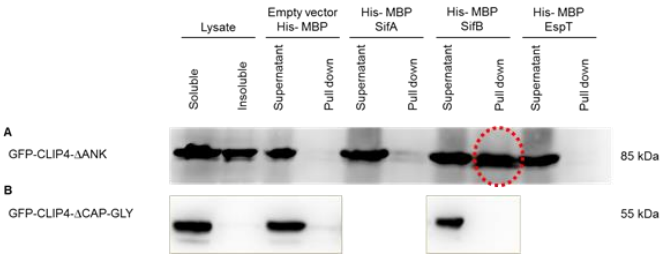


**Figure 26: Pull-down assays of SifB and C-terminal CAP-Gly-domains or an N-terminal ANK-repeats of CLIP4.** Hek293T cells were transfected with respective GFP-tagged constructs of CLIP4, lysed with ice-cold IP buffer and the lysates were incubated with recombinant proteins as described in chapter 3.3.5. Samples were analyzed by SDS-PAGE and visualized by Western Blotting with anti-GFP antibody. (A) Note that construct lacking the ANK repeats domains of GFP-CLIP4 binds SifB. (B) Note that construct lacking the CAP-Gly domains of GFP-CLIP4 does not bind SifB.

In summary, the above assays confirmed that SifB readily binded to CLIP4; this binding depended on the C-terminus of CLIP4 that harbored the CAP-Gly-domains (Figure 26 A) but not the N-terminal ANK repeats (Figure 26 B).

In order to confirm that the CAP-Gly domain region of CLIP4 was essential for the interaction with SifB, different deletion mutants of the C-terminal part of the full-length CLIP4 were tested in a subsequent pull-down assay.

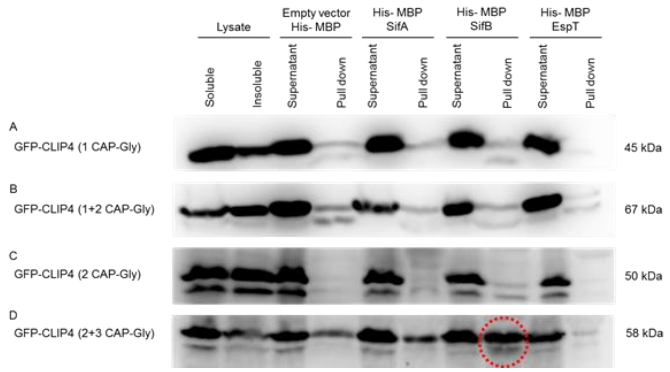


**Figure 27: Pull-down assays of SifB and C-terminally truncated CLIP4 mutants.** Hek293T cells were transfected with various truncated forms of GFP-CLIP4 constructs, lysed with ice-cold IP buffer and the lysates were incubated with recombinant proteins as described in chapter 3.3.5. Samples were analyzed by SDS-PAGE and visualized by Western Blotting with anti-GFP antibody. Note that constructs comprising the 1st CAP-Gly domain alone (A) or the 1st and 2nd CAP-Gly domain of CLIP4 (B) did not bind to SifB Δext, whereas a construct comprising the C-terminal 2nd and 3rd CAP-Gly domains significantly bound to SifB Δext.

The data showed that the region of CLIP4, which enclosed the 2$^{nd}$ and 3$^{rd}$ CAP-Gly domain and a basic serine region in between them at its C-terminal part, was necessary and sufficient for the interaction with SifB (Figure 27 D). An overview of the used domain constructs along with the results has been depicted in Figure 28.

Taken together, these results supported the idea that the full-length CLIP4 protein specifically interacted with the WxxxE domain of SifB (SifBΔext), but not with SifA (Figure 25 B). Furthermore, these experiments demonstrated that SifB-binding depended on the C-terminal CAP-Gly-domains (Figure 26 A), whereas no binding could be detected by either the N-terminal ANK-repeats (Figure 26 B) or the 1st CAP-Gly domain (Figure 4.18 A). Noteworthy, the 2nd and 3rd CAP-Gly domains also surrounded a central basic region which was apparently required in addition to the CAP-Gly domains (Figure 27 D).

Figure 28 illustrates the results of mapping of the interaction surface of CLIP4 and SifB.

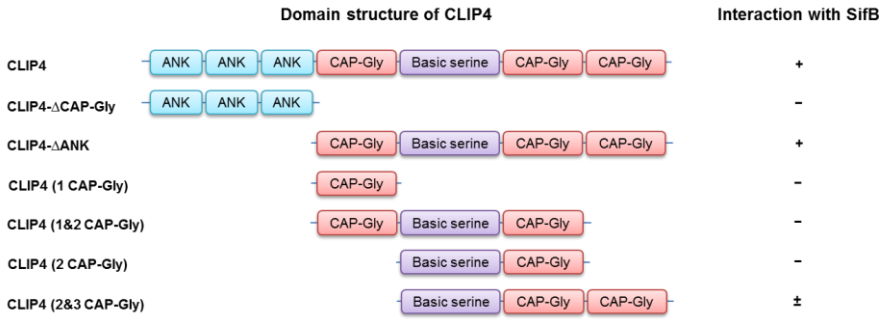


**Figure 28: Schematic summary of protein-protein interaction mapping.**

### 4.7.5 Subcellular localization of GFP-tagged CLIP3

The closest relative of CLIP4 within the CLIP protein family is CLIP3, also known as CLIPR-59 (Lallemand-Breitenbach et al., 2004). CLIP3 had been identified as a neuronal specific protein. Recent studies indicated that CLIP3 (CLIPR-59) interacted with the kinase domain of Akt via its first CAP-Gly domain (Ding et al., 2009). CLIP3 has been reported to regulate the membrane localization of Akt. In contrast to the other CLIP family members, the third member of the CAP-Gly family, CLIP3, localized to the trans-Golgi region and was involved in the early/recycling endosome–TGN transport pathway (Perez et al., 2002).

In order to investigate whether the interaction of SifB was specific to CLIP4 or also occured with CLIP3, we used full-length wild-type and mutant constructs of human CLIP3, a courtesy of Franck Perez (Institut Curie, Paris).


**Figure 29: Schematic domain overview of CLIP3 protein.** Abbreviations: ANK, ankyrin repeats; E/P, glutamate-proline rich; PMT, palmitoylation membrane-targeting motif.

In order to analyze intracellular localization of CLIP3 in our experimental system, Cos-7 fibroblasts were transiently transfected with respective GFP-tagged constructs of CLIP3, fixed 24 hours post transfection and labeled with antibodies to stain the Golgi apparatus.

As expected, we observed that ectopically overexpressed GFP-CLIP3 co-localized at the Golgi complex as visualized by the marker Giantin (Figure 30, top panel). In contrast to the wild-type CLIP3 protein, the localization pattern of CLIP3 mutated in two amino acid residues, C534A and C535A, was cytoplasmic (Figure 30, bottom panel). These results were in agreement with the previously published data (Perez et al., 2002).This showed that the CAP-Gly domain of CLIP3 possesses no independent MT-binding activity.

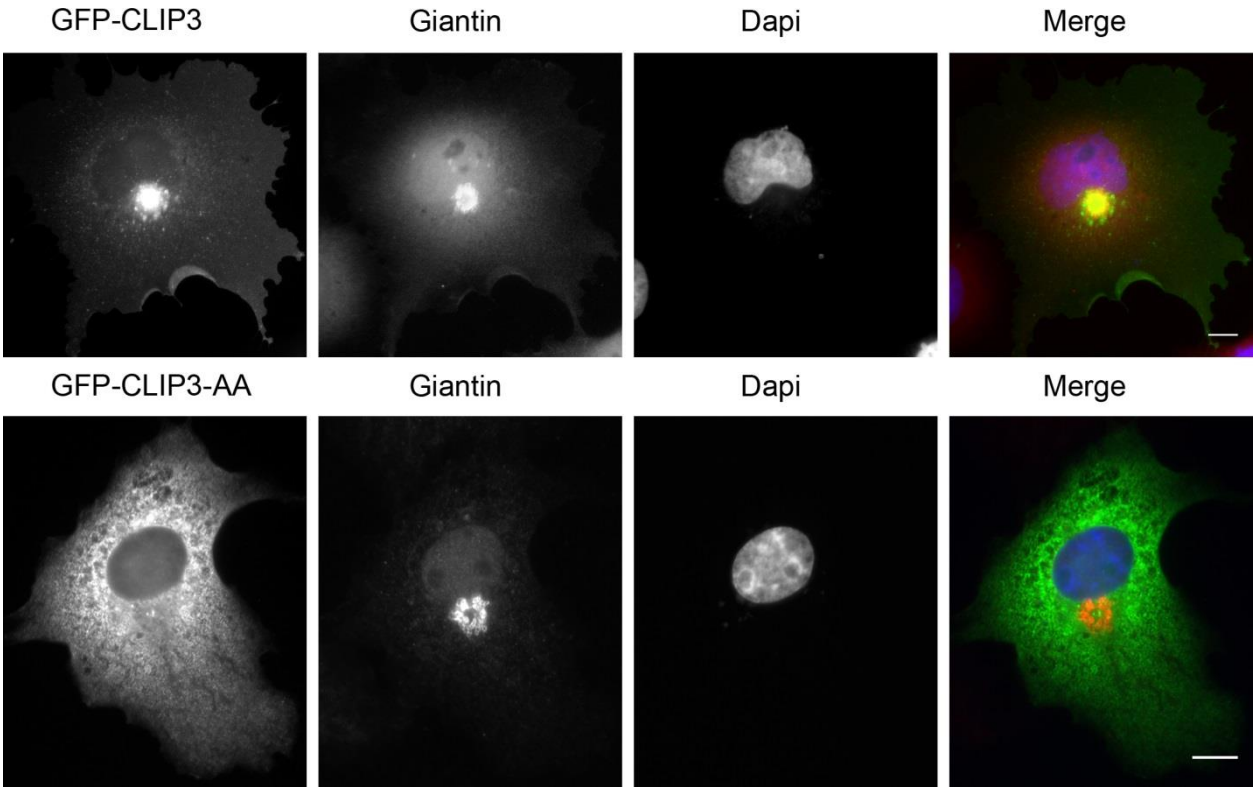


**Figure 30: GFP-CLIP3 localizes to the Golgi apparatus and trans-Golgi via its C-terminal isoprenylation motif (PTM domain).** Cos-7 cells were transfected with CLIP3 and its mutation form and fixed 24 hours later with PFA (chapter 3.4.2). Nuclei were stained with DAPI. Golgi was stained with anti-Giantin rabbit polyclonal antibody. The overlay shows the respective GFP-construct in green, Giantin in red and Dapi in blue. The scale bar indicates 10 µm. Note that the construct lacking the C-terminal isoprenylation motif (PTM domain) lost the ability to target to the Golgi region.

### 4.7.6 Biochemical analysis of the potential interaction between CLIP3 and SifB

In the next step, I investigated whether an interaction between CLIP4 and SifB is specific or whether other CAP-Gly proteins might also interact with SifB. First, I assessed the interaction between CLIP3, the closest relative of CLIP4, and SifB in a pull-down assay, as described above. Similarly to the previous pull-down assays, the purified recombinant His-MBP-EspT, His-MBP-SifA Δext and His-MBP-SifB Δext served as baits whereas the ectopically expressed GFP-CLIP3 protein served as prey. As a negative control, we used His-MBP. The results of the biochemical analyses are shown in Figure 31.

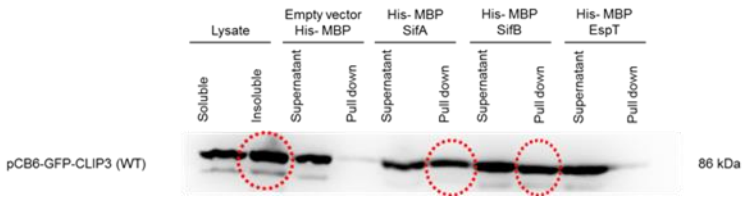


**Figure 31: Pull-down assays to probe binding of SifB to CLIP3.** Hek293T cells were transfected with wild type and mutant GFP-CLIP3 constructs, lysed with ice-cold IP buffer and the lysates were incubated with recombinant proteins. Samples were analyzed by SDS-PAGE and visualized by Western Blotting with anti-GFP antibody. Note that GFP-CLIP3 (WT) is largely insoluble and in addition occurs in the pull-downs of both SifA and SifB.

At this point, it is not clear whether the interaction between CLIP3 and the bacterial factors is plausible. In order to minimize false-positive results, ice-cold IP wash buffer containing 1% Triton X-100 (chapter 3.3.5) was supplemented with various concentrations (10-60 mM) of imidazole.

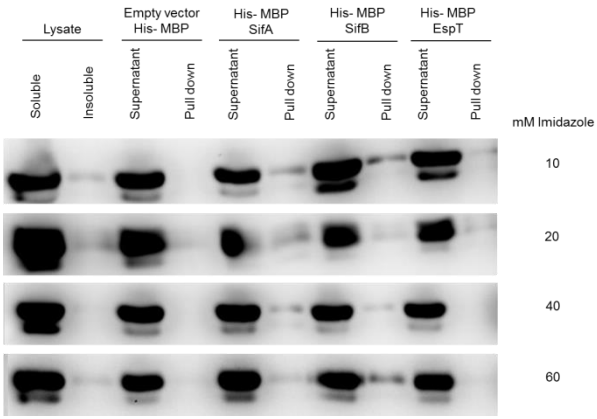


**Figure 32: Pull-down assays to probe binding of SifB to CLIP3 in the presence of imidazole.** Hek293T cells were transfected with GFP-CLIP3 construct, lysed with ice-cold IP buffer and the lysates were incubated with recombinant proteins. Samples were analyzed by SDS-PAGE and visualized by Western Blotting with anti-GFP antibody. Note lack of binding of CLIP3 to the respective bait with increasing imidazole concentration.

The data obtained in these experiments indicate that CLIP3 was not bound to SifA, SifB and EspT (Figure 32), as increasing concentration of imidazole in the wash buffer reduced nonspecific binding. Finally, it was found that CLIP3 is highly expressed in adipose tissue and brain (Ding et al., 2009). Therefore, we considered that CLIP3 unlikely plays a significant role in *Salmonella* infection, and excluded a potential involvement of the third member of CAP-Gly family in this process.

### 4.7.7 Biochemical analysis of the potential interaction between CLIP1-2 and SifB

CLIP1 (170) and CLIP2 (115) have been known as microtubule (MT)-Tip proteins. Both GFP-CLIP1-FL and GFP-CLIP2-FL localized to microtubule plus ends, a feature referred to as "plus-end tracking" ("+TIPs") (Akhmanova & Steinmetz., 2010; Akhmanova & Steinmetz., 2008; Galjart, 2005). Since CLIP4 binded to SifB via its CAP-Gly domains, and since this feature might be conserved in CLIP3 (see 4.7.6), I aimed at investigating whether the CAP-Gly domains of CLIP1 and CLIP2 had any affinity for SifB. To probe for the binding, I used the isolated CAP-Gly domains of CLIP1 (CLIP170) and CLIP2 (CLIP115), a courtesy of Dr. Marco Van Ham (HZI, Braunschweig). In Figure 33, the domain structures of mutant CLIP1 and CLIP2 have been presented.

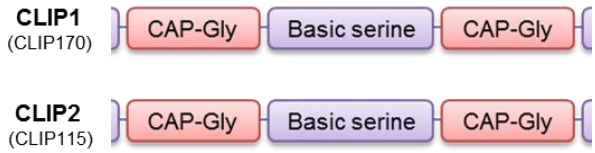


**Figure 33: Schematic representation of truncated CLIP1 and CLIP2 constructs used for pull-down assays.**

The potential interaction between the bacterial virulence protein SifA/B and the host protein CLIP1 or CLIP2 was further studied in the pull-down assays as described in chapter 3.3.5. Purified recombinant His-MBP-SifA Δext and His-MBP-SifB Δext were used as baits, and expressed GFP-CLIP1 or GFP-CLIP2 protein served as prey. As a negative control for our experiment, we used His-MBP and His-MBP-EspT.Representative results of the biochemical analysis have been illustrated in Figure 34.

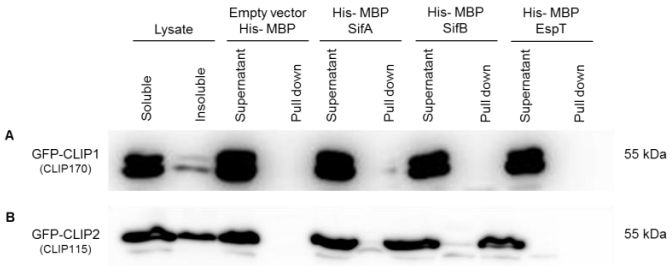


**Figure 34: Pull-down assays to probe for binding of SifB to CLIP1 and CLIP2.** Hek293T cells were transfected with GFP-CLIP1 or GFP-CLIP2 constructs, lysed with ice-cold IP buffer, and the lysates were incubated with recombinant proteins as described in chapter 3.3.5. Samples were analyzed by SDS-PAGE and visualized by Western Blotting with anti-GFP antibody. Note that neither GFP-CLIP1 nor GFP-CLIP2 bound by SifB.

Therefore, these results indicated that His-MBP-tagged SifB did not interact with +TIPs, such as GFP-tagged CLIP1 or CLIP2 (Figure 34).

In summary, the results presented in this section suggest that the bacterial virulence factor SifB specifically interacts with the fourth member of CAP-Gly family (CLIP4), but does not interact with other members of this family, although they share significant sequence similarities including common CAP-Gly domains, connected by a basic serine stretch.

### 4.7.8 Expression profile of CLIP4 in primary human and mouse tissues

To gain more insights into the expression pattern of CLIP4 I have searched in the NCBI GEO database (http://www.ncbi.nlm.nih.gov/geo/). The data were complemented with those from the human Protein Atlas (http://www.proteinatlas.org/). High expression of endogenous CLIP4 was observed in smooth, skeletal and heart muscles, bone marrow and some inner organs including the gut, whereas no expression was observed e.g. in thyroid gland, spleen and liver (Figure 35).

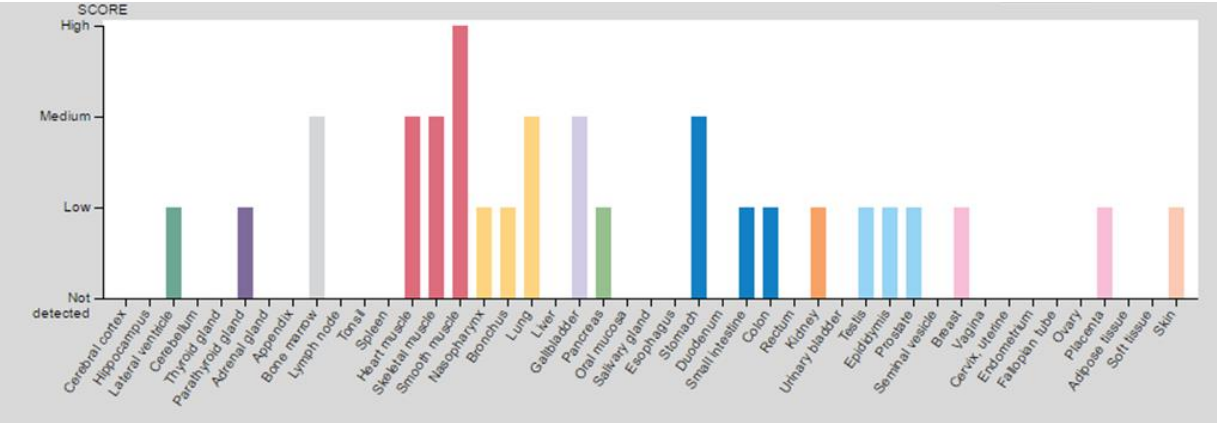


**Figure 35: Expression of CLIP4 in primary human tissues.** Data were extracted from the human Protein Atlas resource.

According to the NCBI database and Ensembl genome browser, there have been four splice variants of CLIP4 reported in mice (Table 39).

**Table 39: Mouse CLIP4 splice variants**

| Splice variants | Amino Acids | Molecular weight |
|---|---|---|
| CLIP4-isoform 1 | 704 | 76 kDa |
| CLIP4-isoform 2 | 551 | 59 kDa |
| CLIP4-isoform 3 | 694 | 75 kDa |
| CLIP4-isoform 4 | 598 | 64 kDa |

Next, I asked where CLIP4 protein might be expressed in primary mouse tissues. To answer this question, I analyzed protein expression of CLIP4 in murine tissue lysates by Western blotting using a polyclonal antibody against CLIP4 and compared it to that in human tissues. Isolation of primary mouse tissues was performed by Stephanie Stahnke (HZI, Braunschweig) as described in the chapter 3.7. It should be noted that splice variants of a significantly reduced size were present in the muscle, but not depicted on the gel below.

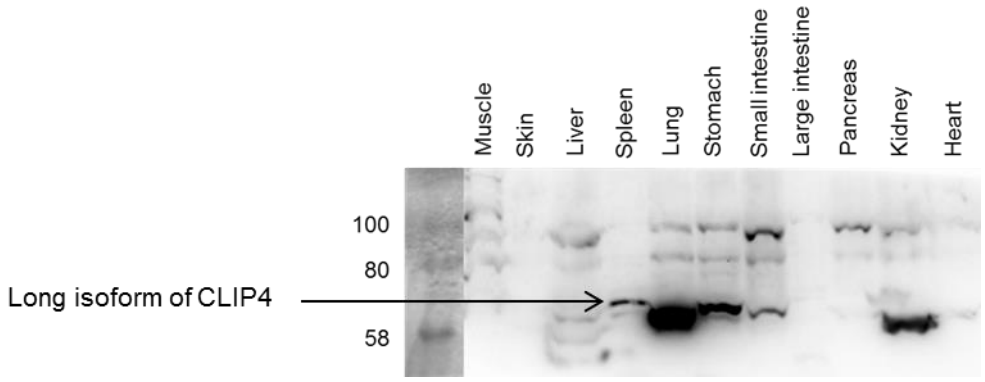


**Figure 36: Expression pattern of CLIP4 in primary mouse tissues visualized on Western blot.** Lysates of mouse tissue samples were mixed with 4x SDS sample buffer, subjected to SDS-PAGE and the endogenous level of CLIP4 was detected by Western blotting using polyclonal anti-CLIP4 antibody. The expected molecular weight of long form of CLIP4 is 76 kDa

I observed that the CLIP4 protein was expressed in stomach, spleen and small intestine. In addition, a slightly smaller band was observed in lung and kidney that might likely correspond to a CLIP4 splice variant. Note that all bands detected in tissues might not correspond to the longest splice variant, because the latter showed an apparent molecular weight of 76 kDa (compare Figure 38). In other tissues, expression of the long variant of CLIP4 was either absent or close to the detection limit of Western blotting. CLIP4 in heart and skeletal muscle most likely corresponded to the short variants (personal communication with Prof. Dr. Holly Goodson) and the specific antibody used here could not detect it.

### 4.7.9 Characterization of CLIP4 protein expression in different cell types.

Next, we compared the mRNA expression profile of CLIP4 to that of other members of CAP-Gly family in different cell lines. For that, we analyzed the datasets from Gene Chip analysis that were obtained in earlier projects.

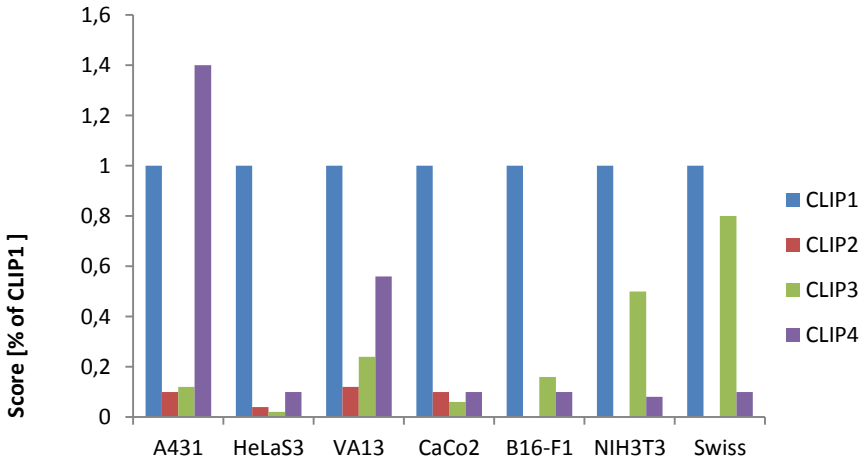


**Figure 37: Expression levels of CLIP2-4 normalized to CLIP1 assessed by microarray analyses of different cell lines.**
Note high expression of CLIP4 mRNA levels in A431.

Significant differences of CLIP4 expression levels were observed between cell lines: a relatively high and an average amount of RNA in A431 and VA13, respectively, and its virtual absence in the other lines tested, such as HeLaS3, CaCo2, B16-F1, NIH3T3 and Swiss3T3. It would be worth to mention that the expression of CLIP4 in A431 cells was even higher than that of the abundant CLIP1, which was set to the arbitrary level 1 for comparability. Analysis of CLIP2-4 expression profiles indicated that these proteins had similar expression levels in HeLaS3 and CaCo2 cells. I also observed that CLIP3, which was the closest relative to CLIP4, was expressed (8 times more than CLIP4) in the Swiss cell lines. In conclusion, the data suggested that CLIP4 RNA was absent in virtually every cell line studied, except A431 and VA13 cell lines. Next, the protein expression of the endogenous CLIP4 protein was analyzed in human and mouse cell lines using Western blotting. For that, Hek293T cells were transfected with untagged CLIP4, which served as control for the determination of the apparent molecular weight in SDS-PAGE.

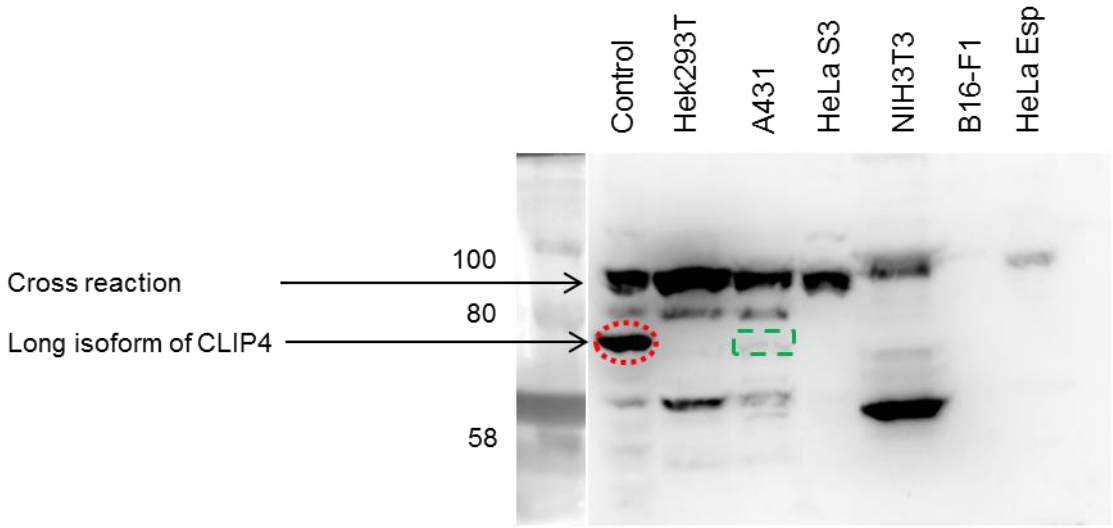


**Figure 38: Western blotting analysis of CLIP4 protein expression in human and mouse tissues.** Cells were lysed with 4x SDS buffer, the lysates were applied to SDS-PAGE and the proteins were visualized by Western blotting using polyclonal anti-CLIP4 antibody. Hek293T cells transfected with untagged CLIP4 served as control.

Expression of CLIP4 was hardly detectable in almost all cell lines. In accordance with GeneChip analyses, mRNA of CLIP4 was absent in Hek293 and NIH3T3 cells. However, the CLIP4 protein was weakly expressed in A431 cells as a weak signal corresponding to the predicted molecular weight of CLIP4 (76 kDa) could be observed. The presence of additional bands indicated non-specific binding of polyclonal antibodies to the membrane because these bands were equally present in cells lacking CLIP4 RNA and, hence, the protein. We could not exclude that the band at ~59 kDa corresponded to a smaller splice variant.

It would be worth mentioning that the expression of endogenous CLIP4 protein was found predominantly in tissues that contain mainly quiescent or postmitotic cells (GEO database), but not in constantly dividing cells such as continuously cultivated tissue cells, where the amount of CLIP4 was about the detection limit of Western blot analysis or absent (see Figure 37 and 38).

### 4.7.10 Generation of human CLIP4 knockout cell lines using CRISPR/Cas9 Genome Engineering Tool

Since nothing was known about the biological function of the fourth member of CAP-Gly family (CLIP4), we aimed to address this question using the CRISPR/Cas9 system, which allowed to knock out a gene of interest in any cell lines. For this purpose, we employed A431 cell lines using this powerful and elegant technique. We generated several constructs of pSpCas9 (BB)-2A-GFP which harbors sgRNAs targeting CLIP4, as described in chapter 3.6. Representative sequencing results of a plasmid DNA comprising guide sequences have been demonstrated in Figure 39.

**pSpCas9 (BB)-2A-GFP containing sgRNA targeting CLIP4 (exon 2)**

AAAGGACGAAACACCGTCCTGGCATGATGCATCATTGTTTTAGAGCTTTTCCTGC
TTTGTGGCAGGACCGTACTACGTAGTAACAAAATCTCGA

**pSpCas9 (BB)-2A-GFP containing sgRNA targeting CLIP4 (exon 4)**

AAAGGACGAAACACCGACATTAGTTTGCGGAGTCGCGTTTTAGAGCTTTTCCTGC
TTTGTGGCTGTAATCAAACGCCTCAGCGCAAAATCTCGA

**WT pSpCas9 (BB)-2A-GFP**

AAAGGACGAAACACCGGGTCTTCGAGAAGACCTGTTTTAGAGCT

TTTCCTGCTTTGTGGCCCAGAAGCTCTTCTGGACAAAATCTCGA

**Figure 39: Sequencing results confirm cloning of sgRNAs into pSpCas9(BB)-2A-GFP.**The color code is as follows: annealed sgRNAs targeting the gene of interest (black), U6 promoter (green), overhangs (blue), additional G or C (red), and sgRNA scaffold (orange).

According to the standard procedure, A431 cells were transfected with two different pSpCas9 (BB)-2A-GFP plasmids which carry the sgRNA targeting CLIP4. I then analyzed the transfected cells using flow cytometry by Lothar Gröbe (HZI, Braunschweig). The results of the FACS analysis have been depicted in Figure 40.

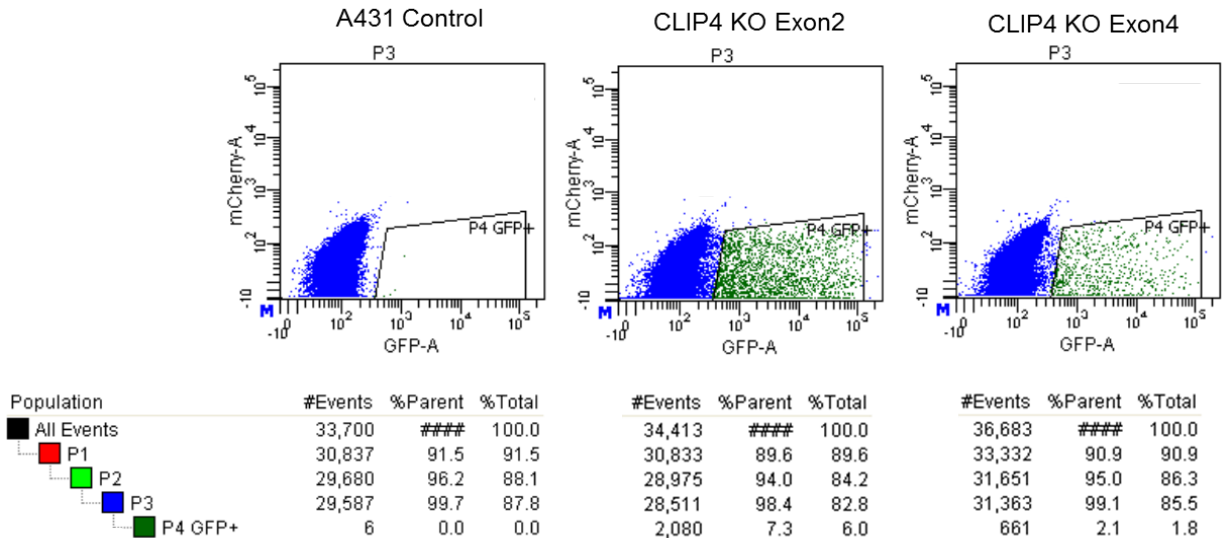


| Population | #Events | %Parent | %Total | #Events | %Parent | %Total | #Events | %Parent | %Total |
|---|---|---|---|---|---|---|---|---|---|
| All Events | 33,700 | #### | 100.0 | 34,413 | #### | 100.0 | 36,683 | #### | 100.0 |
| P1 | 30,837 | 91.5 | 91.5 | 30,833 | 89.6 | 89.6 | 33,332 | 90.9 | 90.9 |
| P2 | 29,680 | 96.2 | 88.1 | 28,975 | 94.0 | 84.2 | 31,651 | 95.0 | 86.3 |
| P3 | 29,587 | 99.7 | 87.8 | 28,511 | 98.4 | 82.8 | 31,363 | 99.1 | 85.5 |
| P4 GFP+ | 6 | 0.0 | 0.0 | 2,080 | 7.3 | 6.0 | 661 | 2.1 | 1.8 |

**Figure 40:Flow cytometric analysis of human epithelial tumor A431 cells transfected with pSpCas9 (BB)-2A-GFP which contains sgRNAs targeting for CLIP4.** CLIP4 KO Exon2 and CLIP4 KO Exon4 cells were transfected with the respective pSpCas9 (BB)-2A-GFP-tagged constructs. All Events = total cell population, P1 = living cells, P2 = single living cells, P3 = single living cells, GFP- and mCherry-negative, P4 = single living cells, GFP- positive.

During flow cytometry, we detected a small population of about 6% of GFP-positive A431 cells transfected with pSpCas9 (BB)-2A-GFP containing sgRNAs targeting the second exon of CLIP4. As shown in Figure 40, around 1.8% of living A431 cells were positive for pSpCas9 (BB)-2A-GFP containing sgRNAs targeting the fourth exon of CLIP4. In this experimental setup, A431 WT cells served as negative control for GFP expression. From this, we isolated more than 96 clones of a potential CLIP4 knockout cells in the locus. Next, the cells were expanded and cryopreserved as described in chapter 3.2.3.

In parallel to the generation of knockout cell lines, we continued to monitor CLIP4 protein expression. However, we were unable to detect significant protein amount of endogenous CLIP4 (76 kDa) in WT A431 cells after long-time tissue culturing and subcloning. Since the expression of CLIP4 was no longer detectable in WT A431 cells, I could not confirm protein rundown in potential CLIP4 knockout cell lines using Western blot analysis (data not shown). Therefore, at this point, I couldnot carry out experiments with possible CLIP4 knockout A431 cell lines. In the future I would plan to target CLIP4 in C2C12 cells and differentiate these into myotubes expressing CLIP4. The upregulation of CLIP4 in C2C12 cells upon myotube differentiation was repeated before us by colleagues (personal communication with Prof. Dr. Holly Goodson and PhD Thesis of Jill S. Voreis).

### 4.7.11 Generation of monoclonal antibodies to SifA and SifB

It has been well known that SifA plays a key role in SIFs formation, but a particular function of SifB during *Salmonella* infection has still remained poorly understood. To further study physiological properties of SifB, I aimed at generating specific antibodies against SifA and SifB in collaboration with Sabine Buchmeier from the Antibody Facility of the Technical University Braunschweig. For this purpose, SifA Δext and SifB Δext proteins were overexpressed in *E. coli* BL21 (DE3) using the pET-41vector and purified as 6xHis-tagged fusion proteins as described in chapter 3.3.4. The immunization procedure lasted around 7-10 weeks and was performed as follows. Briefly, BALB/c mice were immunized with 50 mg of the purified SifA and SifB proteins, and the following steps of antibody generation were carried out according to the standard procedure. The first ELISA screening results indicated 96 positive clones for SifA and 65 positive clones for SifB. Next, in order to identify the most promising ones, the clones were expanded and the antibody titers were determined by ELISA. To confirm ELISA results and to assess specificity of the antibody, we employed Western blot assays using different controls. Of all clones tested, only clone 7H8 and corresponding subclones demonstrated a satisfactory signal (Figure 41). No antibody to SifB, however, could beisolated.

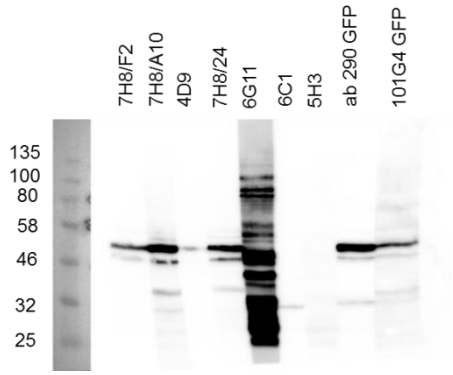


**Figure 41:Western blot analysis using the newly generated anti-SifA antibody.** Hek293T cells were transfected with GFP-SifA and then lysed with 4x SDS buffer. The lysates were subjected to SDS-PAGE and analyzed by Western blotting using newly generated anti-SifA (7H8/F2, 7H8/A10, 4D9, 7H8/24, 6G11, 6C1 and 5H3) and anti-GFP (ab 290 and 101G4) antibodies. The expected molecular weight of SifA is 54 kDa.

As depicted in Figure 41, the produced antibodies against SifA, such as 7H8/F2, 7H8/A10 and 7H8/24, allowed to detect protein bands corresponding to the predicted molecular weight of SifA (54 kDa) in extracts of GFP-SifA transfected cells. Detection with anti-GFP (ab290 and 101G4) antibodies served as positive control.

Finally, the positive clones of SifA antibody (7H8/F2, 7H8/A10 and 7H8/24) were chosen based on the results obtained from ELISA and Western blot analysis of recombinant and over expressed proteins.

However, our attempts to produce anti-SifB antibodies were not successful in two independent rounds. Nevertheless, the produced SifA (7H8/F2, 7H8/A10 and 7H8/24) antibodies were shown to specifically recognize the protein of interest.

### 4.7.12 Subcellular localization of GFP-tagged SifB and the co-localization studies of GFP-CLIP4 and Myc-SifB

Although SifB by sequence would be highly related to SifA, the exact functions of SifB were still not well defined. In order to gain insights into subcellular localization of the bacterial virulence factor SifB, we performed immunofluorescence analysis of Cos-7 fibroblasts transiently transfected with GFP-SifB. Cells were fixed 24 hours post transfection, permeabilized and stained with phalloidin to label F-actin and with DAPI to visualize nuclei. The results of this experiment indicated that the ectopically expressed GFP-SifB Δext widely distributed in the cytoplasm (Figure 42, top panel).

Next, I extended my observation and examined a potential co-localization of CLIP4 and SifB in Cos-7 fibroblasts. As observed earlier, SifB alone appeared mainly cytoplasmic (Figure 42, top panel), whereas overexpression of both GFP-CLIP4 and Myc-SifB proteins strikingly resulted in a partial co-localization on microtubules (Figure 42, middle panel). These data suggested that the microtubule-binding protein CLIP4 in principle had the capability to recruit SifB to microtubules. This finding together with the results of Y2H screening and pull-down assays corroborated the specificity of CLIP4-SifB interaction.

In Figure 42 (bottom panel), cells expressing GFP-CLIP4 were also labeled with an antibody against Myc-tag and stained with DAPI. We observed that, in some cases, anti-Myc antibodies weakly stained microtubule-like pattern in untransfected Cos-7 cells. However, there was a significant difference between the background staining of Myc antibodies in the cells expressing only GFP-CLIP4 or co-expressing GFP-CLIP4 and Myc-SifB.

Taken together, the data presented in Figure 42 reveal that the bacterial virulence factor SifB alone was distributed in the cytoplasm, but was recruited to MTs in the presence of GFP-CLIP4. It should be emphasized that association of SifB with CLIP4 occurred most

prominently on microtubules. These data strongly supported the idea that host microtubule-binding protein CLIP4 interacted with and recruited the bacterial virulence factor SifB onto microtubules. Besides, it was clearly shown that SifB, although binds in the CAP-Gly region of CLIP4, does not interfere with microtubule-binding of CLIP4.

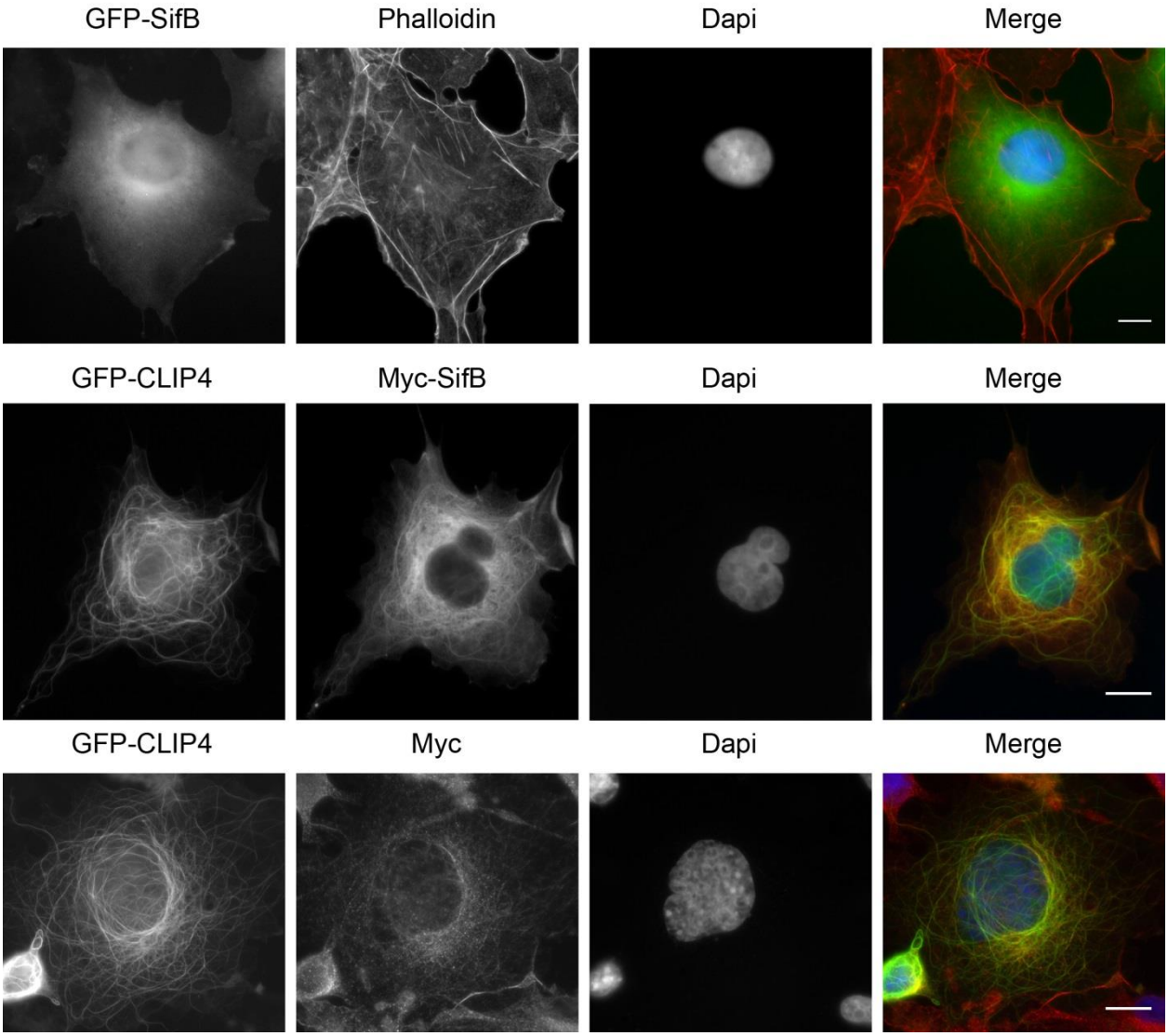


**Figure 42: Subcellular localization of GFP-tagged SifB and co-localization studies of CLIP4 & SifB in Cos-7 fibroblasts.** Cos-7 cells were transfected with respective constructs, fixed 24 hours later with PFA and permeabilized (chapter 3.4.2). Nuclei were stained with DAPI. The actin cytoskeleton was stained with red phalloidin. Myc-tagged SifB protein was labeled with mouse anti-Myc antibody. Merge shows an overlay of green (the respective GFP-construct), red (phalloidin or anti-Myc) and blue (Dapi) channels. The scale bar indicates 10 μm.

### 4.7.13 Formation of *Salmonella*-induced filaments (SIFs) during infection with WT *Salmonella* in host cells

Many research groups contributed to the investigation of *Salmonella*-Induced Filaments (SIFs) from different aspects. During the last decade, growing interest within this area helped to deepen our understanding of *Salmonella* infection.

In order to analyze a possible function of CLIP4 during *Salmonella* infection, I first studied SIFs formation using time-lapse microscopy. Previous studies demonstrated that SIFs were rich in late endocytic markers, such as lysosome-associated membrane proteins (LAMPs). This fact made it possible to monitor the dynamic process of formation of a *Salmonella*-induced tubular network in a time-lapse experiment using cells stably expressing GFP-tagged LAMP1.

HeLa cells stably expressing GFP-LAMP1 (a courtesy of Prof. Dr. Mischael Hensel, University of Osnabrück) were seeded onto Ø 35 mm glass bottom µ-dishes (Ibidi) coated with fibronectin (chapter 3.4.2.5). Next, we infected these cells with wild type *Salmonella enterica* serovar Typhimurium SL1344 as described in chapter 3.5.

As expected, after 2 h.p.i. intracellular bacteria (visible in phase contrast, not shown) were detected in the SCV (yellow arrows Figure 43 left top panel). Approximately 2.5 h.p.i., elongated filaments started to form from SCV in infected cells (red arrows, Figure 43). Later, long highly dynamic membrane tubules and a tubular network developed over time. The data of time-lapse microscopy represented in Figure 43 perfectly demonstrate almost the entire process of infection starting with the formation of the specialized vacuole (SCV) during the early stage of infection and the appearance of LAMP1-containing membrane tubules emanating from the SCV at later time points p.i. In agreement with previously published results, we confirmed that SIFs are extensive, highly dynamic membrane tubules, which start appearing upon infection with *Salmonella* (Garcia-del Portillo et al., 1993).

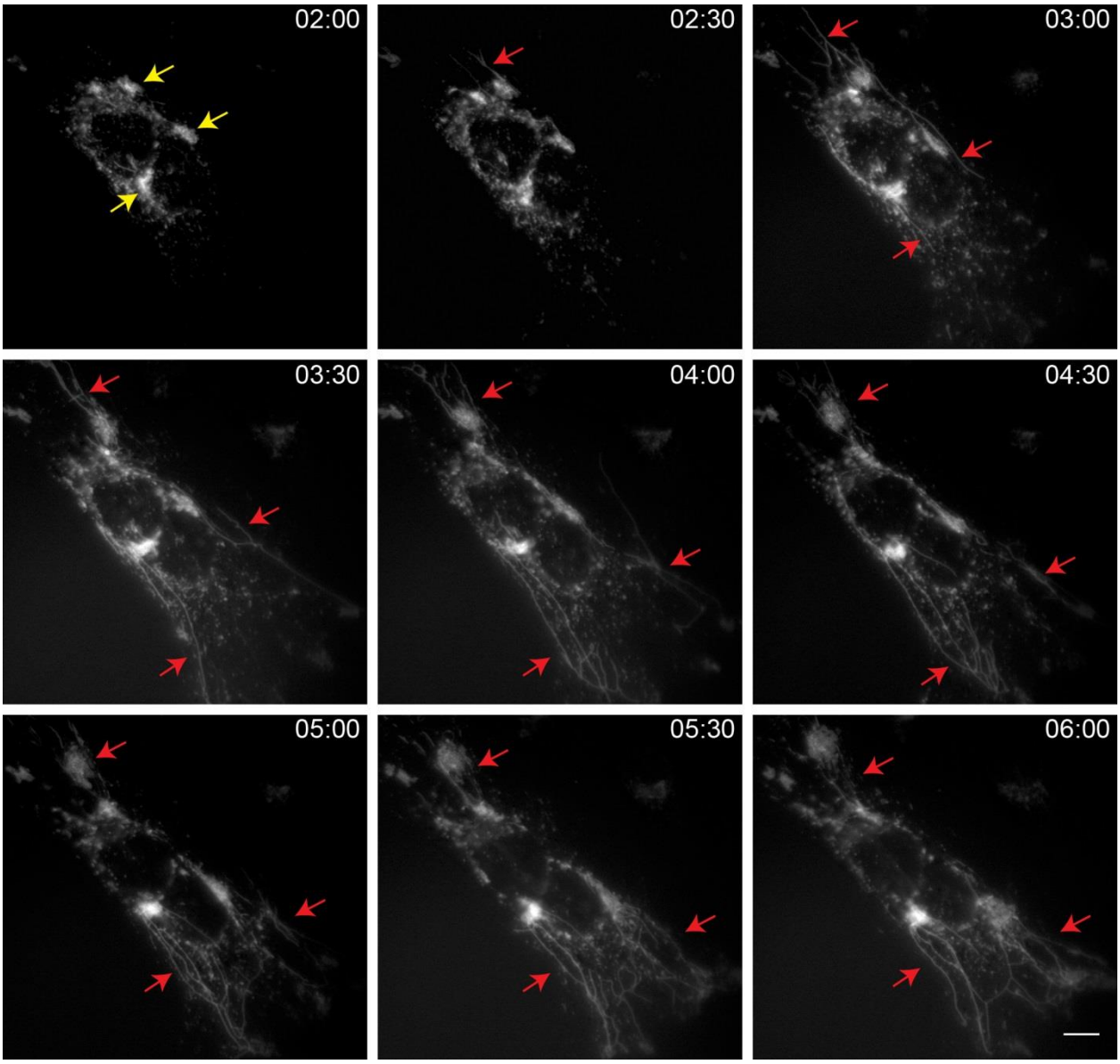


**Figure 43: Time-lapse imaging of the formation of *Salmonella*-induced filaments (SIFs).** HeLa cells stably expressing GFP-LAMP1 were seeded on a 3.5 cm glass bottom dish (Ibidi) coated with fibronectin and then infected with wild type Salmonella. After 20 min of infection cells were washed several times and incubated for 1 h in medium containing 100 µg/ml gentamicin. The concentration of gentamicin was then decreased to 10 µg/ml for the rest of the infection. Dynamics of the formation Salmonella-induced filaments (SIFs) in host cells was visualized using a Nikon BioStation IM (40X magnification) over 12 hours in 5 min intervals as described in chapter 3.4.2.5. Yellow arrows highlight SCVs (Salmonella not shown), demonstrating apparent enrichment in GFP-LAMP1. SIFs emanating from the SCV are marked with red arrows. The scale bar indicates 10 µm. The images were extracted from the supplementary movie 2. The time is shown in the upper right corner of each image and indicates hours starting from the time point of infection.

### 4.7.14 Infection assay with WT *Salmonella* in host cells

To gain more insight into the possible function of CLIP4 during *Salmonella* infection, I performed time-lapse microscopy. I aimed at designing an experiment that could uncover the role of host CLIP4 interacting with the bacterial factor SifB. For this purpose, HeLa cells stably expressing GFP-LAMP1 were transfected with mCherry-labeled CLIP4 and then re-plated onto glass-bottom dishes coated with fibronectin. Next, we infected these cells with wild type, SifA- and SifB-defective *Salmonella* as described in chapter 3.5. Comparison of the processes of infection with a wild type and a mutant *Salmonella enterica* serovar Typhimurium were expected to be appropriate to uncoverthe molecular role of this interaction. However, it was rather difficult to perform this experiment because the mCherry signal of CLIP4 was weak and very sensitive to bleaching.

As shown in Figure 44, two processes could be simultaneously monitored over time in HeLa cells stably expressing GFP-LAMP1: 1) the formation of SCV and SIFs upon infection with WT *Salmonella enterica* serovar Typhimurium SL1344 (left panel), and 2) the dynamics of host microtubules decorated with mCherry CLIP4 protein (middle panel). In the upper panel at 2 h.p.i. the formation of SCV (left top panel, yellow arrows) is shown. In accordance with previous studies, approximately after 5 h.p.i. LAMP1-positive filamentous structures extend from this special vacuole. It was worth noting that SIFs align along MTs which were decorated with CLIP4. In order to perform detailed visualization of co-localization of CLIP4 and SIFs, high-resolution microscopy should be employed. In the future we would use a super resolution video microscope, namely 3D-SIM, in order to visualize this situation.

The results of time-lapse imaging of two simultaneous processes indicated that SIFs, which embody highly dynamic membrane tubules, aligned along CLIP4-labelled MTs during infection with WT *Salmonella*.

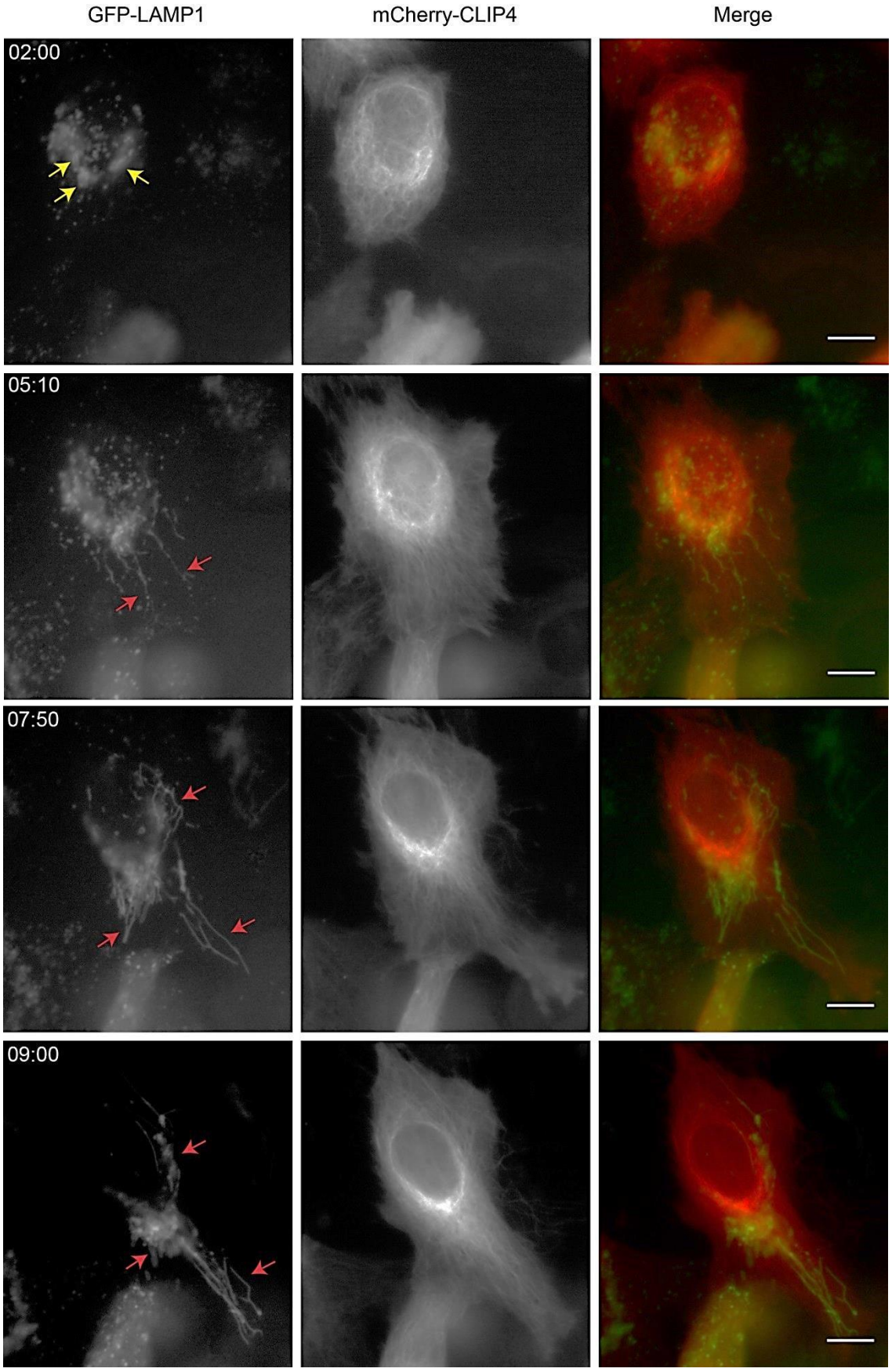


**Figure 44: Time-lapse imaging of mCherry-CLIP4 during infection with WT Salmonella in GFP-LAMP1-expressing cells.**

HeLa cells stably expressing GFP-LAMP1 were transfected with mCherry-tagged CLIP4 construct and seeded on a 3.5 cm glass bottom dish (Ibidi) coated with fibronectin. Cells were infected with wild type *Salmonella*, washed after 20 min and incubated for 1 h in the medium containing 100 µg/ml gentamicin. The concentration of gentamicin was then decreased to10 µg/ml for the rest of the infection. mCherry and GFP -signals were visualized using Nikon BioStation IM (40X magnification) over 12 hours in 10 min intervals. Merge shows an overlay of green (GFP-LAMP1) and red (mCherry-CLIP4) channels. Yellow arrows highlight SCVs (*Salmonella* not shown), clearly enriched in GFP-LAMP1. SIFs emanating from the SCV are marked with red arrows. The scale bar indicates 10 µm. The images were extracted from the supplementary movie 3. Time points are indicated as h:min in the upper left corner of each image starting from the time point of infection.

### 4.7.15 Infection assay with SifA defective *Salmonella* in host cells

SifA is fundamental for the formation of tubular membrane extensions from SCV in HeLa cells, and its deficiency would result in complete loss of SIFs (Mills, 1998; Stein, 1996). In HeLa cells infected with a *Salmonella* strain lacking SifA, but harboring SifB, the latter could not induce SIFs. In this study, we were therefore interested whether the presence of CLIP4 might enable *Salmonella* to form SIFs via SifB in the absence of SifA. Pursuing the aim to study this possibility, HeLa cells stably expressing GFP-LAMP1 were transfected with mCherry-labeled CLIP4 and then infected with a mutant *Salmonella* strain deficient in SifA (as described in chapter 3.5.).

The data presented in Figure 45 nicely demonstrate that CLIP4-positive transfected cells were infected with *Salmonella* SifA mutant strain. In addition, after 2 h.p.i. mature SCVs were formed as shown in Figure 45 (top panel), with yellow arrows pointing to intracellular niches of bacteria. Even after 5 h.p.i. we did not observe the appearance of SIFs network (Figure 45, middle panel). Even after 7 hours,overexpression of CLIP4 inHeLa cells stably expressing GFP-LAMP1 and infected with SifA-defective *Salmonella* did not induce formation of tubular networks (Figure 45, bottom panel), in contrast to the cells infected with WT *Salmonella* (Figure 43).

Furthermore, microscopic time-lapse studies of the behavior of individual cells during *Salmonella* infection with a SifA-defective strain demonstrated no formation of SIFs in the presence of CLIP4 over the 12 hours observation period (not shown). This led to the conclusion that CLIP4 dids not enable formation of extensive tubular membrane network upon infection with SifA-deficient *Salmonella* in HeLa cells. However, as shown by Freeman et al., SifB was expressed very late, after approximately 20 hours post infection (Freeman et al., 2003).Therefore, it was concluded that SifA, but not SifB, is essential for SIF formation. However, no binding partner for SifB has been known (Freeman et al., 2003) and neither of

currently available cell lines expressed CLIP4. Current experiments would aim at studying the behavior of ΔSifA *Salmonella* in CLIP4-expressing cells upon prolonged infection beyond 20 h.p.i.

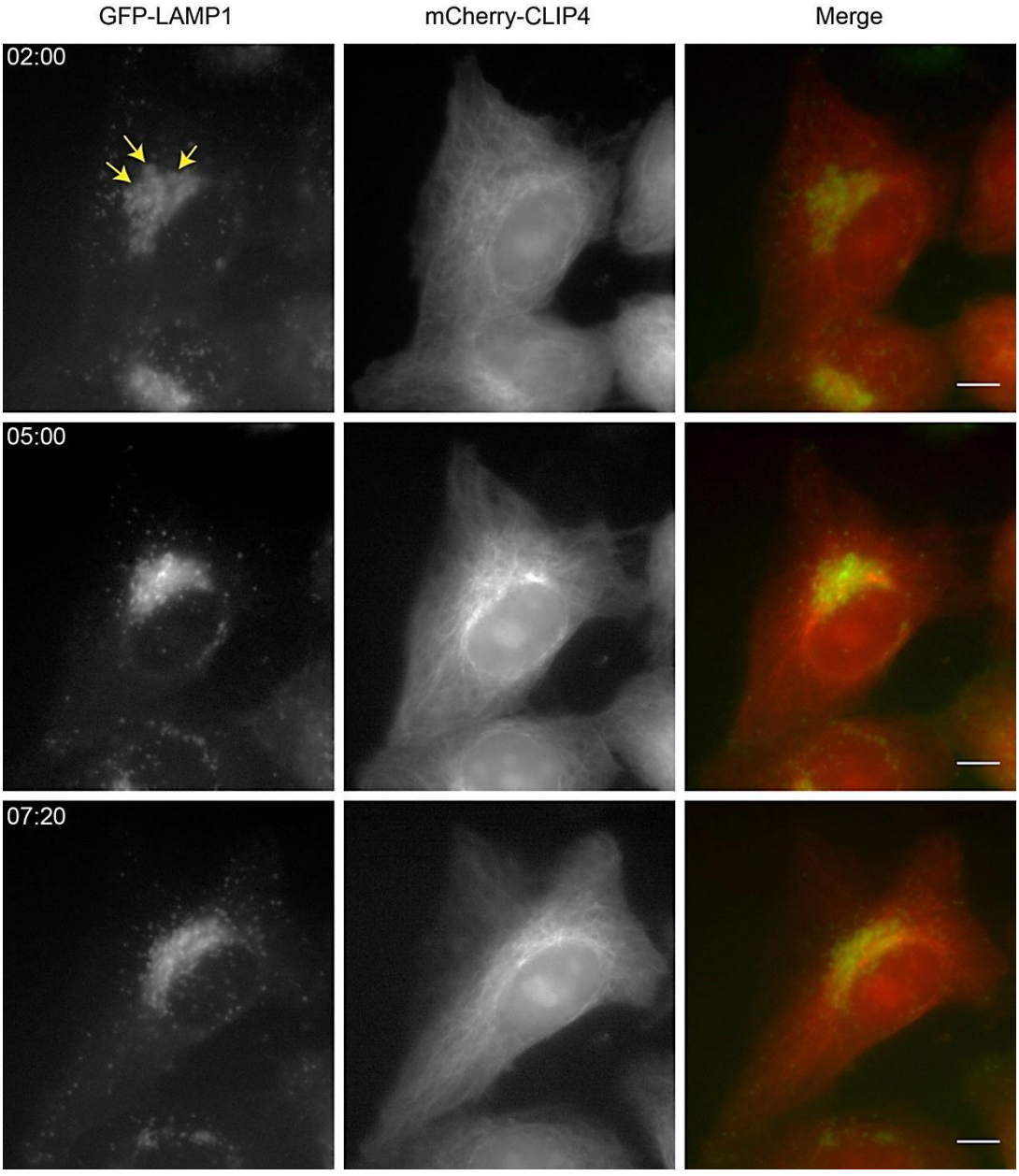


**Figure 45: Time-lapse imaging of mCherry-CLIP4 during infection with SifA defective Salmonella in GFP-LAMP1-expressing cells.** HeLa cells stably expressing GFP-LAMP1 and transiently transfected with mCherry-tagged CLIP4 construct were seeded on a 3.5 cm glass bottom dish (Ibidi) coated with fibronectin. Cells were infected with SifA-defective Salmonella. After 20 min post infection, the cells were washed several times and incubated for 1 h in the medium containing 100 μg/ml gentamicin. The concentration of gentamicin was then decreased to 10 μg/ml for the rest of the infection. mCherry and GFP-signals were visualized using a Nikon BioStation IM (40X magnification) over 12 hours in 10 min intervals. Merge shows an overlay of green (GFP-LAMP1) and red (mCherry-CLIP4) channels. Yellow arrows highlight SCVs (Salmonella not shown), demonstrating apparent enrichment in GFP-LAMP1. SIFs emanating from the SCV are marked with red arrows.

### 4.7.16 Infection assay with SifB defective *Salmonella* in host cells

In contrast to the critical role of SifA in the formation of SIFs, SifB was not known to be involved in this process. In the next experiments, I tested whether intracellular phenotypic differences occur when the cells were infected with a SifB mutant strain. Corresponding images have been shown in Figure 46.

I observed a typical formation of the SCV membrane and long tubules enriched in LAMP1, which extended from the SCV also with SifB-defective *Salmonella* (Figure 46, left panel). In accordance with the previously published data (Freeman et al., 2003), deletion of the bacterial virulence factor SifB appeared to have no dramatic effect on the cell's behavior during *Salmonella* infection and in the presence of CLIP4 (Figure 46).

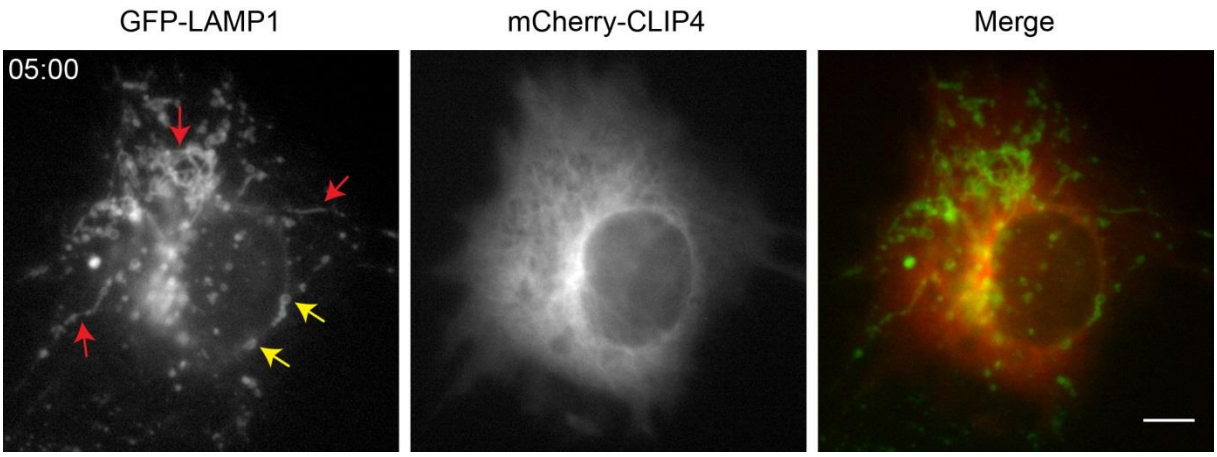


**Figure 46: Time-lapse imaging of mCherry-CLIP4 during infection with SifB defective Salmonella in GFP-LAMP1-expressing cells.** HeLa cells stably expressing GFP-LAMP1 and transfected with mCherry-tagged CLIP4 were seeded on a 3.5 cm glass bottom dish (Ibidi) coated with fibronectin. Cells were infected with SifB-defective *Salmonella*, washed after 20 min post infection and incubated for 1 h in the medium containing100 µg/ml gentamicin. The concentration of gentamicin was then decreased to10 µg/ml for the rest of the infection. mCherry-CLIP4 and GFP-LAMP1 were visualized with Nikon BioStation IM (40X magnification) over 8 hours in 10 min intervals. Merge shows an overlay of green (GFP-LAMP1) and red (mCherry-CLIP4) channels. Yellow arrows highlight SCVs (*Salmonella* not shown), clearly enriched in GFP-LAMP1. SIFs emanating from the SCV are marked with red arrows. The scale bar indicates 10 µm. The time is indicated in h: min, starting from the time point of infection.

Taken together, the above data allowed me to conclude that there was no significant difference in SIF formation regardless of presence or absence of CLIP4 or SifB. The presence or absence of neither SifB nor CLIP4 affected the known dynamics of SIF-formation in HeLa cells. However, the long-term fate of *Salmonella* and very late stages of SIF formation would still need to be analyzed.

# 5. DISCUSSION

This study aims at determining novel binding partners of bacterial virulence factors that belong to the WxxxE family. First, the Y2H screening is performed to identify new host-pathogen interactions where WxxxE effector proteins were used as baits and a human cDNA-based protein library as prey. The identified Y2H hits are evaluated and pre-selected based on known or expected biological functions and localization of these proteins.Next, we define a set of putative interaction pairs, among them APPL1/EspT, Cep70/SifA, DYNLRB1/SifA, and CLIP4/SifB, and analyse them using biochemical and microscopic techniques. Unfortunately, the interaction between APPL1 and EspT cannot be readily confirmed under the chosen experimental conditions. Therefore, I did not continue this subproject in the framework of this thesis. Notwithstanding this, EspT is included as a control for biochemical experiments with SifA and SifB because it belongs to the same protein family but is expected to have entirely different functions.

## 5.1 SifA and its host interaction partners

*Salmonella* that successfully reached the intracellular space secretes an array of bacterial virulence factors, among themSifA, into the host cytoplasm via the T3SS II (Miao et al., 2000). A significant feature of SifA as a key virulence factor in the pathogenesis of *Salmonella* is the maintenance of the SCV and the involvement in the formation of SIFs (LAMP-1-enriched membrane tubules) which originate from SCV, spreading out along microtubules. Furthermore, the *Salmonella* effector protein SifA belongs to the WxxxE family that is composed of 24 members that share the conserved WxxxE motif (Alto at al., 2006). Some members of this family function as bacterial GEFs to activate Rho GTPases, but so far it is not yet demonstrated whether SifA has a GEF activity similar to the EPEC/EHEC effector Map and *Shigella* effectors IpgB1 and IpgB2 (Huang et al., 2009; Klink et al., 2010). Nevertheless, Ohlson and colleagues have earlier reported that SifA binds to the GDP-bound inactive form of the GTPase RhoA (Ohlson et al., 2008). Furthermore, recent studies reveal that SifA interacts with several host proteins during *Salmonella* infection as described below.

One molecular target of SifA is the host protein SKIP (SifA and kinesin-interacting protein) that downregulates kinesin motor activity on the SCV and regulates bacterial vacuole dynamics (Boucrot et al., 2005). This interaction is mediated via the pleckstrin homology

(PH) domain of SKIP (Diacovich et al., 2009). On the other hand, SKIP interacts specifically and directly with the late endosomal marker Rab9 through the same PH domain, but in the presence of SifA this interaction is affected (Jackson et al., 2008). Furthermore, in the work of Jackson and colleagues it is postulated that WxxxE motif of SifA is essential for the interaction with host proteins. Finally, McEwan and colleagues have recently demonstrated that the host Pleckstrin homology domain-containing protein family member 1 (PLEKHM1), which shares a similar domain structure with SKIP, interacts with the N-terminal domain of SifA through its second PH domain (PH2) (McEwan et al., 2015). In their work, a specific interaction between the PH2 and C1/ZnF domains of PLEKHM1 and a small GTPase Rab7, but not Rab9, can be shown.

Among several putative interaction partners of SifA identified in the Y2H screen, I select two proteins, Cep70 and DYNLRB1, for our study. Furthermore and following independent lines of evidence, I include analyses on the interaction of SifA with the GTPases Rab6 and Rab9.

### 5.1.1 Cep70 as a potential target of SifA

The first interaction pair to be validated is Cep70 and SifA. Cep70 is a protein of 70 kDa, which belongs to the centrosomal protein (Cep) family comprising 31 members (Andersen et al., 2003; Kumar et al., 2013). Cep proteins are components of centrosome that functions as a microtubule-organizing center (MTOC). The centrosome is involved in various fundamental processes, including mitosis, cell migration and polarization (Doxsey et al., 2005). Shi and colleagues have observed that the centrosomal localization of Cep70 is dependent on its N-terminal coiled-coil domains that also mediate the interaction with γ-tubulin (Shi et al., 2011). Using microtubule depolymerization assays, the authors demonstrate that this N-terminal region of Cep70 regulates microtubule stability by increasing tubulin acetylation (Shi et al., 2015). It is worth to notice that knockdown of Cep70 expression significantly reduces the level of tubulin acetylation (Shi et al., 2015). The interaction between Cep70 and the microtubule-associated deacetylase HDAC6 is also mediated by the coiled-coil domains of Cep70 (Hubbert et al., 2002; Shi et al., 2015). Thus, the authors come to the conclusion that Cep70 promotes microtubule stabilization via directly binding to and inhibiting HDAC6 (Shi et al., 2015). The biological functions of Cep70 as listed above allow us to assume the existence of an interaction between the centrosomal protein Cep70 and the WxxxE effector protein SifA, which is important for positioning of the SCV in the centrosomal region and for spreading SIFs along stable microtubules.

In my experimental setup, I show by immunofluorescence microscopy thatectopically expressed Cep70 in most cases exclusively accumulates at the two centrioles (Figure 13, top panel). However, in some cases, Cep70 displays a distinct phenotype, which is reflected by so called centriolar satellites (CS) that cluster in the vicinity of the centrosome. This phenotype is similar to that observed for other CS proteins such as Cep72, Cep90 and Cep131 (Tollenaere et al., 2015). Akin to Cep70, the pericentriolar material 1 protein (PCM1) – one of the first CS proteins discovered – contains a coiled-coil motif at the N-terminal region that is essential for protein-protein interactions (Tollenaere et al., 2015). Furthermore, CS proteins are involved in centrosome biogenesis, ciliogenesis, and neurogenesis.At the same time, our co-localization studies of Cep70 and the *Salmonella* bacterial virulence factor SifA reveal that SifA distributes throughout the cell but with clear accumulation in the vicinity of Cep70, which localizes in small granules (Figure 13, bottom panel). These data suggest that Cep70 and SifA can in principle co-localize in the same cell compartment.

However, I have not been able to successfully perform biochemical studies due to technical problems intrinsic to Cep70: Cep70 concentrated mainly in the triton-insoluble fraction when preparing cell lysates. Thus, protein/protein interaction studies are hampered by the virtual absence of Cep70 in the soluble fraction. Nevertheless, Cep70 protein remains an interesting candidate for our research as it is associated with centrosomes, a position of mature SCV in the later stage of infection with *Salmonella*, and/or potential component of centriolar satellites. Thus, the interaction between centrosomal protein Cep70 and SifA may well exist and be relevant, yet a comprehensive analysis is needed in order to verify this possibility.

### 5.1.2 DYNLRB1 might be a potential SifA target

According to the data from the previously conducted Y2H screen, DYNLRB1, a member of the roadblock dynein light chain family, has been identified as a potential interacting partner of SifA. Cytoplasmic dynein consists of two heavy chains (DYNC1H1 and DYNC2H1), which are required for microtubule binding and ATPase activity; two intermediate chains (DYNC1I1 and DYNC1I2); two light intermediate chains (DYNC1LI1 and DYNC1LI2); and several light chains, including DYNLRB1 and DYNLRB2 proteins (Pfister et al., 2006; Wanschers et al., 2008). Dyneins embody one of the two families of molecular motors, namely kinesins and dyneins, accomplishing the transport of intracellular cargos in eukaryotic cells along microtubule tracks (Figure 47). In fact, intracellular *Salmonella* at early time points post infection exploits the minus-end-directed motor dynein, to reach the final SCV

position in the perinuclear area. Localization of the SCV is highly coordinated by T3SS-2 effector proteins including SifA (Henry et al., 2006), why we consider DYNLRB1 and SifA as a potential biologically relevant pair of interaction partners.

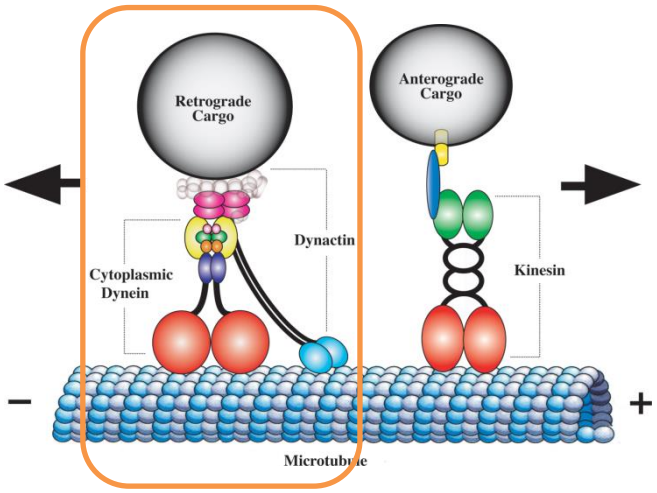


**Figure 47: Molecular motors along microtubular tracks.**

Cytoplasmic dynein is essential for minus end-directed transport towards the perinuclear region whereas kinesin moves various cargoes towards the plus ends in the cell periphery. Cytoplasmic dynein consists of heavy chains (red) that are required for microtubule binding and ATPase activity; intermediate chains (yellow); light intermediate chains (indigo) and several light chains (light pink, green, orange). Dynactin interacts with dynein and harbors several subunits, among them $p150^{Glued}$ (turquoise), that binds to the dynein intermediate chain (yellow) and to microtubules via a CAP-Gly motif at the tip of its globular heads. Association of Dynactin with cargo is mediated by the dynactin subunit p50 (dark pink).

Kinesin comprises two heavy chains, known as microtubule binding and motor subunits (red), and two light chains (green). Cargo-binding is mediated by an intermediate scaffold protein (blue) that can bind to transmembrane cargos (yellow) (Duncan & Goldstein, 2006).

The cytoplasmic localization of DYNLRB1 in transiently transfected Cos-7 cells (Figure 15, top panel) is in line with earlier observations made by the group of Jack Fransen (Wanschers et al., 2008). Detailed co-localization analysis of DYNLRB1 and Rab6 reveal that cytoplasmic DYNLRB1 is recruited to the Golgi region in a Rab6-dependent manner (Wanschers et al., 2008). My results are fully consistent with these published data demonstrating that DYNLRB1 interacts and co-localizes with Rab6 in the Golgi region (Figure 16, upper middle panel). Furthermore, the small GTPase Rab6 is known to be essential for the retrograde transport pathway from endosomes through the Golgi to the endoplasmic reticulum (White et al., 1999). In addition, Rab6 interacts with the $p150^{Glued}$ subunit of the dynactin complex and recruits dynactin to the Golgi membrane. Likewise, Rab6 specifically interacts with the cargo adaptor protein Bicaudal D2 (BICD2) that couples to the p50 subunit of the dynactin complex (Short et al., 2002). Noteworthy, cytoplasmic dynein

interacts with dynactin to drive cargo along microtubules. The stable dynein-dynactin-BICD2N (DDB) complex is formed only when all three proteins are present (Splinter et al., 2012; McKenney et al., 2014; Urnavicius et al., 2015; Matanis et al., 2002). In addition, the DDB complex binds to microtubules as exemplified by using negative stain electron microscopy and 2D analysis (Chowdhury et al., 2015).

Noteworthy, co-localization of the small GTPase Rab6 with SifA is very apparent at the Golgi complex (Figure 16, lower middle panel). This finding allows me to conclude that Rab6 alone already has a significant ability to recruit SifA from the cytoplasm to the Golgi region. Furthermore, simultaneous overexpression of three proteins – DYNLRB1, SifA and Rab6 – resulted in their pronounced accumulation at the Golgi complex, close to the replication position of *Salmonella* (Figure 16, bottom panel).I hypothesize that Rab6 might be required for the interaction of SifA with DYNLRB1. This might in turn be important for intracellular replication of *Salmonella* which takes place in the SCV in close vicinity of the Golgi apparatus. As previously mentioned, this special localization of the SCV in the perinuclear region is tightly regulated by T3SS-2 effector proteins, including SseG, SseF and SifA.

Despite the interaction between DYNLRB1 and SifA in our Y2H screen, I cannot readily observe binding of the two proteins in our pull-down assays. Notwithstanding this, I have found a weak interaction under buffer conditions where no detergent was present or the water activity was reduced (high salt), which is conclusive with a near-membrane-interaction in the cell (Figure 17). Since the small GTPase Rab6 has the ability to recruit SifA and DYNRB1 to the Golgi, we tested whether the presence of Rab6 would bind to SifA or promote a putative interaction between SifA and DYNLRB1. However, neither Rab6 binding nor increased DYNLRB1 binding is observed under our experimental conditions (Figure 18). It may be worth to revisit this question using different ‘membrane-friendly’ conditions such as cell fractionation.

Intracellular pathogenic *Salmonella* exploits host cell trafficking pathways, which are regulated by a complex network of Rab GTPases, in order to promote SCV maturation (Brumell & Scidmore, 2007). Furthermore, Rabs concentrate at distinct subcellular compartments in mammalian cells (Figure 48) (Zerial & McBride, 2001; Jean & Kiger, 2012; Hutagalung and & Novick, 2011).

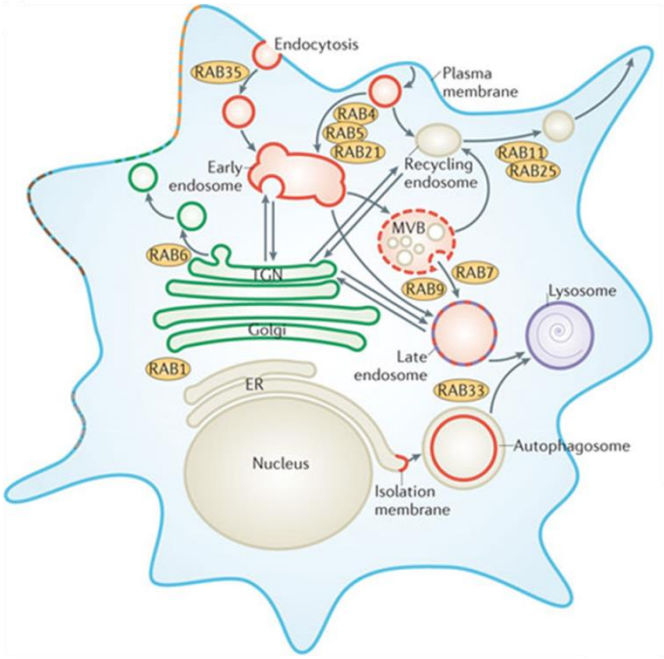


**Figure 48: Intracellular localization of Rab GTPases in eukaryotic cells.** Rab1 regulates ER-Golgi traffic. Rab4, Rab5 and Rab21 associate to early endosomes. Rab6 is involved in retrograde Golgi-ER and intra Golgi- transport pathways. Rab7 and Rab9 both localize to late endosomes, and Rab9 also regulates membrane traffic between late endosomes and the trans-Golgi network (Hutagalung and & Novick, 2011). Rab11, Rab25 and Rab35 localize to recycling endosomes. Rab33 associates with the Golgi apparatus (Jean & Kiger, 2012).

Among 18 Rabs proteins that have been found to be present at the SCV during maturation, only two, namely Rab7 and Rab9, are required for the formation of SIFs (Brumell & Scidmore, 2007). Thus I probed the ability of these Rab GTPases to bind to SifA or to impact on SifA/DYNLRB1 binding. Using pull-down assays, we identify the ability of the WxxxE domain of SifA to bind specifically to the late endosomal marker Rab9 (Figure 19 and preliminary work in the PhD Thesis of S. Arens). This finding certainly has biological relevance since SifA and Rab9 are both involved in the formation of SIFs and plus Rab9 shares a binding partner, namely SKIP, with SifA. Since no target GTPase for SifA can be identified among the Rho-family of small GTPases, it is tempting to speculate that SifA embodies a bacterial GEF for Rab9. SifA shares the GEF-like fold with the Rac/Cdc42 GEF SopE.(Alto et al., 2006; Ohlson et al., 2008) but not with other known bacterial Rab-GEFs. Moreover, despite SifA binds to a GDP-bound RhoA (Ohlson et al., 2008), recent structure models of the IpgB2-RhoA complex and its overlay with SifA structure reveal that interaction between SifA and RhoA is highly unfavorable since SifA harbors a more extended catalytic loop when compared to IpgB2 (Klink et al., 2010).Since Rab-GTPases are distantly related to Rho GTPases (both belong to the Ras-superfamily), a potential evolution of Rab-GEF activity within this branch of bacterial GEFs is thinkable and attractive.

In my thesis work, I can readily confirm a significant interaction between SifA and Rab9 (but not Rab6) in pull-down assays (Figure 19). Hence, I here suggest that SifA may function as bacterial GEF for Rabs (i.e.Rab9) rather than Rho-GTPases. This will also be compatible with either exclusive or competitive binding of Rab9 to its GEF (SifA) or effector (SKIP) as

described (Ohlson et al., 2008). It will be exciting to experimentally challenge this hypothesis e.g. by solving the crystal structure of WxxxE domain of SifA from *Salmonella* in complex with Rab9 and/or by conducting *in vitro* GTP-exchange assays. However, this aim lies beyond the scope of the present thesis and must be addressed in further studies.

Nonetheless, I analyze whether interaction between SifA and Rab9 has an influence on the binding of SifA to DYNLRB1. However, the interaction between DYNLRB1 and SifA remain at or below detection levels as before, despite the presence of the small GTPase Rab9 and its clear binding to SifA (Figure 20). Also here a fine tuning of experimental conditions may help to dissect DYNLRB1, Rab6 or Rab9 binding to SifA.

Remarkably, Rab9 subcellularly localizes in a manner similar to the Rab6 (Figure 21, top panel). Our data demonstrate that the expression of Rab9 has a dramatic effect on the subcellular distribution of SifA, leading to a virtually complete recruitment of cytoplasmic SifA to the Golgi region by Rab9 (Figure 21, lower middle panel). Finally, co-overexpression of Rab9 and SifA leads to partial re-localization of cytoplasmic DYNLRB1 to the Golgi region (Figure 21, bottom panel). Interestingly, in contrast to Rab6, Rab9 cannot translocate DYNLRB1 to the Golgi in the absence of SifA, suggesting a different behavior of Rab9 compared to Rab6. Figure 49 illustrates different cascades of recruitment of DYNLRB1 and SifA to the Golgi by Rab6 and Rab9 GTPases.

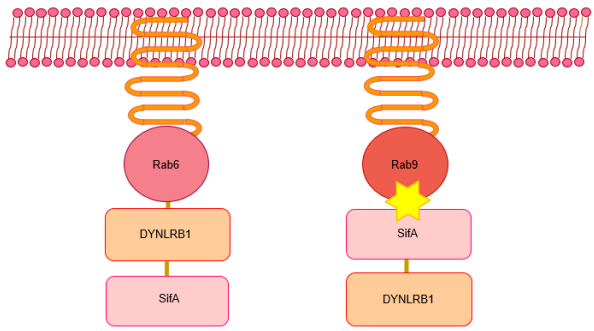


**Figure 49: Schematic illustration of the potential signaling/recruitment cascades of Rab6 and Rab9 leading to translocation of SifA DYNLRB1.** Aster marks a potential GEF activity of SifA towards Rab9.

However, in this study neither Rab6 nor Rab9 can promote the interaction between SifA and DYNLRB1. Hence, in addition to the above experiments, comprehensive studies must be conducted to determine whether the interaction between cytoplasmic dynein, DYNLRB1, and WxxxE effector protein SifA depends on the presence of additional cofactors. Currently, I cannot exclude the possibility that SifA binds indirectly to the microtubule motor protein, DYNLRB1. Considering the fact that Rab6 has a unique ability to recruit a large dynein-

dynactin-BICD2N complex, which transports various cellular cargo towards the minus ends of microtubules and *Salmonella* to their specific subcellular location, it is reasonable to probe the members of this complex for such a role. Strikingly, bicaudal has also been identified in the Y2H list of potential interactors but as yet no further analysis is done. This explains the fact that progress of the SifB/Clip4 interaction outperforms this subproject (see 5.2).

## 5.2 The interaction between CLIP4 and SifB

Based on the results of Y2H screening, CLIP4 has been identified to be a potential target of the *Salmonella* effector protein SifB. The *Salmonella* virulence factor SifB, similarly to SifA, belongs to a large family of 24 proteins that harbor a common WxxxE motif at the C-terminal region (Alto et al., 2006). Within this protein, SifA and SifB form a subgroup because they both harbor a conserved N-terminal extension, which in the case of SifA connects to SKIP and kinesin (see above). Since this work and the prior Y2H screen is set out to identify interactors of WxxxE proteins, I have designed and used throughout SifA- and SifB variants lacking the N-terminal extension (termed Δext) if not stated otherwise. It is known that SifB is translocated by the SPI2-encoded T3SS into the host cell at late to very late stages (after 20 hours post infection) (Freeman et al., 2003), but the exact role of SifB in the course of *Salmonella* infection is not understood. In fact, a mutant lacking SifB did not show any phenotype in *vitro* infection assays using HeLa cells (Rajashekar et al., 2014).

CLIP4, in turn, belongs to the CAP-GLY Domain Containing Linker Proteins family. The members of this family are defined based on the presence of an ~80 amino acids protein module, which is highly conserved among organisms ranging from yeast to human (Riehemann & Sorg, 1993; Weisbrich et al., 2007). This module, called cytoskeleton-associated protein-glycine-rich (CAP-Gly) domain, has been first discovered in 1993 (Riehemann & Sorg, 1993) and found in functionally diverse proteins, such as cytoplasmic linker proteins (CLIPs and CLIPRs), large subunit of the dynactin complex p150Glued, tubulin-folding cofactors B and E, centrosome-associated protein-350 (CAP350), the kinesin protein KIF13B or the familial cylindromatosis tumor suppressor CYLD (Weisbrich et al., 2007; Steinmetz & Akhmanova, 2008).

CLIP1 and CLIP2 (also known as CLIP170 and CLIP115, respectively) are the best characterized representatives of the CAP-Gly family and are known as microtubule plus-end tracking proteins (+TIPs) (Pierre et al., 1992; Akhmanova & Steinmetz., 2010; Akhmanova &

Steinmetz., 2008; Galjart, 2005). In contrast to CLIP2, CLIP1 contains zink-binding domains (ZnF) and an EEY/F motif necessary for interaction with the CAP-Gly domain of p150Glued, and the dynein regulator LISI (Lansbergen et al., 2004; Coquelle et al., 2002). Two major +TIPs, CLIP170 and p150Glued, bind to the C-terminal EEY/F motifs of end-binding (EB) proteins through their CAP-Gly domains. Interestingly, CLIP3 (CLIPR-59), which is closely related in its sequence to CLIP4 (Steinmetz & Akhmanova, 2008), exclusively localizes to the Golgi and *trans*-Golgi region. This is shown to solely depend on a palmitoylated membrane-targeting motif (PMT) enclosed within the last 30 amino acid residues (Figure 30, top panel). CLIP3 is believed to be involved in the early/recycling endosome–TGN transport pathway (Perez et al., 2002; Lallemand-Breitenbach et al., 2004 ) and has been shown to interact with the kinase domain of Akt by means of its first CAP-Gly domain, regulating its membrane localization (Ding et al., 2009). Finally, CLIP3 expressed in the neuronal system and a knockout show defects in neuromuscular junction formation leading to late embryonic or neonatal lethality (Couesnon et al., 2013)

CLIP4 contains three ankyrin-repeats in its N-terminus, followed by three CAP-Gly domains, with a basic serine region in between 1$^{st}$ and 2$^{nd}$ CAP-Gly domains (Figure 22). Regarding the biological function, subcellular localization or protein expression of CLIP4, there are no studies available. In contrast to the well-studied CLIP1 and CLIP2, the fourth member of the CAP-Gly family, CLIP4, is a yet uncharacterized protein. Therefore, I started studying subcellular localization of CLIP4 in Cos-7 cells transiently transfected with its GFP-fusion construct. Microscopy analysis demonstrates that CLIP4 is a microtubule-binding protein (Figure 23, top panel) rather than a +TIP, like CLIP1 and CLIP2. I perform time-lapse microscopy in order to visualize dynamic behavior of individual GFP-CLIP4-transfected Cos-7 cells (Figure 24), supporting the notion that is decorating microtubules along their length and is not enriched at their tips. Moreover, I observe substantial bundling of microtubules which is augmented with increasing ectopic expression levels.

In order to identify the domains required for microtubule localization, I design constructs that harbor ankyrin-repeats and CAP-Gly-domains with a basic serine region of human protein CLIP4. The results unambiguously demonstrate that the CAP-Gly domains with the basic serine stretch are essentially required and sufficient for microtubule binding and bundling, whereas the localization of the isolated Ankyrin repeats remains cytoplasmic (Figure 23). Interestingly, similar binding characteristics have been described for the CAP-Gly-domainy of CYLD (Wickström et al., 2010) and the basic region within Ras association domain family

1A (RASSF1A) that also stabilizes and bundles MTs via this basic region (Rong et al., 2004; Arnette et al., 2014).

Strikingly, these proteins belong to a class of structurally very divergent proteins that all share a role as tumor suppressors as they all stabilize interphase microtubules and (epithelial) cell polarity, thus prohibiting proliferation and migration (Hernandez & Tirnauer, 2010). Merlin (Muranen et al, 2007) and von-Hippl-Lindau-Syndrome-protein (Hergovich et al, 2003) also belong to this class of proteins. A hallmark of this feature is that i) microtubules are stabilized in a way that they are protected from the de-polymerizing effect of nocodazole and ii) that microtubules are then longer lived and thus accumulate post-translational modifications such as acetylation of alpha-tubulin. These effects have been observed for the above mentioned members of this call of tumor suppressing protein and have prompted members of the lab here to probe this features also for CLIP4. In fact, both parameters could be detected (see supplemental Figure 50; a courtesy of Theresia Stradal & Annette Otto, HZI, Braunschweig), suggesting that CLIP4 also functions as tumor suppressor.

In this context I then analyze the expression pattern of CLIP4 in human and mouse tissues using data available from different data bases e.g. the GEO database providing GeneChip datasets. In fact these analyses uncover that CLIP4 is not expressed in constantly dividing cells (see Figure 37 and 38) and even downregulated in cells that are experimentally stimulated to proliferate. This is a clear indication for CLIP4 acting as tumor suppressor gene in selected tissues- according to its expression pattern- in skeletal muscle and/or parts of the digestive tract. This in turn highlights its potential involvement in *Salmonella* infection.

Thus, CLIP4 interaction with SifB may play a role in very late stages of *Salmonella* infection, when bacteria has reached tissues consisting mostly of quiescent, non-cycling cells and thus expressing CLIP4. To corroborate this at least *in vitro*, I examine the distribution and behavior of GFP-SifB when transiently transfected into Cos-7 cells (that lack endogenous CLIP4) or ectopically co-expressing with CLIP4. As shown in Figure 42 (top panel), SifB alone is mostly dispersed throughout the cell. Furthermore, I provide evidence that CLIP4 and SifB co-localize significantly on microtubules (Figure 42, middle panel).

The interaction between the host protein CLIP4 and the T3SS-2 effector protein SifB is further verified by pull-down assays. The specificity of this interaction can be confirmed since none of the other WxxxE effector proteins such as SifA and EspT, interacts with CLIP4 (Figure 25 B). Moreover, I successfully map interaction surfaces between the two proteins,

SifB and CLIP4, using individual domain-based constructs of CLIP4 in pull-down assays. I demonstrate that the C-terminal region harboring CAP-Gly domains and basic serine stretch of CLIP4 is necessary and sufficient for the interaction with SifB, but not with the related protein SifA (Figure 26A). In contrast to CLIP4, I did not observe an interaction between SifB and CLIP1 or CLIP2 in our pull-down assays, although the latter two proteins belong to the same protein family and share similar CAP-Gly domains with CLIP4 (Figure 34). Despite the weak but significant ability of CLIP3 to interact with *Salmonella* effector protein SifB in the pull-down assay, this interaction is not likely of biological relevance, since the third member of CAP-Gly family, CLIP3, appears to be expressed in adipose and brain tissue (Ding et al., 2009), which are normally not infected by *Salmonella*.

The data suggests that CLIP4 specifically interacts with the WxxxE domain of SifB via its second and third CAP-Gly domains, which follow the central basic serine region (Figure 27 D).

In order to gain insight into interaction between virulence factors and host proteins, we aim to generate mouse monoclonal antibodies against SifA and SifB, in collaboration with colleagues from the TU Braunschweig (Sabine Buchmeier), a specific anti-SifA monoclonal antibody is established, which will be a valuable tool in future studies. However, despite our careful attempts, we did not succeed in producing anti-SifB antibodies.

In this study, in order to analyze cellular phenotypes as well as alterations during infections with wild-type and SifB-defective *Salmonella*, I also aim at generating somatic knockouts for CLIP4 using the CRISPR-Cas technology. Although I find small amounts of CLIP4 to be endogenously expressed in the A431 cell line, I fail with this approach because all clones, no matter if treated with guide RNAs specific to CLIP4 or not, did not lose residual expression. One possible and likely explanation is that subcloning of the cells during establishment of targeted clones selects the cells for continuous cycling, which in turn results in shutting down CLIP4 expression. Therefore, I have discontinued further experiments in this direction. Here, I also emphasize that in the majority of immortal cell lines I did not detect any CLIP4 (Figure 38), which is in accordance with the data obtained with Gene Chip analysis (Figure 37). In the future, it may be useful to target stem cell-like cells and then differentiate them into specific lines that are capable of CLIP4 expression.

Next, I investigate localization of CLIP4 with respect to SIF-dynamics in *Salmonell*a infected cells. First, we study the dynamic process of formation SIFs in HeLa cells stably expressing

GFP-tagged Lamp1 infected with wild-type *Salmonella spp*. using long-term time-lapse microscopy (Figure 43). These results are consistent with previously published data, which demonstrated that SIFs spread throughout the entire cell to form a complex network (Garcia-del Portillo et al., 1993; Rajashekar et al., 2008). Furthermore, Brumell and colleagues demonstrate that SIFs are formed along microtubules that serve as cytoskeleton scaffold for them, and that depolymerization of the microtubule network disrupted SIFs (Brumell et al., 2002; Garcia-del Portillo et al., 1993). Next, I analyze the behavior of CLIP4 in HeLa cells stably expressing GFP-LAMP1 and transiently transfected with mCherry-CLIP4 upon infection with wild-type, SifA- or SifB-defective *Salmonella*. Remarkably, extensive highly dynamic SIFs align along microtubule-binding protein CLIP4 during the course of infection with wild-type *Salmonella* (Figure 44) or SifB-deficient bacteria. However, the presence of CLIP4 is not sufficient to induce SIF-formation upon infection with SifA-defective *Salmonella* (Figure 45) in infection experiments up to 12 hours. Notwithstanding this, it is still reasonable to assume that SifB has such (or similar) function in late stages, because in an earlier report it was described to occur not before 20 hours post infection in vivo. Due to the lack of a good antibody the time point of expression of SifB in the current thesis is not monitored.

Therefore, a potential role of SifB in the formation of SIFs has not been found until now probably because SifB did not induce SIFs when studied in immortal cell lines lacking endogenous CLIP4 such as HeLa.

## 5.3 Concluding remarks

In this study, I validate several hits from a previous Y2H screen for host-specific interactors of members of the WxxxE family. By using biochemical and microscopic techniques, in order to identify new host binding proteins of bacterial virulence effectors, I here report the validation of two interactions. This study provides strong indications for an interaction between SifA and Cep70, which might well be involved in SCV positioning. Also, this work corroborates the intimate interplay with Rab-GTPase signaling and highlights a potential additional function for the WxxxE domain of SifA as GEF for Rab9. Finally it provides strong evidence for the interaction between the host microtubule-binding protein CLIP4 and the *Salmonella* WxxxE effector protein SifB. The interaction surface between these two proteins to the C-terminal region containing CAP-Gly domains and a basic serine stretch of CLIP4 is mapped. Moreover, both proteins have been shown to co-localize on microtubules. In addition, CLIP4 behaves similarly to other tumor suppressor proteins such as RASSF1A and VHL-Sp, which stabilize interphase-microtubules, thus prohibiting cell cycle. Therefore, we assume that CLIP4 may also serve as a tumor suppressor protein in certain tissues. However, the biologic relevance of the interaction between CLIP4 and SifB – although anticipatable- remains to be shown.

Investigation of how WxxxE effector proteins manipulate host proteins will offer deeper insights into the multitude of biologic activities exerted by these bacterial virulence factors during infection. Exact molecular mechanisms of these host-pathogen interactions in the course of infection will lead to new strategies in fighting infectious disease.

# 6. SUMMARY

Even in the twenty-first century, infectious diseases remain a global health problem. The World Health Organization (WHO) continuously registers incidents of *Salmonella* infections in both developed and developing countries. During long-standing co-evolution with their hosts, pathogenic bacteria have evolved multiple strategies to survive and replicate within the host by manipulating intracellular signaling pathways. Furthermore, an array of bacterial virulence factors is delivered into the host cytoplasm upon infection via the type three secretion system (T3SS). Alto and colleagues grouped 24 effector proteins, including Map, EspM and EspT of EHEC/EPEC and the related *Citrobacter rodentium*, IpgB1 and IpgB2 of *Shigella sp*, and SifA and SifB of *Salmonella sp*, that share a common motif WxxxEinto a single family (Alto et al., 2006). These WxxxE proteins mostly act as bacterial guanine nucleotide exchange factors (GEFs) towards Rho GTPases. Structural studies of WxxxE-family GEFs showed that these effectors share a common fold with *Salmonella* SopE and SopE2 (Buchwald et al., 2002; Ohlson et al., 2008; Huang et al., 2009). The latter are known to mimic eukaryotic GEFs by targeting Rho GTPases. However, WxxxE effectors SifA and SifB appear to lack GEF-activity towards Rho-GTPases, which opens up new questions on investigating the molecular function of these effector proteins during infection.

In this regard, the present study focuses on the identification of new host cell targets of a number of various bacterial virulence factors, including SifA, SifB and EspT. Based on the results of a previously conducted Y2H screening, we preselect four most prominent host-pathogen pairs (APPL1 and EspT, Cep70 and SifA, DYNLRB1 and SifA, CLIP4 and SifB) for our study.

I perform pull-down assays in order to validate the interactions predicted by the Y2H screen. Interaction of EspT and APPL1 can not be confirmed with this approach and thus it has been excluded from further analyses.

Similarly, an interaction between a host protein Cep70 and a bacterial virulence factor SifA, can not be demonstrated in these experiments, because Cep70 accumulated in the triton-insoluble fraction. Centrosomal proteins form complexes that can either be included in the centrosome or in so calledcentriolar satellites. Taking into account the fact that Cep70 localizes at centrosomes, where also *Salmonella*-containing vacuoles (SCVs) migrate after 2

hours post invasion, the putative interaction between Cep70 and SifA is still considered to be of potential interest. However, this is not followed further in this thesis.

Another predicted interaction partner of the WxxxE effector SifA is DYNLRB1. It is difficult to demonstrate the interaction under chosen experimental conditions in pull-down assays. However, when using immunofluorescence microscopy, a partial co-localization of DYNLRB1 with SifA is readily observed; at the same time, the small GTPase Rab6 can recruit DYNLRB1 to the Golgi in accordance with the previously published data (Wanschers et al., 2008). Furthermore, co-expression of DYNLRB1, Rab6 and SifA leads to compact localization of all three proteins at the Golgi structure. Therefore, the results of our Y2H screen together with co-localization studies support idea that DYNLRB1 interacts with SifA.

Within the framework of this study, I have succesfully identified a novel interaction between the host protein CLIP4, the function of which has been unknown until now, and the bacterial virulence factor SifB. The interaction surface of these two proteins has been mapped to the C-terminal CAP-Gly domains of CLIP4. Furthermore, SifB is shown to specifically interact with CLIP4, but not with other members of The CAP-Gly family (CLIP1, CLIP2, or CLIP3). Using microscopic techniques, it has been revealed that CLIP4 is a microtubule-binding protein. In particular, it demonstrates that this feature is mediated via the Cap-Gly-domains and not the ankyrin repeats. In addition, the work presented here shows that the bacterial virulence protein SifB alone is diffusely distributed throughout the cytoplasm, but is recruited to microtubules in the presence of CLIP4. Finally, co-localization of *Salmonella*-induced membrane tubules, termed SIFs, with CLIP4-labelled microtubules can be visualized using time-lapse microscopy. In the view of the different approaches, these data strongly suggest that *Salmonella* effector protein SifB specifically targets the host microtubule-binding protein CLIP4.

Together, this study identifies new interaction partners of SifA and SifB and paves the way to a deeper understanding of the late steps of *Salmonella* infection.

# I List of abbreviations

| | |
|---|---|
| A | Ampere |
| aa | amino acid(s) |
| amp | Ampicillin |
| ANK | ankyrin repeat |
| ApE | a plasmid editor |
| APPL1 | adaptor protein, phosphotyrosine interacting with PH domain and leucine zipper 1 |
| APS | ammonium persulfate |
| BICD2 | bicaudal D homolog 2 |
| BLAST | basic local alignment search tool |
| bp | Base pair |
| BSA | bovine serum albumin |
| cDNA | complementary DNA |
| °C | degree Celsius |
| Cep70 | centrosomal protein 70 |
| CLIP4 | CAP-Gly Domain Containing Linker Protein Family Member 4 |
| CRISPR | Clustered regularly interspaced short palindromic repeats |
| CS | centriolar satellites |
| C-terminus | carboxy-terminus |
| CYLD | cylindromatosis (turban tumor syndrome) |
| Δ | delta |
| Ø | diameter |
| DAPI | 4',6-diamidino-2-phenylindole |
| DDB | dynein-dynactin-BICD2N |
| DKFZ | German Cancer Research Center |
| DNA | deoxyribonucleic acid |
| dNTP | deoxynucleotide-triphosphate |
| DMEM | Dulbeccos' modified Eagle medium |
| DMSO | dimethyl sulfoxide |
| DYNLRB1 | Dynein Light Chain Roadblock type-1 protein |
| EB | end-binding proteins |
| *E. coli* | *Escherichia coli* |

| | |
|---|---|
| ECDC | European Centre for Disease Prevention and Control |
| EDTA | ethylenediaminetetraacetic acid |
| EEA | European Economic Area |
| EEA1 | early endosomal antigen 1 |
| e.g. | exempli gratia |
| EHEC | enterohemorrhagic *E.coli* |
| EPEC | enteropathogenic *E.coli* |
| E/P | glutamate-proline rich |
| ER | endoplasmic reticulum |
| ELISA | enzyme-linked immunosorbent assay |
| et al. | et alii |
| EU | European Union |
| FACS | fluorescence-activated cell sorting |
| FCS | fetal calf serum |
| FL | full-length |
| For | forward |
| g | gram |
| GAP | GTPase activating protein |
| GDI | guanosine nucleotide dissociation inhibitors |
| GDP | guanosine diphosphate |
| GEO | Gene Expression Omnibus |
| GFP | green fluorescent protein |
| GEF | guanosine nucleotide exchange factor |
| GTP | guanosine triphosphate |
| h | hour(s) |
| HDAC6 | histone deacetylase 6 |
| HEK | human embryonic kidney |
| HRP | horseradish peroxidase |
| HZI | Helmholtz Centre for Infection Research |
| IF | immunofluorescence microscopy |
| IM | inner membrane |
| IPTG | isopropyl β-D-1-thiogalactopyranosid |
| kana | kanamycin |
| kDa | kilodalton |

| | |
|---|---|
| KO | knockout |
| l | liter(s) |
| LAMPs | lysosome-associated membrane proteins |
| LB | Luria Bertani broth |
| LC3 | microtubule-associated protein 1 light chain 3 |
| LE | late endosome markers |
| LNTs | LAMP1-negative tubules |
| Lys | lysosome markers |
| µ | micro- |
| m | milli- or meter(s) |
| M | molar |
| MBP | maltose binding protein |
| mc | monoclonal |
| MHH | Medizinischen Hochschule Hannover |
| min | minute(s) |
| mRNA | messenger RNA |
| Mm | Mus musculus |
| MS | membrane and supramembrane |
| MTOC | microtubule-organizing centre |
| MTs | microtubules |
| n | nano- |
| NAGK | N-acetylglucosamine kinase |
| NCBI | National Center for Biotechnology Information |
| N-terminus | amino-terminus |
| NTS | non-typhoidal *Salmonella* |
| $OD_{600}$ | optical density at 600 nm |
| OM | outer membrane |
| OPTN | optineurin |
| PAGE | polyacrylamide gel electrophoresis |
| PBS | phosphate-buffered saline |
| PCR | polymerase chain reaction |
| pc | polyclonal |
| PFA | paraformaldehyde |
| PH | pleckstrin homology |

| | |
|---|---|
| $P_i$ | phosphate |
| p.i. | post invasion |
| % | percent |
| PCM1 | pericentriolar material 1 protein |
| PLEKHM1 | pleckstrin homology domain-containing protein family member 1 |
| ® | registered trademark symbol |
| RASSF1A | Ras association domain family 1A |
| RILP | Rab-interacting lysosomal protein |
| PMT | palmitoylation membrane-targeting motif |
| P/S | penicillin/streptomycin |
| PVDF | polyvinylidenfluorid |
| RFP | red fluorescent protein |
| Rev | reverse |
| RNAi | RNA interference |
| rpm | rounds per minute |
| RT | room temperature |
| s | second(s) |
| SCV | *Salmonella* containing vacuole |
| Sct | secretion and cellular translocation |
| SDS | sodium dodecyl sulfate |
| sgRNA | single guide RNA |
| SIFs | *Salmonella* induced filaments |
| SISTs | *Salmonella*-induced secretory carrier membrane protein 3 (SCAMP3) tubules |
| SKIP | SifA and kinesin-interacting protein |
| SLRs | sequestosome 1/p62-like receptors |
| SNX | sorting nexin tubules |
| SPI | *Salmonella* pathogenicity island |
| Sip | *Salmonella* invasion protein |
| Sop | *Salmonella* outer protein |
| t | time |
| TAE | tris base, acetic acid and EDTA containing buffer |
| TBS | tris-buffered saline |
| TBS/T | tris-buffered saline / Tween 20 |
| TEMED | N, N, N, N,-Tetramethylethylenediamine |

| | |
|---|---|
| TGN | trans-Golgi network |
| T3SS | type 3 secretion system |
| TIF | tagged image file format |
| +TIPs | microtubule plus-end tracking proteins |
| ™ | trademarkt |
| TU | Technical University |
| U | unit |
| UV | ultraviolet |
| V | volt |
| vATPase | vacuolar ATPase |
| VHL-Sp | von-Hippl-Lindau-Syndrome-protein |
| v/v | volume per volume |
| WHO | world health organization |
| w/v | weight per volume |
| WT | wild type |
| x | times magnification |
| xg | times gravitation constant |
| Y2H | yeast two hybrid |
| ZnF | zinc finger domain |

## II List of figures

# III List of tables

# IV Supplementary data

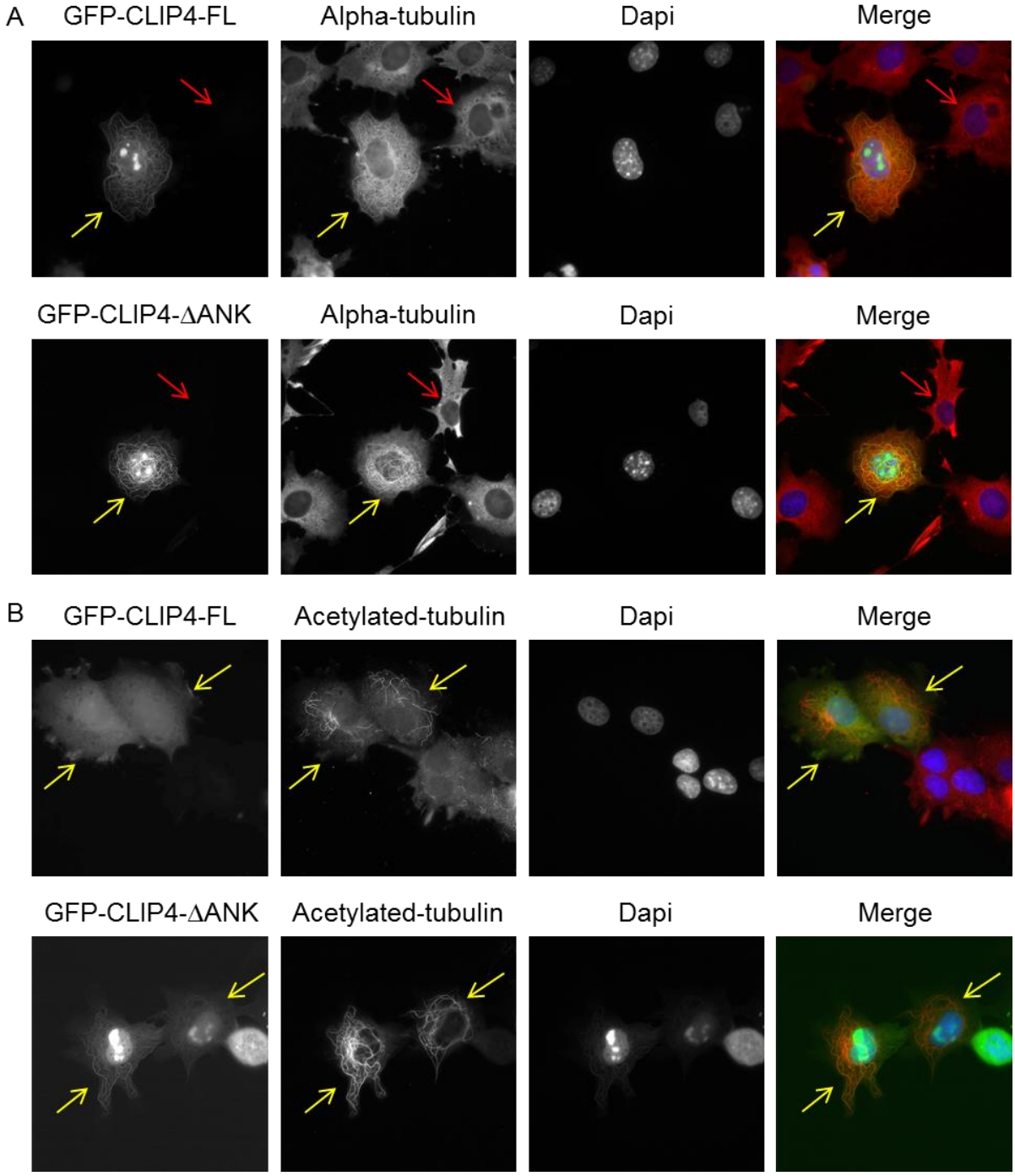


**Figure 50: CLIP4-FL and CLIP4-ΔANK stabilize microtubules upon treatment with microtubule-depolymerizing drug nocodazole.**Cos-7 cells were transfected with respective GFP-tagged constructs of CLIP4, 24 hours later cells were treated with nocodazole and fixed with PFA and permeabilized. Nuclei were stained with DAPI (blue). (A) Staining of cells with anti-α-tubulin antibody revealed that CLIP4-FL and CLIP4-ΔANK stabilize microtubules in the presence of nocodazole. (B) Staining of cells with anti-acetylated tubulin antibody revealed that CLIP4-FL and CLIP4-ΔANK protect mainly acetylated microtubules from nocodazole. Merge shows an overlay of the green, red and blue channel. Yellow and red arrows highlight transfected GFP-CLIP4-FL or GFP-CLIP4-ΔANK and untransfected cells, respectively.

# V List of references

Abrahams, G. L., P. Müller and M. Hensel (2006). "Functional Dissection of SseF, a Type III Effector Protein Involved in Positioning the Salmonella-Containing Vacuole." Traffic 7(8): 950-965.

Agbor, T. A. and B. A. McCormick (2011). "Salmonella Effectors: Important players modulating host cell function during infection." Cellular Microbiology 13(12): 1858-1869.

Akeda, Y. and J. E. Galan (2005). "Chaperone release and unfolding of substrates in type III secretion." Nature 437(7060): 911-915.

Akhmanova, A. and M. O. Steinmetz (2008). "Tracking the ends: a dynamic protein network controls the fate of microtubule tips." Nat Rev Mol Cell Biol 9(4): 309-322.

Akhmanova, A. and M. O. Steinmetz (2010). "Microtubule +TIPs at a glance." Journal of Cell Science 123(20): 3415-3419.

Akhmanova, A. and M. O. Steinmetz (2015). "Control of microtubule organization and dynamics: two ends in the limelight." Nat Rev Mol Cell Biol 16(12): 711-726.

Aktories, K. and J. T. Barbieri (2005). "Bacterial cytotoxins: targeting eukaryotic switches." Nat Rev Micro 3(5): 397-410.

Alto, N. M., F. Shao, C. S. Lazar, R. L. Brost, G. Chua, S. Mattoo, S. A. McMahon, P. Ghosh, T. R. Hughes, C. Boone and J. E. Dixon (2006). "Identification of a Bacterial Type III Effector Family with G Protein Mimicry Functions." Cell 124(1): 133-145.

Andersen, J. S., C. J. Wilkinson, T. Mayor, P. Mortensen, E. A. Nigg and M. Mann (2003). "Proteomic characterization of the human centrosome by protein correlation profiling." Nature 426(6966): 570-574.

Arnette, C., N. Efimova, X. Zhu, G. J. Clark and I. Kaverina (2014). "Microtubule segment stabilization by RASSF1A is required for proper microtubule dynamics and Golgi integrity." Molecular Biology of the Cell 25(6): 800-810.

Ashokkumar, B., S. M. Nabokina, T. Y. Ma and H. M. Said (2009). "Identification of dynein light chain road block-1 as a novel interaction partner with the human reduced folate carrier." American Journal of Physiology - Gastrointestinal and Liver Physiology 297(3): G480-G487.

Birmingham, C. L., A. C. Smith, M. A. Bakowski, T. Yoshimori and J. H. Brumell (2006). "Autophagy Controls Salmonella Infection in Response to Damage to the Salmonella-containing Vacuole." Journal of Biological Chemistry 281(16): 11374-11383.

Bishop, A. L. and A. Hall (2000). "Rho GTPases and their effector proteins." Biochemical Journal 348(Pt 2): 241-255.

Boquet, P. (2000). "Small GTP binding proteins and bacterial virulence." Microbes and Infection 2(7): 837-843.

Boucrot, E., T. Henry, J.-P. Borg, J.-P. Gorvel and S. Méresse (2005). "The Intracellular Fate of Salmonella Depends on the Recruitment of Kinesin." Science 308(5725): 1174-1178.

Bradford, M.M. (1976), "Rapid and sensitive method for the quantitation of microgram quantities of protein utilizing the principle of protein-dye binding", Anal. Biochem., 72: 248–254.

Braun, V., A. Wong, M. Landekic, W. J. Hong, S. Grinstein and J. H. Brumell (2010). "Sorting nexin 3 (SNX3) is a component of a tubular endosomal network induced by Salmonella and involved in maturation of the Salmonella-containing vacuole." Cellular Microbiology 12(9): 1352-1367.

Brumell, J. H., C. M. Rosenberger, G. T. Gotto, S. L. Marcus and B. B. Finlay (2001). "SifA permits survival and replication of Salmonella typhimurium in murine macrophages." Cellular Microbiology 3(2): 75-84.

Brumell, J. H., D. L. Goosney and B. B. Finlay (2002). "SifA, a Type III Secreted Effector of Salmonella typhimurium, Directs Salmonella-Induced Filament (Sif) Formation Along Microtubules." Traffic 3(6): 407-415.

Brumell, J. H. and M. A. Scidmore (2007). "Manipulation of Rab GTPase Function by Intracellular Bacterial Pathogens." Microbiology and Molecular Biology Reviews : MMBR 71(4): 636-652.

Buchwald, G., A. Friebel, J. E. Galán, W.-D. Hardt, A. Wittinghofer and K. Scheffzek (2002). "Structural basis for the reversible activation of a Rho protein by the bacterial toxin SopE." The EMBO Journal 21(13): 3286-3295.

Bujny, M. V., P. A. Ewels, S. Humphrey, N. Attar, M. A. Jepson and P. J. Cullen (2008). "Sorting nexin-1 defines an early phage of *Salmonella*-containing vacuole-remodeling during *Salmonella* infection." Journal of Cell Science 121(12): 2027-2036.

Bulgin, R., B. Raymond, J. A. Garnett, G. Frankel, V. F. Crepin, C. N. Berger and A. Arbeloa (2010). "Bacterial Guanine Nucleotide Exchange Factors SopE-Like and WxxxE Effectors." Infect Immun 78(4): 1417-1425.

Bulgin, R. R., A. Arbeloa, J. C. S. Chung and G. Frankel (2009). "EspT triggers formation of lamellipodia and membrane ruffles through activation of Rac-1 and Cdc42." Cellular Microbiology 11(2): 217-229.

Burkinshaw, B. J. and N. C. J. Strynadka (2014). "Assembly and structure of the T3SS." Biochimica et Biophysica Acta (BBA) - Molecular Cell Research 1843(8): 1649-1663.

Cirillo, D. M., R. H. Valdivia, D. M. Monack and S. Falkow (1998). "Macrophage-dependent induction of the Salmonella pathogenicity island 2 type III secretion system and its role in intracellular survival." Molecular Microbiology 30(1): 175-188.

Cherfils, J. and M. Zeghouf (2013). "Regulation of Small GTPases by GEFs, GAPs, and GDIs." Physiological Reviews 93(1): 269-309.

Chowdhury, S., S. A. Ketcham, T. A. Schroer and G. C. Lander (2015). "Structural organization of the dynein-dynactin complex bound to microtubules." Nat Struct Mol Biol 22(4): 345-347.

Conde, C. and A. Caceres (2009). "Microtubule assembly, organization and dynamics in axons and dendrites." Nat Rev Neurosci 10(5): 319-332.

Coquelle, F. M., M. Caspi, F. P. Cordelières, J. P. Dompierre, D. L. Dujardin, C. Koifman, P. Martin, C. C. Hoogenraad, A. Akhmanova, N. Galjart, J. R. De Mey and O. Reiner (2002). "LIS1, CLIP-170's Key to the Dynein/Dynactin Pathway." Molecular and Cellular Biology 22(9): 3089-3102.

Cornelis, G. R. (2006). "The type III secretion injectisome." Nat Rev Micro 4(11): 811-825.

Couesnon, A., N. Offner, V. Bernard, N. Chaverot, S. Backer, A. Dimitrov, F. Perez, J. Molgó and E. Bloch-Gallego (2013). "CLIPR-59: a protein essential for neuromuscular junction stability during mouse late embryonic development." Development 140(7): 1583-1593.

Cullen, P. J. (2008). "Endosomal sorting and signalling: an emerging role for sorting nexins." Nat Rev Mol Cell Biol 9(7): 574-582.

de Jong, H. K., C. M. Parry, T. van der Poll and W. J. Wiersinga (2012). "Host–Pathogen Interaction in Invasive Salmonellosis." PLoS Pathogens 8(10): e1002933.

Deretic, V. (2012). "Autophagy as an innate immunity paradigm: expanding the scope and repertoire of pattern recognition receptors." Current Opinion in Immunology 24(1): 21-31.

Desai, A. and T. J. Mitchison (1997). "Microtubule polymerization dynamics." Annual Review of Cell and Developmental Biology 13(1): 83-117.

Diacovich, L., A. Dumont, D. Lafitte, E. Soprano, A.-A. Guilhon, C. Bignon, J.-P. Gorvel, Y. Bourne and S. Méresse (2009). "Interaction between the SifA Virulence Factor and Its Host Target SKIP Is Essential for Salmonella Pathogenesis." The Journal of Biological Chemistry 284(48): 33151-33160.

Diepold, A. and S. Wagner (2014). "Assembly of the bacterial type III secretion machinery." FEMS Microbiology Reviews 38(4): 802-822.

Ding, J. and K. Du (2009). "ClipR-59 Interacts with Akt and Regulates Akt Cellular Compartmentalization." Molecular and Cellular Biology 29(6): 1459-1471.

Donnenberg, M. S. (2000). "Pathogenic strategies of enteric bacteria." Nature 406(6797): 768-774.

Doxsey, S., W. Zimmerman and K. Mikule (2005). "Centrosome control of the cell cycle." Trends in Cell Biology 15(6): 303-311.

Drecktrah, D., S. Levine-Wilkinson, T. Dam, S. Winfree, L. A. Knodler, T. A. Schroer and O. Steele-Mortimer (2008). "Dynamic Behavior of Salmonella-Induced Membrane Tubules in Epithelial Cells." Traffic 9(12): 2117-2129.

Duncan, J. E. and L. S. B. Goldstein (2006). "The Genetics of Axonal Transport and Axonal Transport Disorders." PLoS Genet 2(9): e124.

Etienne-Manneville, S. and A. Hall (2002). "Rho GTPases in cell biology." Nature 420(6916): 629-635.

Figueira, R. and D. W. Holden (2012). "Functions of the Salmonella pathogenicity island 2 (SPI-2) type III secretion system effectors." Microbiology 158(5): 1147-1161.

Freeman, J. A., M. E. Ohl and S. I. Miller (2003). "The Salmonella enterica Serovar Typhimurium Translocated Effectors SseJ and SifB Are Targeted to the Salmonella-Containing Vacuole." Infection and Immunity 71(1): 418-427.

Friebel, A., H. Ilchmann, M. Aepfelbacher, K. Ehrbar, W. Machleidt and W.-D. Hardt (2001). "SopE and SopE2 from Salmonella typhimurium Activate Different Sets of RhoGTPases of the Host Cell." Journal of Biological Chemistry 276(36): 34035-34040.

Fu, Y. and J. E. Galan (1999). "A Salmonella protein antagonizes Rac-1 and Cdc42 to mediate host-cell recovery after bacterial invasion." Nature 401(6750): 293-297.

Galjart, N. (2005). "CLIPs and CLASPs and cellular dynamics." Nat Rev Mol Cell Biol 6(6): 487-498.

Garcia-del Portillo, F., J. W. Foster and B. B. Finlay (1993). "Role of acid tolerance response genes in Salmonella typhimurium virulence." Infect Immun 61(10): 4489-4492.

Giacomodonato, M. N., S. Uzzau, D. Bacciu, R. Caccuri, S. H. Sarnacki, S. Rubino and M. C. Cerquetti (2007). "SipA, SopA, SopB, SopD and SopE2 effector proteins of Salmonella

enterica serovar Typhimurium are synthesized at late stages of infection in mice." Microbiology 153(4): 1221-1228.

Gupta, K. K., M. V. Joyce, A. R. Slabbekoorn, Z. C. Zhu, B. A. Paulson, B. Boggess and H. V. Goodson (2010). "Probing Interactions between CLIP-170, EB1, and Microtubules." Journal of Molecular Biology 395(5): 1049-1062.

Hänisch, J., R. Kölm, M. Wozniczka, D. Bumann, K. Rottner and Theresia E. B. Stradal (2011). "Activation of a RhoA/Myosin II-Dependent but Arp2/3 Complex-Independent Pathway Facilitates Salmonella Invasion." Cell Host & Microbe 9(4): 273-285.

Haraga, A., M. B. Ohlson and S. I. Miller (2008). "Salmonellae interplay with host cells." Nat Rev Micro 6(1): 53-66.

Hardt, W.-D., L.-M. Chen, K. E. Schuebel, X. R. Bustelo and J. E. Galán (1998). "S. typhimurium Encodes an Activator of Rho GTPases that Induces Membrane Ruffling and Nuclear Responses in Host Cells." Cell 93(5): 815-826.

Harrison, R. E., J. H. Brumell, A. Khandani, C. Bucci, C. C. Scott, X. Jiang, B. B. Finlay and S. Grinstein (2004). "Salmonella Impairs RILP Recruitment to Rab7 during Maturation of Invasion Vacuoles." Molecular Biology of the Cell 15(7): 3146-3154.

Heasman, S. J. and A. J. Ridley (2008). "Mammalian Rho GTPases: new insights into their functions from in vivo studies." Nat Rev Mol Cell Biol 9(9): 690-701.

Henry, T., J.-P. Gorvel and S. Méresse (2006). "Molecular motors hijacking by intracellular pathogens." Cellular Microbiology 8(1): 23-32.

Hensel, M. (2000). "Salmonella Pathogenicity Island 2." Molecular Microbiology 36(5): 1015-1023.

Hensel, M., J. Shea, C. Gleeson, M. Jones, E. Dalton and D. Holden (1995). "Simultaneous identification of bacterial virulence genes by negative selection." Science 269(5222): 400-403.

Hergovich, A., J. Lisztwan, R. Barry, P. Ballschmieter and W. Krek (2003). "Regulation of microtubule stability by the von Hippel-Lindau tumour suppressor protein pVHL." Nat Cell Biol 5(1): 64-70.

Hernandez, P. and J. S. Tirnauer (2010). "Tumor suppressor interactions with microtubules: keeping cell polarity and cell division on track." Disease Models & Mechanisms 3(5-6): 304-315.

Horio, T. and H. Hotani (1986). "Visualization of the dynamic instability of individual microtubules by dark-field microscopy." Nature 321(6070): 605-607.

Huang, Z., S. E. Sutton, A. J. Wallenfang, R. C. Orchard, X. Wu, Y. Feng, J. Chai and N. M. Alto (2009). "Structural insights into host GTPase isoform selection by a family of bacterial GEF mimics." Nat Struct Mol Biol 16(8): 853-860.

Hubbert, C., A. Guardiola, R. Shao, Y. Kawaguchi, A. Ito, A. Nixon, M. Yoshida, X.-F. Wang and T.-P. Yao (2002). "HDAC6 is a microtubule-associated deacetylase." Nature 417(6887): 455-458.

Humphreys, D., P. J. Hume and V. Koronakis (2009). "The Salmonella Effector SptP Dephosphorylates Host AAA+ ATPase VCP to Promote Development of its Intracellular Replicative Niche." Cell Host & Microbe 5(3): 225-233.

Hutagalung, A. H. and P. J. Novick (2011). "Role of Rab GTPases in Membrane Traffic and Cell Physiology." Physiological reviews 91(1): 119-149.

Islam, M. A., S. R. Sharif, H. Lee, D.-H. Seog and I. S. Moon (2015a). "N-acetyl-D-glucosamine kinase interacts with dynein light-chain roadblock type 1 at Golgi outposts in neuronal dendritic branch points." Experimental & Molecular Medicine 47(8): e177.

Islam, M. A., S. R. Sharif, H. Lee and I. S. Moon (2015b). "N-Acetyl-D-Glucosamine Kinase Promotes the Axonal Growth of Developing Neurons." Molecules and Cells 38(10): 876-885.

Jackson LK, N. P., Hentea C, Roark EA, Haldar K. (2008). The Salmonella virulence protein SifA is a G protein antagonist. Proc Natl Acad Sci U S A. 105: 14141–14146.

Jaffe, A. B. and A. Hall (2005). "Rho GTPases: biochemistry and biology." Annu Rev Cell Dev Biol 21: 247-269.

Javier Ruiz-Albert, X.-J. Y., Carmen R. Beuzón, Abigail N. Blakey, Edouard E. Galyov, David W. Holden (2002). "Complementary activities of SseJ and SifA regulate dynamics of the Salmonella typhimurium vacuolar membrane." Mol Microbiol 44: 645-661.

Jean, S. and A. A. Kiger (2012). "Coordination between RAB GTPase and phosphoinositide regulation and functions." Nat Rev Mol Cell Biol 13(7): 463-470.

Klink, B. U., S. Barden, T. V. Heidler, C. Borchers, M. Ladwein, T. E. B. Stradal, K. Rottner and D. W. Heinz (2010). "Structure of Shigella IpgB2 in Complex with Human RhoA: Implications for the mechanism of bacterial guanine nucleotide exchange factor mimicry." The Journal of Biological Chemistry 285(22): 17197-17208.

Knodler, L. A. (2015). "Salmonella enterica: living a double life in epithelial cells." Current Opinion in Microbiology 23: 23-31.

Knodler, L. A. and O. Steele-Mortimer (2005). "The Salmonella Effector PipB2 Affects Late Endosome/Lysosome Distribution to Mediate Sif Extension." Mol Biol Cell 16(9): 4108-4123.

Knodler, L. A., V. Nair and O. Steele-Mortimer (2014). "Quantitative Assessment of Cytosolic Salmonella in Epithelial Cells." PLoS ONE 9(1): e84681.

Kreibich, S., M. Emmenlauer, J. Fredlund, P. Rämö, C. Münz, C. Dehio, J. Enninga and W.-D. Hardt (2015). "Autophagy Proteins Promote Repair of Endosomal Membranes Damaged by the Salmonella Type Three Secretion System 1." Cell Host & Microbe 18(5): 527-537.

Krieger, V., D. Liebl, Y. Zhang, R. Rajashekar, P. Chlanda, K. Giesker, D. Chikkaballi and M. Hensel (2014). " Reorganization of the endosomal system in Salmonella-infected cells: the ultrastructure of Salmonella-induced tubular compartments." PLoS Pathog 10(9): e1004374.

Kuhle, V., D. Jäckel and M. Hensel (2004). "Effector Proteins Encoded by Salmonella Pathogenicity Island 2 Interfere with the Microtubule Cytoskeleton after Translocation into Host Cells." Traffic 5(5): 356-370.

Kumar, A., V. Rajendran, R. Sethumadhavan and R. Purohit (2013). "CEP proteins: the knights of centrosome dynasty." Protoplasma 250(5): 965-983.

Laemmli, U. K. (1970). Cleavage of structural proteins during the assembly of the head of bacteriophage T4. Nature, 227(5259), 680–5.

Lallemand-Breitenbach, V., M. Quesnoit, V. Braun, A. El Marjou, C. Poüs, B. Goud and F. Perez (2004). "CLIPR-59 Is a Lipid Raft-associated Protein Containing a Cytoskeleton-associated Protein Glycine-rich Domain (CAP-Gly) That Perturbs Microtubule Dynamics." Journal of Biological Chemistry 279(39): 41168-41178.

Lansbergen, G., Y. Komarova, M. Modesti, C. Wyman, C. C. Hoogenraad, H. V. Goodson, R. P. Lemaitre, D. N. Drechsel, E. van Munster, T. W. J. Gadella, F. Grosveld, N. Galjart, G. G. Borisy and A. Akhmanova (2004). "Conformational changes in CLIP-170 regulate its binding to microtubules and dynactin localization." The Journal of Cell Biology 166(7): 1003-1014.

Lemichez, E. and K. Aktories (2013). "Hijacking of Rho GTPases during bacterial infection." Experimental Cell Research 319(15): 2329-2336.

Li, J., X. Mao, L. Q. Dong, F. Liu and L. Tong (2007). "Crystal Structures of the BAR-PH and PTB Domains of Human APPL1." Structure 15(5): 525-533.

Liss, V. and M. Hensel (2015). "Take the tube: remodelling of the endosomal system by intracellular Salmonella enterica." Cellular Microbiology 17(5): 639-647.

Liu, J., F. Yao, R. Wu, M. Morgan, A. Thorburn, R. L. Finley and Y. Q. Chen (2002). "Mediation of the DCC Apoptotic Signal by DIP13α." Journal of Biological Chemistry 277(29): 26281-26285.

Lommel, S., S. Benesch, M. Rohde, J. Wehland and K. Rottner (2004). "Enterohaemorrhagic and enteropathogenic Escherichia coli use different mechanisms for actin pedestal formation that converge on N-WASP." Cellular Microbiology 6(3): 243-254.

Maikke B. Ohlson, Z. H., Neal M. Alto, Marie-Pierre Blanc, Jack E. Dixon, Jijie Chai, Samuel I. Miller (2008). "Structure and function of Salmonella SifA indicate that its interactions with SKIP, SseJ, and RhoA family GTPases induce endosomal tubulation." Cell Host Microbe 4: 434-446.

Malik-Kale, P., C. E. Jolly, S. Lathrop, S. Winfree, C. Luterbach and O. Steele-Mortimer (2011). "Salmonella – At Home in the Host Cell." Front Microbiol 2.

Malik-Kale, P., S. Winfree and O. Steele-Mortimer (2012). "The Bimodal Lifestyle of Intracellular Salmonella in Epithelial Cells: Replication in the Cytosol Obscures Defects in Vacuolar Replication." PLoS ONE 7(6): e38732.

Mao, X., C. K. Kikani, R. A. Riojas, P. Langlais, L. Wang, F. J. Ramos, Q. Fang, C. Y. Christ-Roberts, J. Y. Hong, R.-Y. Kim, F. Liu and L. Q. Dong (2006). "APPL1 binds to adiponectin receptors and mediates adiponectin signalling and function." Nat Cell Biol 8(5): 516-523.

Marlovits, T. C., T. Kubori, A. Sukhan, D. R. Thomas, J. E. Galán and V. M. Unger (2004). "Structural Insights into the Assembly of the Type III Secretion Needle Complex." Science 306(5698): 1040-1042.

Matanis, T., A. Akhmanova, P. Wulf, E. Del Nery, T. Weide, T. Stepanova, N. Galjart, F. Grosveld, B. Goud, C. I. De Zeeuw, A. Barnekow and C. C. Hoogenraad (2002). "Bicaudal-D regulates COPI-independent Golgi-ER transport by recruiting the dynein-dynactin motor complex." Nat Cell Biol 4(12): 986-992.

McEwan, David G., B. Richter, B. Claudi, C. Wigge, P. Wild, H. Farhan, K. McGourty, Fraser P. Coxon, M. Franz-Wachtel, B. Perdu, M. Akutsu, A. Habermann, A. Kirchof, Miep H. Helfrich, Paul R. Odgren, W. Van Hul, Achilleas S. Frangakis, K. Rajalingam, B. Macek, David W. Holden, D. Bumann and I. Dikic (2015). "PLEKHM1 Regulates Salmonella-Containing Vacuole Biogenesis and Infection." Cell Host & Microbe 17(1): 58-71.

McGhie, E. J., L. C. Brawn, P. J. Hume, D. Humphreys and V. Koronakis (2009). "Salmonella takes control: effector-driven manipulation of the host." Current Opinion in Microbiology 12(1): 117-124.

McKenney, R. J., W. Huynh, M. E. Tanenbaum, G. Bhabha and R. D. Vale (2014). "Activation of cytoplasmic dynein motility by dynactin-cargo adapter complexes." Science (New York, N.Y.) 345(6194): 337-341.

Miaczynska, M., S. Christoforidis, A. Giner, A. Shevchenko, S. Uttenweiler-Joseph, B. Habermann, M. Wilm, R. G. Parton and M. Zerial (2004). "APPL Proteins Link Rab5 to Nuclear Signal Transduction via an Endosomal Compartment." Cell 116(3): 445-456.

Miao, E. A. and S. I. Miller (2000). "A conserved amino acid sequence directing intracellular type III secretion by Salmonella typhimurium." Proceedings of the National Academy of Sciences 97(13): 7539-7544.

Mullis, K., Faloona, F., Scharf, S., Saiki, R., Horn, G., & Erlich, H. (1986). Specificenzymatic amplification of DNA in vitro: the polymerase chain reaction. Cold Spring Harbor Symposia on Quantitative Biology, 51 Pt 1, 263–73.

Mills, S. D., S. R. Ruschkowski, M. A. Stein and B. B. Finlay (1998). "Trafficking of Porin-Deficient Salmonella typhimurium Mutants inside HeLa Cells: ompR and envZ Mutants Are Defective for the Formation of Salmonella-Induced Filaments." Infection and Immunity 66(4): 1806-1811.

Mitsuuchi Y, Johnson SW, Sonoda G, Tanno S, Golemis EA, Testa JR.(1999) "Identification of a chromosome 3p14.3-21.1 gene, APPL, encoding an adaptor molecule that interacts with the oncoprotein-serine/threonine kinase AKT2". Oncogene. 18:4891–4898.

Moest, T. P. and S. Méresse (2013). "Salmonella T3SSs: successful mission of the secret(ion) agents." Current Opinion in Microbiology 16(1): 38-44.

Mota Lí, J., A. E. Ramsden, M. Liu, J. D. Castle and D. W. Holden (2009). "SCAMP3 is a component of the Salmonella-induced tubular network and reveals an interaction between bacterial effectors and post-Golgi trafficking." Cell Microbiol 11(8): 1236-1253.

Muranen, T., M. Grönholm, A. Lampin, D. Lallemand, F. Zhao, M. Giovannini and O. Carpén (2007). "The tumor suppressor merlin interacts with microtubules and modulates Schwann cell microtubule cytoskeleton." Human Molecular Genetics 16(14): 1742-1751.

Muresan, V., M. C. Stankewich, W. Steffen, J. S. Morrow, E. L. F. Holzbaur and B. J. Schnapp (2001). "Dynactin-Dependent, Dynein-Driven Vesicle Transport in the Absence of Membrane Proteins: A Role for Spectrin and Acidic Phospholipids." Molecular Cell 7(1): 173-183.

Nechamen, C. A., R. M. Thomas and J. A. Dias (2007). "APPL1, APPL2, Akt2 and FOXO1a Interact with FSHR in a Potential Signaling Complex." Molecular and cellular endocrinology 260-262: 93-99.

Niskanen, T., Giovanna Ciaravino, G. and Takkinen, J. (2015). "Surveillance of seven priority food- and waterborne diseases in the EU/EEA 2010-2012". ECDC surveillance report. 1-262.

Ohlson, M. B., Z. Huang, N. M. Alto, M. P. Blanc, J. E. Dixon, J. Chai and S. I. Miller (2008). "Structure and function of SifA indicate that interactions with SKIP, SseJ, and RhoA family GTPases induce endosomal tubulation." Cell Host Microbe 4(5): 434-446.

Ohya, K., Y. Handa, M. Ogawa, M. Suzuki and C. Sasakawa (2005). "IpgB1 Is a Novel Shigella Effector Protein Involved in Bacterial Invasion of Host Cells: Its activity to promote membrane ruffling via Rac1 and Cdc42 activation." Journal of Biological Chemistry 280(25): 24022-24034.

Orchard, R. C. and N. M. Alto (2012). "Mimicking GEFs: A Common Theme For Bacterial Pathogens." Cellular Microbiology 14(1): 10-18.

Owen, Katherine A. and James E. Casanova (2015). "Salmonella Manipulates Autophagy to "Serve and Protect"." Cell Host & Microbe 18(5): 517-519.

Perez, F., G. S. Diamantopoulos, R. Stalder and T. E. Kreis (1999). "CLIP-170 Highlights Growing Microtubule Ends In Vivo." Cell 96(4): 517-527

Perez, F., K. Pernet-Gallay, C. Nizak, H. V. Goodson, T. E. Kreis and B. Goud (2002). "CLIPR-59, a new trans-Golgi/TGN cytoplasmic linker protein belonging to the CLIP-170 family." The Journal of Cell Biology 156(4): 631-642.

Pfister, K. K., P. R. Shah, H. Hummerich, A. Russ, J. Cotton, A. A. Annuar, S. M. King and E. M. C. Fisher (2006). "Genetic Analysis of the Cytoplasmic Dynein Subunit Families." PLoS Genetics 2(1): e1.

Pierre, P., J. Scheel, J. E. Rickard and T. E. Kreis (1992). "CLIP-170 links endocytic vesicles to microtubules." Cell 70(6): 887-900.

Rajashekar, R. and M. Hensel (2011). "Dynamic modification of microtubule-dependent transport by effector proteins of intracellular Salmonella enterica." European Journal of Cell Biology 90(11): 897-902.

Rajashekar, R., D. Liebl, D. Chikkaballi, V. Liss and M. Hensel (2014). "Live Cell Imaging Reveals Novel Functions of Salmonella enterica SPI2-T3SS Effector Proteins in Remodeling of the Host Cell Endosomal System." PLoS One 9(12).

Rajashekar, R., D. Liebl, A. Seitz and M. Hensel (2008). "Dynamic Remodeling of the Endosomal System During Formation of Salmonella-Induced Filaments by Intracellular Salmonella enterica." Traffic 9(12): 2100-2116.

Ramsden, A. E., L. J. Mota, S. Münter, S. L. Shorte and D. W. Holden (2007). "The SPI-2 type III secretion system restricts motility of Salmonella-containing vacuoles." Cellular Microbiology 9(10): 2517-2529.

Ran, F. A., P. D. Hsu, J. Wright, V. Agarwala, D. A. Scott and F. Zhang (2013). "Genome engineering using the CRISPR-Cas9 system." Nat. Protocols 8(11): 2281-2308.

Raymond, B., V. F. Crepin, J. W. Collins and G. Frankel (2011). "The WxxxE effector EspT triggers expression of immune mediators in an Erk/JNK and NF-κB-dependent manner." Cellular microbiology 13(12): 1881-1893.

Riehemann, K. and C. Sorg (1993). "Sequence homologies between four cytoskeleton-associated proteins." Trends in Biochemical Sciences 18(3): 82-83.

Ridley, A. J. and A. Hall (1992). "The small GTP-binding protein rho regulates the assembly of focal adhesions and actin stress fibers in response to growth factors." Cell 70(3): 389-399.

Ridley, A. J., H. F. Paterson, C. L. Johnston, D. Diekmann and A. Hall (1992). "The small GTP-binding protein rac regulates growth factor-induced membrane ruffling." Cell 70(3): 401-410.

Riesenberg-Wilmes, M. R., B. Bearson, J. W. Foster and R. Curtis (1996). "Role of the acid tolerance response in virulence of Salmonella typhimurium." Infect Immun 64(4): 1085-1092.

Rong, R., W. Jin, J. Zhang, M. Saeed Sheikh and Y. Huang (2004). "Tumor suppressor RASSF1A is a microtubule-binding protein that stabilizes microtubules and induces G2//M arrest." Oncogene **23**(50): 8216-8230.

Rottner, K., T. E. B. Stradal and J. Wehland (2005). "Bacteria-Host-Cell Interactions at the Plasma Membrane: Stories on Actin Cytoskeleton Subversion." Developmental Cell 9(1): 3-17.

Ruiz-Albert, J., X.-J. Yu, C. R. Beuzón, A. N. Blakey, E. E. Galyov and D. W. Holden (2002). "Complementary activities of SseJ and SifA regulate dynamics of the Salmonella typhimurium vacuolar membrane." Molecular Microbiology 44(3): 645-661.

Schlumberger, M. C. and W.-D. Hardt (2006). "Salmonella type III secretion effectors: pulling the host cell's strings." Current Opinion in Microbiology 9(1): 46-54.

Schlumberger, M. C., A. J. Müller, K. Ehrbar, B. Winnen, I. Duss, B. Stecher and W. D. Hardt (2005). "Real-time imaging of type III secretion: Salmonella SipA injection into host cells." Proc Natl Acad Sci U S A 102(35): 12548-12553.

Schraidt, O. and T. C. Marlovits (2011). "Three-Dimensional Model of Salmonella's Needle Complex at Subnanometer Resolution." Science 331(6021): 1192-1195.

Schroeder, N., L. J. Mota and S. Méresse (2011). "Salmonella-induced tubular networks." Trends in Microbiology 19(6): 268-277.

Schroeder, N., T. Henry, C. de Chastellier, W. Zhao, A.-A. Guilhon, J.-P. Gorvel and S. Méresse (2010). "The Virulence Protein SopD2 Regulates Membrane Dynamics of Salmonella-Containing Vacuoles." PLoS Pathogens 6(7): e1001002.

Shea, J. E., C. R. Beuzon, C. Gleeson, R. Mundy and D. W. Holden (1999). "Influence of the Salmonella typhimurium Pathogenicity Island 2 Type III Secretion System on Bacterial Growth in the Mouse." Infection and Immunity 67(1): 213-219.

Shi, X., X. Sun, M. Liu, D. Li, R. Aneja and J. Zhou (2011). "CEP70 Protein Interacts with γ-Tubulin to Localize at the Centrosome and Is Critical for Mitotic Spindle Assembly." The Journal of Biological Chemistry 286(38): 33401-33408.

Shi, X., M. Liu, D. Li, J. Wang, R. Aneja and J. Zhou (2012a). "Cep70 contributes to angiogenesis by modulating microtubule rearrangement and stimulating cell polarization and migration." Cell Cycle 11(8): 1554-1563.

Shi, X., J. Wang, Y. Yang, Y. Ren, J. Zhou and D. Li (2012b). "Cep70 promotes microtubule assembly in vitro by increasing microtubule elongation." Acta Biochimica et Biophysica Sinica 44(5): 450-454.

Shi, X., Y. Yao, Y. Wang, Y. Zhang, Q. Huang, J. Zhou, M. Liu and D. Li (2015). "Cep70 regulates microtubule stability by interacting with HDAC6." FEBS Letters 589(15): 1771-1777.

Short, B., C. Preisinger, J. Schaletzky, R. Kopajtich and F. A. Barr (2002). "The Rab6 GTPase Regulates Recruitment of the Dynactin Complex to Golgi Membranes." Current Biology 12(20): 1792-1795.

Smith, A. C., W. D. Heo, V. Braun, X. Jiang, C. Macrae, J. E. Casanova, M. A. Scidmore, S. Grinstein, T. Meyer and J. H. Brumell (2007). "A network of Rab GTPases controls phagosome maturation and is modulated by Salmonella enterica serovar Typhimurium." The Journal of Cell Biology 176(3): 263-268.

Splinter, D., D. S. Razafsky, M. A. Schlager, A. Serra-Marques, I. Grigoriev, J. Demmers, N. Keijzer, K. Jiang, I. Poser, A. A. Hyman, C. C. Hoogenraad, S. J. King and A. Akhmanova (2012). "BICD2, dynactin, and LIS1 cooperate in regulating dynein recruitment to cellular structures." Molecular Biology of the Cell 23(21): 4226-4241.

Steele-Mortimer, O. (2008). "The Salmonella-containing Vacuole – Moving with the Times." Curr Opin Microbiol 11(1): 38-45.

Stein, M. A., K. Y. Leung, M. Zwick, F. G.-d. Portillo and B. B. Finlay (1996). "Identification of a Salmonella virulence gene required for formation of filamentous structures containing lysosomal membrane glycoproteins within epithelial cells." Molecular Microbiology 20(1): 151-164.

Steinmetz, M. O. and A. Akhmanova (2008). "Capturing protein tails by CAP-Gly domains." Trends in Biochemical Sciences 33(11): 535-545.

Tang, Q., C. M. Staub, G. Gao, Q. Jin, Z. Wang, W. Ding, R. E. Aurigemma and K. M. Mulder (2002). "A Novel Transforming Growth Factor-β Receptor-interacting Protein That Is Also a Light Chain of the Motor Protein Dynein." Molecular Biology of the Cell 13(12): 4484-4496.

Thurston, T. L. M., M. P. Wandel, N. von Muhlinen, A. Foeglein and F. Randow (2012). "Galectin 8 targets damaged vesicles for autophagy to defend cells against bacterial invasion." Nature 482(7385): 414-418.

Tollenaere, M. A. X., N. Mailand and S. Bekker-Jensen (2015). "Centriolar satellites: key mediators of centrosome functions." Cellular and Molecular Life Sciences 72(1): 11-23.

Urnavicius, L., K. Zhang, A. G. Diamant, C. Motz, M. A. Schlager, M. Yu, N. A. Patel, C. V. Robinson and A. P. Carter (2015). "The structure of the dynactin complex and its interaction with dynein." Science 347(6229): 1441-1446.

van Buul, J. D., D. Geerts and S. Huveneers (2014). "Rho GAPs and GEFs: Controling switches in endothelial cell adhesion." Cell Adh Migr 8(2): 108-124.

van de Willige, D., C. C. Hoogenraad and A. Akhmanova (2016). "Microtubule plus-end tracking proteins in neuronal development." Cellular and Molecular Life Sciences 73: 2053-2077.

van Weering, J. R. T., P. Verkade and P. J. Cullen (2010). "SNX–BAR proteins in phosphoinositide-mediated, tubular-based endosomal sorting." Seminars in cell & developmental biology 21(4): 371-380.

Vigil, D., J. Cherfils, K. L. Rossman and C. J. Der (2010). "Ras superfamily GEFs and GAPs: validated and tractable targets for cancer therapy?" Nat Rev Cancer 10(12): 842-857.

Wade, R. H. (2009). "On and Around Microtubules: An Overview." Molecular Biotechnology 43(2): 177-191.

Walker, R. A., E. T. O'Brien, N. K. Pryer, M. F. Soboeiro, W. A. Voter, H. P. Erickson and E. D. Salmon (1988). "Dynamic instability of individual microtubules analyzed by video light microscopy: rate constants and transition frequencies." The Journal of Cell Biology 107(4): 1437-1448.

Wanschers B, van de Vorstenbosch R, Wijers M, Wieringa B, King SM, Fransen J. (2008). "Rab6 family proteins interact with the dynein light chain protein DYNLRB1". Cell Motil. Cytoskeleton. 65 (3): 183–96

Weisbrich, A., S. Honnappa, R. Jaussi, O. Okhrimenko, D. Frey, I. Jelesarov, A. Akhmanova and M. O. Steinmetz (2007). "Structure-function relationship of CAP-Gly domains." Nat Struct Mol Biol 14(10): 959-967.

White, J., L. Johannes, F. Mallard, A. Girod, S. Grill, S. Reinsch, P. Keller, B. Tzschaschel, A. Echard, B. Goud and E. H. K. Stelzer (1999). "Rab6 Coordinates a Novel Golgi to ER Retrograde Transport Pathway in Live Cells." The Journal of Cell Biology 147(4): 743-760.

Wickström, S. A., K. C. Masoumi, S. Khochbin, R. Fässler and R. Massoumi (2010). "CYLD negatively regulates cell-cycle progression by inactivating HDAC6 and increasing the levels of acetylated tubulin." The EMBO Journal 29(1): 131-144.

Wong, A. R. C., J. S. Pearson, M. D. Bright, D. Munera, K. S. Robinson, S. F. Lee, G. Frankel and E. L. Hartland (2011). "Enteropathogenic and enterohaemorrhagic Escherichia coli: even more subversive elements." Molecular Microbiology 80(6): 1420-1438.

Zerial, M. and H. McBride (2001). "Rab proteins as membrane organizers." Nat Rev Mol Cell Biol 2(2): 107-117.

Zhao, W., T. Moest, Y. Zhao, A.-A. Guilhon, C. Buffat, J.-P. Gorvel and S. Méresse (2015). "The Salmonella effector protein SifA plays a dual role in virulence." Scientific Reports 5: 12979.

Zhu, G., J. Chen, J. Liu, J. S. Brunzelle, B. Huang, N. Wakeham, S. Terzyan, X. Li, Z. Rao, G. Li and X. C. Zhang (2007). "Structure of the APPL1 BAR-PH domain and characterization of its interaction with Rab5." The EMBO Journal 26(14): 3484-3493.

**Acknowledgments**

I would like to express my special appreciation and thanks to

My advisor Prof. Dr. Theresia Stradal for her guidance and support at all times of research and writing of this thesis, for the knowledge and experience she has given me, for having her door opened for me at any time, for being literally my “Doktormutter” - I sincerely thank her,

Prof. Dr. Martin Korte for reviewing my PhD thesis as well as Prof. Dr. Ralf R. Mendel for kind participation in my oral defense,

Prof. Dr. Klemens Rottner, Prof. Dr. Lothar Jänsch and Dr. Marco van Ham for kind participation in my thesis committee, scientific discussions and pieces of advice to improve my PhD project,

Prof. Dr. Matthias Epple and his working group 2011/2012 for great scientific experience and knowledge during my research internship,

Prof. Dr. Valeriy Bondarenko, my supervisor for the Master's Thesis, for his kind support throughout my study,

Prof. Dr. Michael Hensel, Dr. Franck Perez, Dr. Marco van Ham for providing me necessary cell line and DNA plasmids to carry out my experiments,

my colleagues, namely PD Dr. Anika Steffen, Dr. Sonia Costa, Stephanie Stahnke, Jessica Halfen, and my friend Dr. Tatyana Danyukova for critical reading of my PhD thesis and valuable comments and suggestions,

Dr. Svitlana Chernousova for teaching me a lot of things and sharing knowledge during my research internship,

Dr. Stefan Arens and Eric Meinhardt for practical tips during the first mounts in the lab,

Dr. Sonia Costa for friendly advising and supporting, for an unforgettable weekend trip to Rome,

PD Dr. Anika Steffen for being always available and keen on helping me,

Annette Otto, Patrik Duwe, Brigitte Denker, Monique Duwe, Karin Littmann-Janßen for their excellent technical assistance,

Astrid Lootz, Daniela Romke and Claudia Bethke-Schönherr for kind assistance with paper work,

Jana Kollasser, Dr. Jan Hänish, Dr. Kai Schlüter, Dr. David de Gorter, Aleks Guledani for helpfulness in the everyday lab life,

Dr. Sabine Kirchoff, Dr. Berenike Henneberg and the rest of the Graduate School for excellent workshops as well as PhD Retreats and Symposiums,

Angela Walter for great assistance to international PhD students,

Helene Todt, Dr. Vladimir Gonçalves Magalhaes, Dr. Sripriya Murthy, Abhishek Bakuli, Neda Tafrishi, Dr. Igor Grekov, Tatjana Hirsch, Oxana Haberkorn and Inga Hochnadel for friendly conversations and support,

Nadine Koch and Tobias Lübke for being with me "DO IT"-speakers, working as a team and sharing a great experience,

Diwali team for enjoyable moments.

Words cannot express how grateful I am to my dearest and beloved family, my friends and relatives, especially

my parents, Elena and Igor, for everything they have been doing for me, in my past and for the sake of my future, their love and belief in me,

my grandmothers, Iulia and Vera, for their unconditional love and care,

my younger sister Tetiana for cheering me up at any occasion and taking care of parents and grandparents at the time when I was far away,

my beloved husband Viktor for his endless love, support and inspiration.